Materials for simultaneous energy conversion and storage

Jérémy Sum

Sorbonne Université

Ecole doctorale 397 : Physique et Chimie des Matériaux

Laboratoire de Chimie de la Matière Condensée de Paris

Matériaux pour Conversion et Stockage simultanés de l'énergie

By **Jérémy SUM**

PhD thesis in Material Chemistry

Directed by Christel LABERTY-ROBERT and

co-supervised by Natacha KRINS

Presentation on January 20, 2022

In front of the jury:

Dr. Nathalie JOB	Associate Professor, Université de Liège	Referee
Pr. Pierre MILLET	Professor, Université Paris-Saclay	Referee
Dr. Benoit LIMOGES	CNRS Director, Université de Paris	Examinator
Dr. Elise NANINI-MAURY	Research-Engineer, ENGIE Laborelec	Examinator
Dr. Hubert PERROT	CNRS Director, Sorbonne Université	Examinator
Dr. Natacha KRINS	Associate Professor, Sorbonne Université	Co-supervisor
Pr. Christel LABERTY-ROBERT	Professor, Sorbonne Université	Director

Remerciements

Avant toute chose, j'aimerais remercier mes encadrants Natacha Krins et Christel Laberty-Robert pour m'avoir permis de rejoindre le LCMCP sur une thématique en accord avec mon projet professionnel et surtout en accord avec mes valeurs. Je les remercie également de m'avoir transmis leurs connaissances en science mais également en diffusion scientifique. Merci pour ces réunions scientifiques se terminant souvent par un débat sur l'amélioration de l'enseignement supérieur, la crise COVID ou autres sujets divers et variés. J'aimerais remercier à titre personnel Christel pour le partage de sa passion qui se traduit en quantité de travail par jour impressionnante tout en restant disponible pour discuter de mes dernières avancées à la paillasse. Pour moi Christel est un modèle de réussite professionnelle grâce à l'équilibre entre sa passion pour les sciences, l'enseignement tout en gardant du temps pour faire du sport. J'aimerais également souligner sa capacité à conduire ses étudiants vers l'excellence avec bienveillance. J'aimerais également remercier Natacha pour sa gentillesse, son empathie mais également ses connaissances qui ont été en open access à n'importe quelle heure et durant toute ma thèse. Je la remercie également de m'avoir transmis son sens de l'esthétisme pour mieux organiser, clarifier et embellir mes figures et schémas.

D'un point de vue plus personnel j'aimerais remercier du fond du cœur ma famille, maman papa et Anthony pour votre soutien, compréhension et surtout tolérance. Je vous aime. Merci à ma famille au sens large : cousins, oncles et tantes qui, par leur diversité de choix de vie m'a ouvert l'esprit. Merci à mon grand-père qui est un modèle de bonheur et de ténacité. Merci à mes proches amis en particulier, Aurore, Romain, Erwan, Léo, Patrick, Hamza mais aussi Robin et Francis que j'ai négligé mais, vous le savez, vous comptez énormément pour moi. Merci à Yacine et Rémi pour votre aide précieuse. Merci à Mélissa pour ton soutien quotidien et sans faille ! Merci à mes camarades de promo mais aussi aux deux CDD, aux anciens et nouveaux doctorants pour la bonne ambiance générée au LCMCP. Merci à mes anciens profs, aux bizounours, à la team RL, la team escalade bref merci à tous ceux qui m'ont apporté leur soutien qui m'a permis de continuer d'avancer et qui a fait l'homme que je suis aujourd'hui.

TABLE of CONTENTS

Résumé (fr) :

Introduction :

L'énergie solaire est l'énergie la plus abondante sur Terre, soit 23 000 TW par an. Cette énergie pourrait satisfaire la consommation annuelle mondiale estimée à 19 TW en 2015 (**figure 1 du manuscrit**).[1,2] Il existe deux moyens pour collecter cette énergie solaire, la voie thermique et la voie photovoltaïque. Nous nous intéresserons tout particulièrement à la valorisation de ce rayonnement solaire par la voie photovoltaïque. Cette voie transforme l'énergie solaire en énergie électrique, grâce aux propriétés que possèdent certains matériaux avec des rendements approchant les 50 % en laboratoire. Différentes technologies ont vu le jour depuis la découverte du phénomène photovoltaïque en 1839 par deux français, Antoine Becquerel et son fils ; les cellules solaire multi-jonction (~47 % de rendement), les cellules perovskites (PSCs, ~25 %), les cellules a colorant (dye sensitized solar cells, DSSCs, 12,6 %), les cellules organiques (OPV, 17,5 %) et la technologie la plus utilisée de nos jours, les cellules à base de silicium qui atteigne les 25 % de rendement (**figure 2 du manuscrit**)[3,4]. Néanmoins l'énergie solaire a l'inconvénient d'être une énergie intermittente et nécessite une utilisation directe. En conséquence, l'utilisation d'un système de stockage de l'énergie est nécessaire pour pallier aux aléas climatique, à l'alternance jour/nuit mais également pour faire correspondre la demande d'énergie des consommateurs avec la production issue du solaire (**figure 3 du manuscrit**). Le stockage électrochimique est parmi les choix les plus attractif pour stocker les énergies renouvelables.[5]

Parmi le stockage électrochimique, les batteries lithium ion sont les plus performantes et est de nos jours, une technologie mature qui jouit de 40 ans de développement et de commercialisation à travers le monde. Elle est considérée comme l'avancé du siècle tout comme l'a été la machine à vapeur et les moteurs à combustion à leur époque. Si nous voulons réduire les émissions de gaz à effet de serre en remplaçant les véhicules thermiques par des véhicules électriques, 2,9 milliards de véhicules sont à remplacer. L'augmentation du nombre de véhicule électrique pourrait alors créer une saturation du réseau électrique. Une des solutions serait de les charger en dehors du réseau électrique et si possible avec de l'énergie verte.

Des prototypes existent déjà comme la voiture Aptera[7] qui peut recharger sa batterie grâce à l'énergie solaire. Nous allons voir par la suite comment coupler ses deux systèmes de conversion et de stockage de l'énergie solaire.

Chapitre 1 : Etat de l'art

Pour collecter l'énergie solaire et la stocker électrochimiquement trois architectures sont reportées dans la littérature. La plus intuitive est l'utilisation des technologies existante et les coupler entre elles pour obtenir un dispositif tandem. Néanmoins, cette architecture est volumineuse et nécessite des adaptations entre les batteries et les cellules solaires. Les deux architectures suivantes sont donc plus compactes. La deuxième architecture est un système avec une photo-électrode et deux électrodes de batterie, la photo-électrode ayant pour rôle de collecter et charge la batterie. La dernière architecture est une architecture a seulement deux électrodes avec une électrode capable de réaliser à la fois la collecte de l'énergie solaire mais également qui aurait la propriété d'insérer réversiblement des cations dans sa structure. Cette architecture peut être sous divisée en deux suivant la nature de cette électrode hybride. Soit celle-ci est composée d'un absorbeur de lumière (colorant ou semi-conducteur par exemple), celui-çi étant déposé sur un matériau de batterie. Soit cette électrode n'est composé que d'un seul matériau capable de réaliser l'absorption à la fois de cations et de l'énergie solaire ; ce matériau sera appelé par la suite un matériau bi-fonctionnel. Le but de ces photo-électrodes étant de photo-recharger les électrodes de batterie pour donc stocker l'énergie solaire de façon électrochimique. Pour ce faire deux types de charges existent. La photo-charge qui est une charge uniquement réalisée grâce au rayonnement solaire, sans apport extérieur et donc réalisé en circuit ouvert (Open Circuit Voltage, OCV). Soit la charge photo-assistée qui, comme son nom l'indique est assisté par une charge électrique. Les deux types de recharge sont présentés dans le **schéma 1** pour les architectures à deux électrodes.

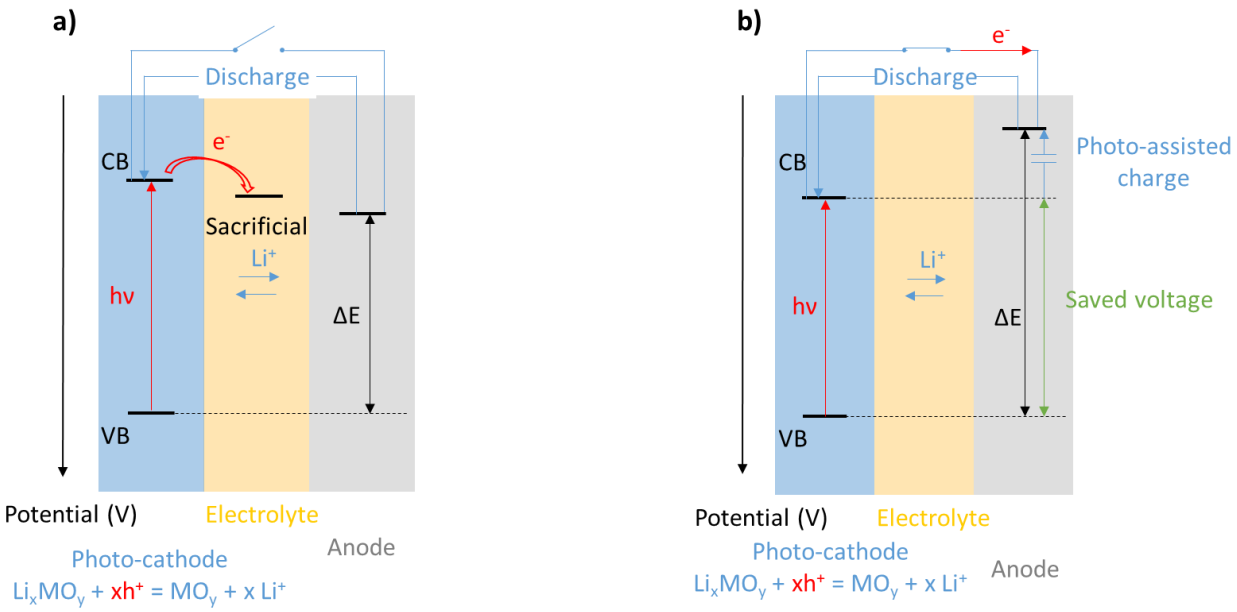

Schéma 1 : a) Illustration d'une photo-charge (OCV sous illumination) d'un système à 2 électrodes, b) Illustration d'une charge photo-assistée (charge électrique sous illumination) d'un système à 2 électrodes.

Les mécanismes de l'architecture à trois électrodes ne seront pas détaillés ici car dans le reste de ce résumé et des travaux réalisés durant cette thèse, seul l'architecture à deux électrodes sera utilisée ; il est néanmoins détaillé dans le **chapitre I**. Pour l'architecture à deux électrodes deux mécanismes sont possible suivant le type de charge cité précédemment. Lors d'une photo-charge l'électrode réalisant la collecte et le stockage généra, en présence de lumière, un exciton c'est-à-dire une paire électron-trou. Le trou peut alors réagir avec le matériau lithié composant cette électrode pour extraire les ions lithiums. On parle alors de photo-extraction. Le photo-électron quant à lui est condamné à réagir en surface de cette électrode avec l'électrolyte ou un élément sacrificiel ; en effet la photo-charge étant réalisé à l'OCV, c'est-à-dire à circuit ouvert, empêchant ainsi le photo-électron de passer par le circuit extérieur (**schéma 1a du manuscrit**). Sous charge photo-assistée le mécanisme du trou est similaire. Le photo-électron quant à lui peut passer par le circuit extérieur entrainé par le flux d'électron dû à la charge électrochimique. L'énergie électrique fourni pour charger la batterie est alors moins conséquente grâce aux charges photo-générées ; on a donc remplacé une partie de l'énergie électrique par de l'énergie solaire.

Cette thèse fait suite à la thèse d'Olivier Nguyen qui travailla sur une électrode bi-fonctionnel de dioxyde de titane (TiO_2) anatase mésoporeuse préparée en film mince.

Le TiO_2 anatase est en effet bien connu pour être capable de stocker les ions lithium réversiblement. C'est également un matériau semi-conducteur photosensible. En absorbant la lumière dans la gamme des Ultra-Violets (UV) celui-ci a la capacité de créer une paire électron-trous. Les mécanismes cités précédemment sont alors envisageable. L'objectif de cette thèse était d'étudier les mécanismes sous-jacents de ces photo-recharges. Pour ce faire une électrode « modèle », c'est-à-dire sans additifs (colorant ou carbone conducteur) a été réalisée pour simplifier l'étude de cette électrode bi-fonctionnelle. Les éléments constituant le système sont : verre/FTO/TiO_2 // $LiPF_6$ 1 M in EC : DMC (1 : 1 en vol) // Li°, ref/Li°. Utilisant ce système O. Nguyen et al ont comparé un cycle de décharge/charge (en mode galvanostatique) dans le noir et sous illumination les résultats sont présentés ci-dessous dans la **figure 1** ci-dessous.

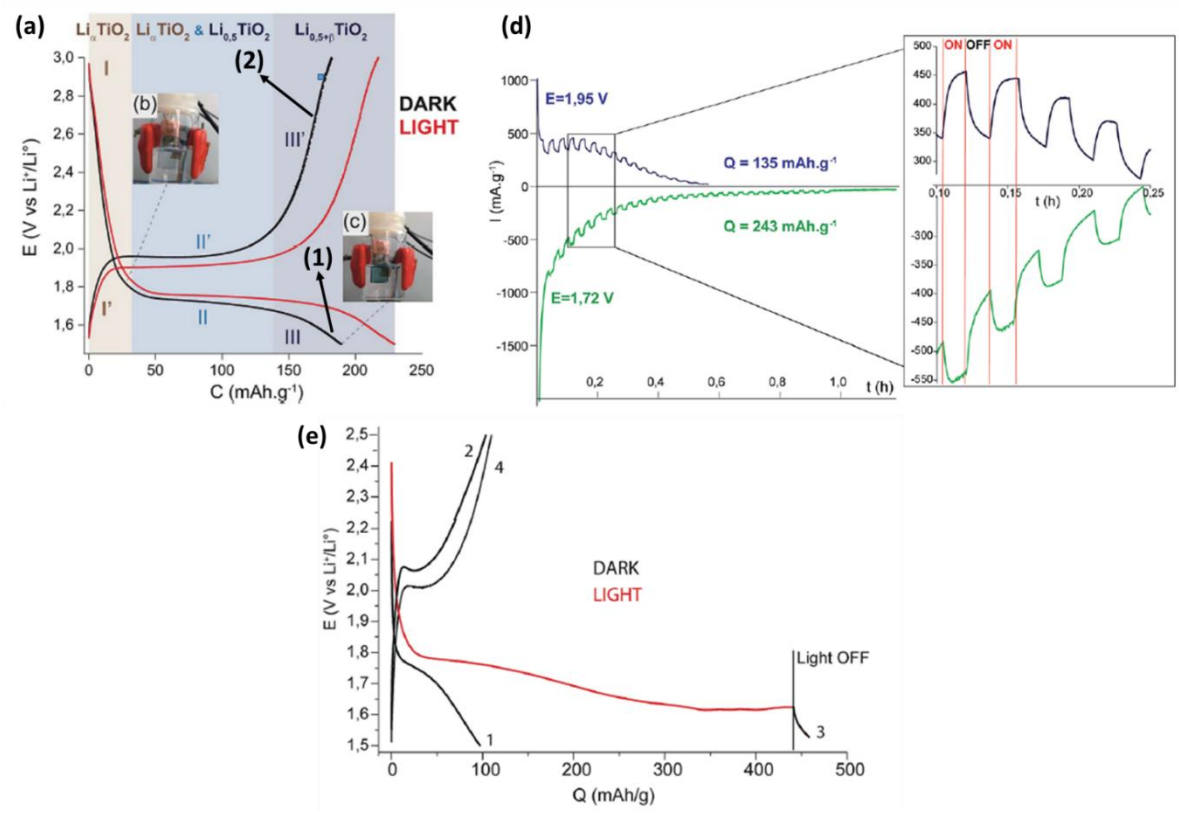

Figure 1 : système : verre/FTO/TiO_2// $LiPF_6$ 1 M in EC : DMC (1 : 1 en vol) // Li°, ref/Li° avec un TiO_2 anatase mésoporeux de 230 nm d'épaisseur. a) Cycle de décharge/charge (2C) dans le noir (courbes noires) et sous illumination (courbes rouges). b) photo du film de TiO_2 en phase pauvre en lithium (électrode transparente). c) photo du film de TiO_2 en phase riche en lithium (électrode bleu). d) Potentiostatique à différents potentiels : 1,95 V et 1,72 V vs Li^+/Li avec une illumination périodique toutes les minutes. e) Illustration de la possible capacité «infinie». 2 décharge/charge consécutives (1-2, 3-4, à i=47 mA/g, C/7) dans le noir (courbes noires) et sous illumination (courbe rouge). L'illumination de la décharge 3 à été arrêté après 8 heures d'illumination.

Suite à ces expériences O. Nguyen et al en déduisent plusieurs hypothèses quant au mécanisme. Le mécanisme de cette photo-recharge repose sur la capacité du trou formé après illumination à réagir avec les centres Ti^{3+} du matériau pour donner Ti^{4+}, ce qui entraîne l'extraction d'un ion Li^{+} par compensation de charge. Néanmoins le mystère sur le devenir du photo-électron persista. L'hypothèse formulée alors était une réduction de l'électrolyte formant une interface solide entre l'électrolyte et l'électrode appelé SEI (Solid Electrolyte Interface).

Cette deuxième réaction n'est pas une réaction souhaitée et est pénalisante sur le long terme, c'est pourquoi durant ma thèse nous avons décidé de changer l'électrolyte, passant d'un électrolyte organique à un électrolyte de type « Water In Salt » (WIS) i.e un sel très concentré dans de l'eau. Ce changement d'électrolyte a pour vocation d'introduire un accepteur de ce photo-électron, ici l'eau, pour former du dihydrogène. Le dihydrogène est considéré comme un vecteur énergétique et est une méthode de stockage de l'énergie ; ainsi les deux charges photo-générée seraient valorisées.

Chapitre II : Partie expérimentale

La partie expérimentale ne sera pas détaillée dans ce résumé.

Chapitre III : Etude electrochimique dans le noir

Comparaison LP30/WIS

Un premier travail de comparaison entre les deux électrolytes est nécessaire pour vérifier que les propriétés sont similaires (**figure 2**).

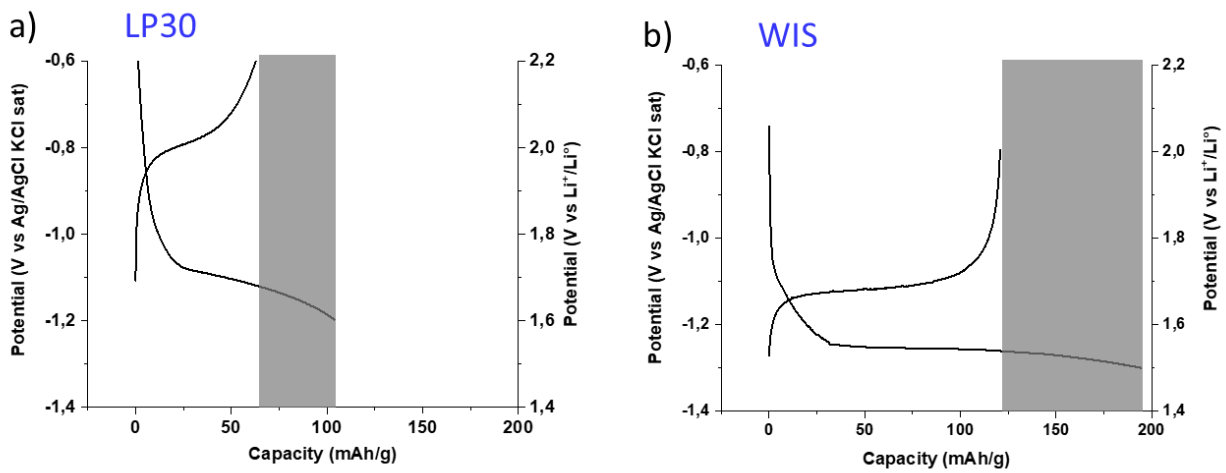

Figure 2 : Charge galvanostatique (2C) a) dans le LP30, b) dans le water in salt (WIS, LiTFSI 20 M).

Des capacités plus élevées sont atteignable en WIS de plus les images SEM-FEG suggèrent moins de dégradation de l'électrolyte à l'interface. Une étude plus approfondi sur la formation de dihydrogène est entrepris dans la partie suivante.

Electrocatalyse de l'eau modulé par la composition en lithium du TiO_2

Un caractère irréversible entre la décharge et la charge est attribué majoritairement à de l'électrocatalyse de l'eau en dihydrogène(EC-HER) confirmé par chromatographie en phase gaz. Il est possible de favoriser l'EC-HER en jouant sur les vitesses de décharge. Néanmoins il est difficile de distinguer les phénomènes d'insertion de lithium de l'EC-HER. C'est pourquoi nous avons utilisé la spectroscopie UV-VIS NIR operando. Durant un cycle galvanostatique à 2C un spectre est effectué toutes les 2 minutes. Il a été constaté que lors de l'insertion de lithium (décharge) une bande à 720 nm augmente. Celle-ci diminue ensuite lors de l'extraction du lithium (charge). Cette longueur d'onde correspondrait à la couleur complémentaire du bleu, couleur du matériau à l'état lithié. Nous avons donc attribué cette bande à l'insertion/extraction des ions lithiums au sein du dioxyde de titane. Grâce à cette bande il est possible de remonter à la capacité « réelle » d'insertion/extraction du lithium, exempté de l'EC-HER. Il est alors possible de suivre l'évolution de l'absorption relative de cette bande au court du cyclage (**figure 3**).

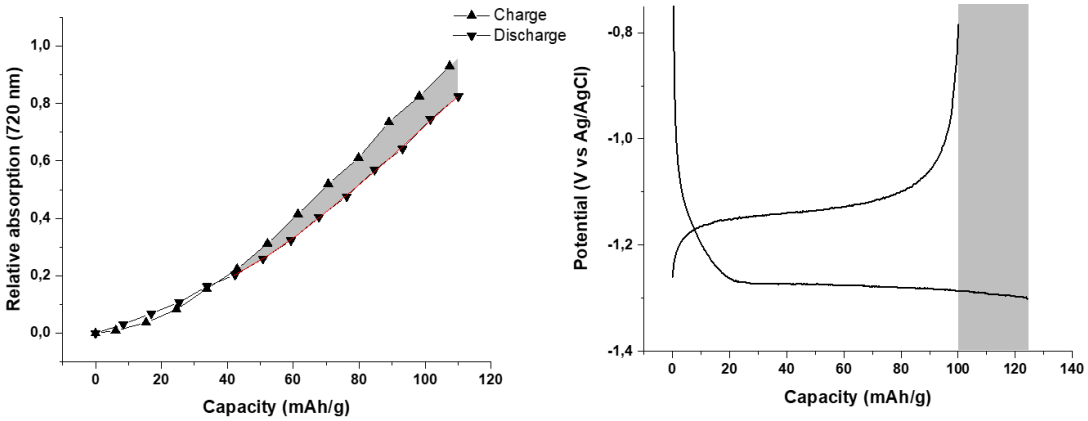

Figure 3 : (gauche) Evolution de l'absorption relative de la bande à 720 nm supposée correspondre au taux de lithium en fonction de la capacité mesurée par électrochimie. La partie grisée correspondant à l'EC-HER, (droite) Charge et décharge galvanostatique avec en gris la capacité supposée d'EC-HER.

On peut noter que pour une même absorbance/ composition en lithium, deux capacités différentes sont observés. Si l'ont fait l'hypothèse que l'EC-HER n'a pas lieu pendant la charge mais seulement pendant la décharge, la différence entre la capacité de décharge par rapport à la capacité de charge représente la production de dihydrogène. Nous avons donc pu montrer qu'une augmentation d'activité vis-à-vis de cette EC-HER s'effectue avec l'augmentation du taux de lithium dans l'électrode de TiO_2. En d'autres termes plus la capacité est élevée plus le matériau est réactif vis-à-vis de la production d'hydrogène.

Au vu de ces résultats nous pouvons également supposer que ce changement de composition peut influencer les photo-recharges. Une première étude a été menée sur la photo-charge.

Chapitre IV : Etude photo-(electro)chimique

Influence de la composition sur les phénomènes de photo-recharge

I) Photo-charge

Pour évaluer l'influence de la composition sur la photo-charge l'électrode a été lithié à différentes compositions. Cela est réalisé en effectuant une décharge en s'arrêtant à différentes capacités. Après chaque capacité une photo-charge est effectuée (**figure 4**).

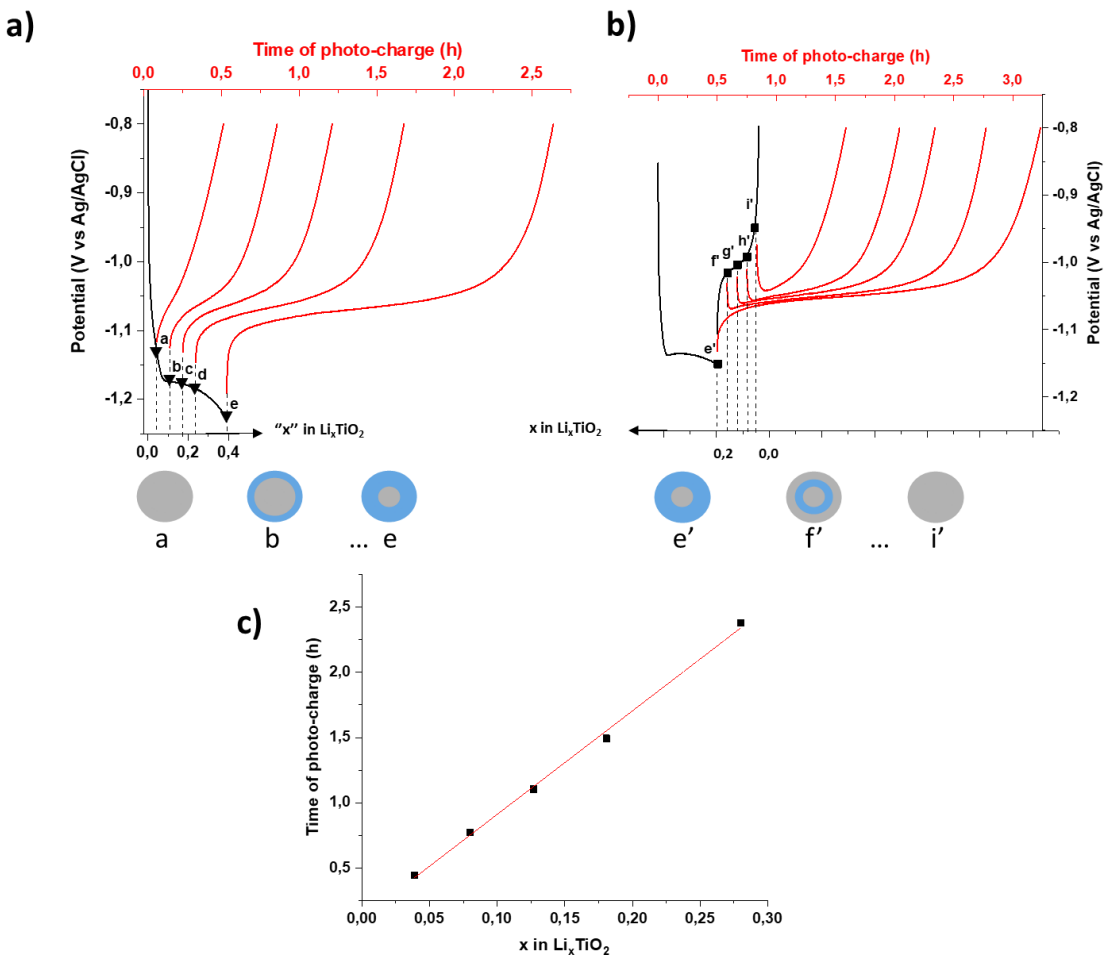

Figure 4 : (a) décharge arrêtée à différentes compositions en lithium suivi d'une photo-charge (OCV sous illumination), (b) vitesse de photo-extraction des ions lithium en fonction du taux de lithium dans l'électrode de TiO_2, c)temps de photo-extraction versus composition en lithium.

D'après la **figure 4c** une fonction affine permet de déduire la vitesse de photo-extraction de lithium grâce à la pente. Cela nous indique que la vitesse de photo-extraction est constante peut importe la composition en lithium.

Il est connu pour des nanoparticules de TiO_2 supérieures à 7 nm, que la lithiation s'effectue en présence de deux phases ; une phase pauvre et une phase riche en lithium. L'arrangement entre ses deux phases peut avoir une incidence sur les vitesses de photo-charge. Suite à une expérience similaire mais avec un arrangement différent entre ces phases, cette expérience révèle une même tendance mais des vitesses plus faibles à celles vu précédemment. Ceci pourrait s'expliquer par l'étude du mécanisme de photo-charge. Puisque nous travaillons à l'OCV, le photo-électron ne peut pas passer par le circuit extérieur, le mécanisme est donc limité à l'échelle de la particule et est comparable à un mécanisme de photo-catalyse. Compte tenu du fait que les conductivités ioniques et

électriques diffèrent entre les phases pauvre et riche en lithium, il est fort probable que l'arrangement spatial entre ses phases ait un impact non négligeable sur les vitesses de photo-extractions des ions lithiums.

II) Charge photo-assistée

Pour poursuivre notre étude sur l'influence de la composition sur les phénomènes de photo-recharge, l'étude de la charge photo-assistée a été étudiée dans une nouvelle partie. La charge photo-assistée regroupe les expériences en galvanostatique, en potentiostatique et en voltametrie cyclique (CV) sous illumination. Dans le cas des expériences en gavanostatiques et des CV on observe sous illumination une augmentation des capacités en réduction et en oxydation.

De plus on peut observer une diminution de la polarisation entre la décharge et la charge et une diminution des surtensions en galvanostatique et en CV respectivement. Cela va dans le sens d'une amélioration sous illumination des phénomènes déjà existant. Néanmoins comme nous l'avons vu précédemment, il est difficile de dissocier les phénomènes. Pour ce faire des expériences sous illumination périodique sont réalisées. Tout d'abord la CV nous montre que seules certaines compositions du TiO_2 sont photo-actives. Il semblerait également qu'une activité électrochimique est nécessaire à la photo-activité (autour de 0 A la photo-activité est nulle). Quant aux expériences en potentiostatique les résultats sont similaires à ceux présentés par O. Nguyen. Les hypothèses ainsi que le mécanisme proposé peuvent être transposé à ce système. La lumière permettrait donc de photo-extraire les ions lithium que ce soit pendant la charge comme pendant la décharge. Le courant circulant entre les deux électrodes, le photo-électron est donc capable de passer par le circuit extérieur. Le mécanisme n'est donc plus à l'échelle de la particule comme en photo-charge mais à l'échelle de la cellule. En effet le photo-électron guidé par le courant imposé pendant la charge photo-assistée pourrait être utilisé à la contre électrode pour former du dihydrogène. Des expériences complémentaires doivent être réalisées pour confirmer cette hypothèse.

Du point de vue de la cyclabilité la charge photo-assistée est en mesure de réaliser plus de cycle avec peu de modification que ce soit en termes de capacité ou en termes de dégradation à la surface.

Le temps d'exposition à la lumière peut également jouer un rôle quant à la possible dégradation de l'électrode. En effet les photo-charges sont plus longue que les charges photo-assistées ce qui favoriserait les réactions de dégradation photo-assisté. De plus si l'hypothèse d'une « délocalisation » de la production d'H_2 à la contre électrode est vérifié celle pourrait permettre de plus facilement le recueillir pour le valorisé ultérieurement.

Chapitre V : Challenges et perspectives

I) b-Si

Plusieurs challenges restent encore à être relevés sur ce sujet notamment les capacités assez limitées obtenu qui s'explique du fait des tailles des nanoparticules mais surtout du fait de la faible stabilité du substrat conducteur transparent de FTO. Plusieurs substrats ont été essayé notamment un substrat de « black » silicium (b-Si) à nano-aiguilles formé par plasma. Ce substrat a été choisi pour plusieurs raisons : une meilleure conductivité, une possible absorption de la lumière, une possible insertion de lithium et une très faible réflectivité (R<5 %). Le système étudié est le suivant : b-Si/TiO_2//LP30 1 M// Li°/Li°. Le choix de repasser en solvant organique a été fait pour éviter à bas potentiel la formation exclusive d'hydrogène. Les résultats préliminaires semblent indiquer qu'à plus bas potentiel le lithium semble s'insérer dans le substrat de b-Si. Ceci semble avoir pour conséquence une faible stabilité au cours du cyclage qui pourrait s'expliquer du fait que le silicium est un matériau de conversion et donc change de volume au cours de la lithiation (jusqu'à 300 %) ce qui aurait une influence sur l'interface avec le TiO_2. Néanmoins sous illumination les capacités en CV sont augmentées. Une possibilité pour éviter l'insertion de lithium dans le substrat de silicium est de déposer une première couche de TiO_2 dense qui empêcherait les ions lithiums d'atteindre le substrat.

II) LIPON

Nous avons vu dans cette thèse un moyen de valoriser le photo-électron généré. Une alternative est envisageable et s'inspire des tendances actuelles dans le secteur des batteries. En effet il est possible d'utiliser un électrolyte solide qui serait stable et donc non réactif vis-à-vis de ce photo-électron qui lui est très réactif. Celui-ci serait alors capable de réduire les ions lithiums à l'anode de lithium métallique. Le système utilisé est le suivant :

verre/FTO/TiO_2// LiPON// Li°. Le LiPON étant des phosphates de lithium dont l'oxygène est partiellement substitué à l'azote. Les résultats sont prometteurs du fait de l'augmentation sous illumination des capacités en oxydation et en réduction. Néanmoins des efforts doivent être fournis sur l'interface entre les différents éléments.

Conclusion générale :

Nous avons vu dans ce manuscrit une méthode innovante de conversion et stockage de l'énergie solaire à travers une électrode bi-fonctionnelle de TiO_2. L'objectif de cette thèse était d'étudier le photo-mécanisme. En effet une question en suspens sur le devenir du photo-électron demeurait dans la littérature. Nous avons alors décidé d'utiliser l'eau comme accepteur de cet électron ce qui a permis de produire du dihydrogène valorisable par la suite. L'ajout d'eau a été fait par le biais d'un électrolyte de type Water In Salt (WIS) ; un sel très concentré dans de l'eau. A propriétés similaire nous avons pu valoriser ce photo-électron comparé à un solvant organique classique.

Le comportement de la production de dihydrogène électrochimique a été étudié au préalable (chapitre III). En effet des propriétés intéressantes en électrocatalyse du TiO_2 lithié ont été remarquées. Suivant la composition en lithium la production de dihydrogène peut être modulée.

Nous avons également étudié cette même évolution de composition sur (1) la photo-recharge du matériau et (2) la production électrochimique d'hydrogène (chapitre IV). Nous avons montré une augmentation de la vitesse de charge sous illumination ainsi qu'une augmentation de la production d'hydrogène dans l'obscurité. L'utilisation de l'énergie solaire permet une charge rapide mais aussi une économie d'énergie puisque pour une même vitesse le temps de charge est réduit sous éclairage. En perspective, nous avons utilisé un électrolyte solide (LiPON) plus stable que le liquide afin d'éviter que le photo-électron ne réagisse avec l'électrolyte permettant de réduire l'ion lithium au niveau de la contre-électrode lithium. Une optimisation du dépôt du LiPON et du lithium métal reste à faire.

Nous avons vu la conclusion de ce travail avec le point de vue de la batterie mais une approche différente pourrait être faite. Nous montrons un moyen d'augmenter la production d'hydrogène en insérant un cation dans un semi-conducteur dans l'obscurité. Ce type de matériau dynamique pourrait être utilisé en photo-catalyseur pour HER ou OER.

Cette thèse ouvre des perspectives dans différents domaines comme le photo-catalyseur pour la production d'hydrogène et le concept pourrait être étendu à d'autres semi-conducteurs rapportés dans la littérature a conditions qu'ils soient capables d'insérer des ions dans leur structure. Ce travail ouvre également la voie au domaine de la batterie avec des moyens innovants de charger une batterie avec de l'énergie renouvelable. Pour la partie batterie on peut coupler cette photo-électrode avec une autre afin d'avoir un appareil complet rechargeable par l'énergie solaire en utilisant encore moins d'énergie électrique.

General Introduction

Solar energy as the largest renewable energy source is regarded as a most promising candidate for addressing the challenges of fossil fuel shortage and environment pollution issues facing current society. The prerequisite of enabling continuous utilization of solar energy is the effective storage and dispatching on demand to the end users in view of the intermittency and low-energy density of solar light. Storage of solar energy in electrochemical devices such as rechargeable lithium batteries provides an attractive approach of reaching this purpose. Currently, the dominant route of storing solar energy in the form of electrical energy involves the conversion of solar energy to electricity in photovoltaic cells and subsequent storage of electricity in electrochemical energy-storage devices such as supercapacitors and lithium batteries. To simplify the storage process of solar energy in the form of electricity, some early attempts have focused on the direct integration of photovoltaic cell and capacitor/battery into one device with the dual function of conversion and storage of solar energy to electricity. However, up to now, electrical energy-storage devices hybridized with photovoltaic cells exhibit low storage capacity, which is inadequate for large-scale solar-energy storage and long-term operation. Moreover, the use of embedded photovoltaic cells greatly increases the cost and also causes additional reliability issues. Consequently, the direct and massive storage of solar energy in electric energy-storage devices without using photovoltaic cells is highly desirable yet remains a challenge.

In this thesis, in contrast to the past designing of using photovoltaic cells to realize solar-energy conversion in the device containing energy-storage component, we are interested in the development of a photo-rechargeable battery based on the use of photo-electrode TiO_2 with a WIS electrolyte to realize the conversion and storage of solar energy in the Li-ion battery. More specifically, the mechanisms underlying the photo-recharge, or the photo-assisted recharge have been studied in details.

CHAPTER I: State of the Art - Coupling Solar Harvesting with Electrochemical Storage

TABLE of CONTENTS

CHAPTER I: State of the Art - Coupling Solar Harvesting with Electrochemical Storage

Introduction

The solar energy is the most abundant energy accessible on Earth around 23 000 TW extractable per year[1,2] and could completely satisfy the global energy consumption estimated at 19 TW per year (**figure 1**). To collect this renewable energy there are two main ways, the thermal and the electrical way. The thermal way uses a material that absorbs the solar radiation, which causes its temperature to increase. This heat will be transferred to a calorific fluid that can be used for several applications.[3]

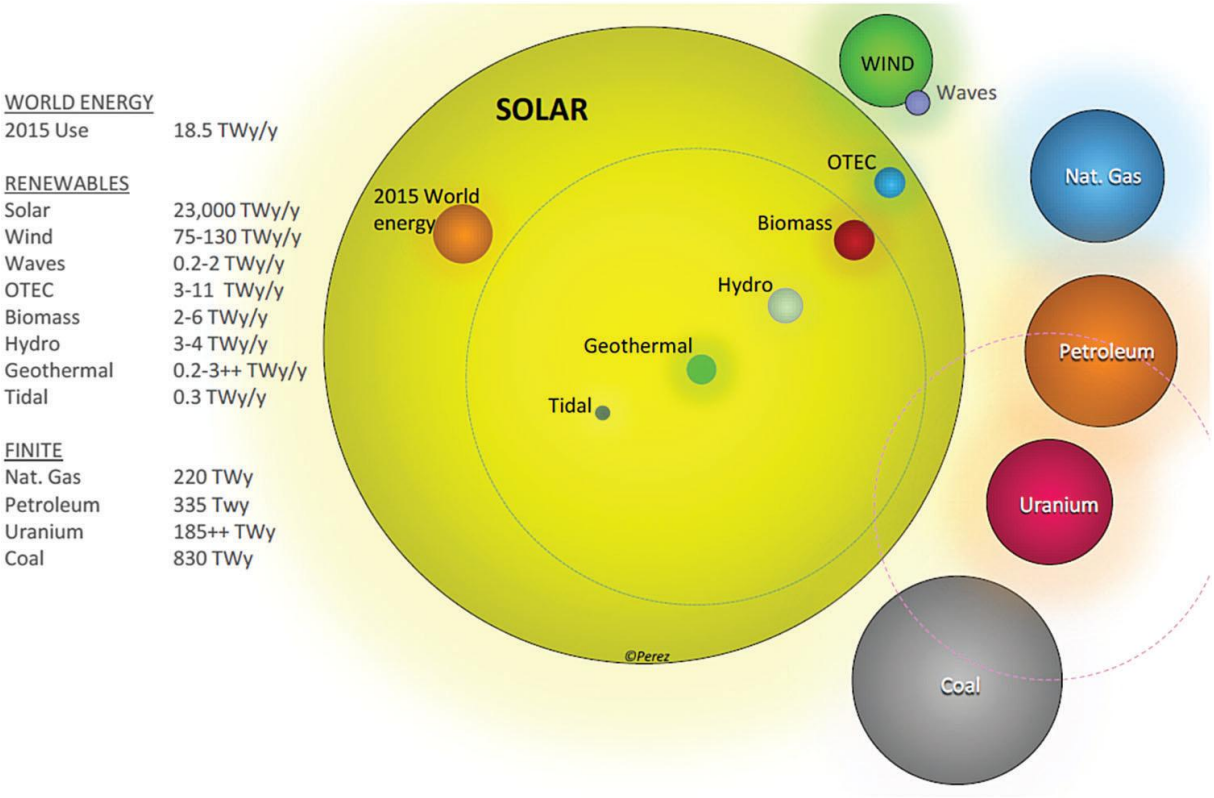

***Figure 1**: Estimated finite and renewable planetary energy reserves (Terawatt-years). Note that total recoverable reserves are shown for the finite resources whereas yearly potential is shown for the renewables. Reproduced with permission from ref. 1 and 2. Copyright 2015 International Solar Energy Society.*

The other way is the use of solar energy to produce electricity thanks to a photovoltaic cell (PV). The most common technologies used in photovoltaic cells are silicon-based (~25 % efficiency), multi-junction (~47 % efficiency), perovskite (PSCs, ~25 % efficiency), dye-sensitized (DSSCs, 12.6 % efficiency) and organic (OPV, 17.5 % efficiency) solar cells.[4] Their evolution over the years are presented in **figure 2.**[4,5]

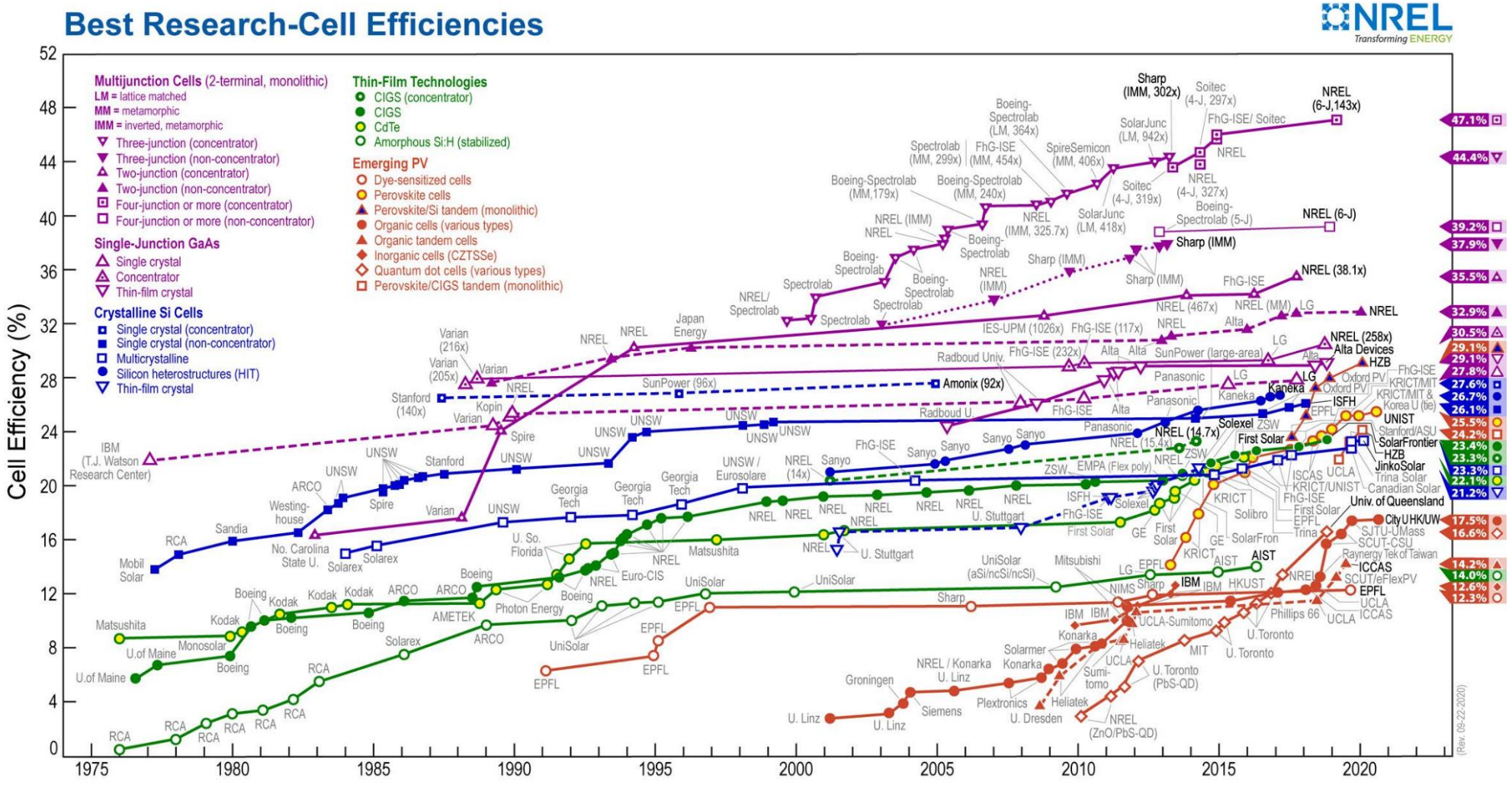

***Figure 2**: Best research-cell Efficiencies over the years.*[4]

Nevertheless, the solar energy is intermittent: the electricity production stops as the sun sets and reduces during cloudy days. When converted into electric energy, this energy is for straight usage only. There is a mismatch between the electricity production and its consumption (**figure 3**). The blue curve indicates the electricity demand and the yellow curve the solar power over a day. We can clearly see that the time of the electricity demand is different from the time for the production. To balance this mismatch, it is important to look for energy conversion-storage combined systems.

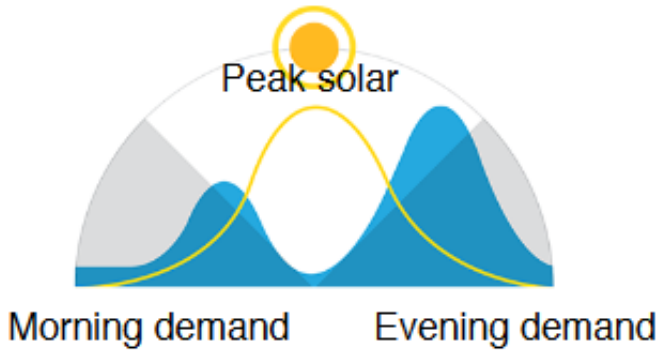

***Figure 3**: Electricity demand (blue curve) compared with solar power (yellow curve) over a day.*[6]

Electrochemical energy storage systems (EESSs) are considered amongst the best choices to store the energy produced from renewable resources.[7]

Among them, Li-ion battery is a mature technology with 40 years of development and worldwide commercialization. The Li-ion battery is considered as one of the biggest advance of the century like the steam machine or the combustion engine at their time. It allows us to consume energy without being plugged into the grid, and so giving access to mobility. In 2019, John B. Goodenough, Stanley Whittingham and Akira Yoshino received the Nobel Prize in chemistry for the development of Li-ion batteries. In 2018, 2 million of electric vehicles based on this technology were sold. The estimate for 2025 is 10 million and 28 million in 2030.[8] In 2017, the European Commission launched the European Battery Alliance to migrate from fossil to electric energy. Even though the market is led by Asian countries, the final objective is to relocate the production of batteries. More recently, the 23rd of February 2021, the European commission allocated 2.9 billion of euros to several countries including France to develop Research and Innovation centers in the field of batteries. In 2020, the number of vehicle was estimated at 1.4 billion.[9]

If we want to reduce the pollution by replacing all thermal vehicles by electric ones, the grid will be saturated and some people might end up having limited access to electricity. To overcome this issue, one idea is to get the electric vehicles off the grid for the recharge. Few solutions are already present on the market like the Aptera[10] car, which was designed to be 100 % rechargeable by sunlight. The technology used is a photovoltaic panel linked to Li-ion batteries. This is one option but there are several ways to convert sunlight and store it in an electrochemical way. In the following chapter, we will present different associations under investigation of solar conversion and electrochemical storage. In several works, a supercapacitor is used in place of a battery for short-term storage, however these examples will not be exposed in this thesis.[11,12] We will review **how a battery can store sunlight and how to evaluate the performances of the device (I.0)** that both harvests light and store energy. We will examine three configurations from the most straightforward and **mature tandem device (I.1)** to **more compact all-in-one devices (I.2)**. Within these more compact devices, we will discuss the set-up with three electrodes (I.2.1) where one electrode is dedicated to sunlight conversion while two battery electrodes are devoted to storing the electricity into chemical bounds. We will finally present some two-electrode set-up (I.2.2) where one electrode is able to both convert and store energy. We will present the state-of-the-art mechanisms for the three configurations, and we will compare them by presenting their pros and cons in terms of durability and performances.

I.0. Basics of solar conversion and electrochemical storage

In order to better apprehend how it is possible to charge a battery using solar energy, it is important to have in mind the parameters that govern the performances of both solar conversion and electrochemical storage. In this section, we will successively present the basics of converting sunlight and of electrochemical energy storage. We will then be able to present the three different configurations that enable to store solar energy.

I.0.1. Solar Conversion

For a material to convert sun light into electricity, it needs to present an electronic structure able to absorb light. The light absorbing element could be **(1)** an inorganic semiconductor **(2)** an organic molecule adsorbed at the surface of an electrode, called a photo-sensitizer or **(3)** plasmonic nanoparticles.

(1) In the case of a semiconductor, the absorption wavelength is determined by the bandgap between the valence band and the conductive band (from 0.5 to 4 eV). The semiconductor can absorb a photon with the same energy or more than the bandgap, $E_{light} = hc/\lambda \geq E_g$. The absorption of the photon will extract an electron (e^-) from the valence band to the conductive band, resulting in a hole (h^+) in the valence band. The pair electron-hole is called an exciton. The charge carriers are attracted to each other by the electrostatic Coulomb force, and they tend to recombine. In order to collect electricity, charges carriers must be separated to be collected at the current collector of opposite electrodes.

(2) For the photo-sensitizer, the absorption wavelength is determined by the gap between the lowest unoccupied molecular orbital (LUMO) and the highest occupied molecular orbital (HOMO). As in semiconductor the photo-charges (the electron and the hole) must be separated in order to collect the solar energy.[13]

(3) For the plasmonic nanoparticles, the collect of the solar energy is realized by using the localized surface plasmon resonance (LSPR) effect. This phenomenon occurs when a conducting material is illuminated at a specific wavelength which will result in a collective oscillation of the free charge in the material. The absorption wavelength could be tuned by the size of the nanoparticles.[14,15]

The major challenges of photo-active material are the photo-absorption and the efficient use of the charge carrier. The photo-absorption represents the amount of solar energy that the material can collect or absorb at various wavelength to create excitons. An example of TiO_2 nanoparticle absorption spectrum is illustrated **figure 4a**. An ideal absorbing material should be able to absorb most of the solar spectrum over a wide range of wavelength (**figure 4b**).

Quantum efficiency is used to compare the efficiency of an absorbing material. Two QE can be defined.

*External Quantum Efficiency (EQE) is the ratio of the number of charge carriers collected by the solar cell to the number of photons of a given energy shining on the solar cell from outside (incident photons). Some authors prefer talking about incident photon-to-current efficiency (IPCE).

*Internal Quantum Efficiency (IQE) is the ratio of the number of charge carriers collected by the solar cell to the number of photons of a given energy shining on the solar cell from outside and that are absorbed by the cell.

$$EQE = \frac{electrons/sec}{photons/sec} = \frac{(current)/(charge\ of\ one\ electron)}{(total\ power\ of\ photons)/(energy\ of\ one\ photon)}$$

$$IQE = \frac{electrons/sec}{absorbed\ photons/sec} = \frac{EQE}{1 - reflection}$$

The IQE is always larger than the EQE. A low IQE indicates that the active layer of the solar cell is unable to make good use of the photons. To measure the IQE, one first measures the EQE of the solar device, then measures its transmission and reflection, and combines these data to infer the IQE.[16]

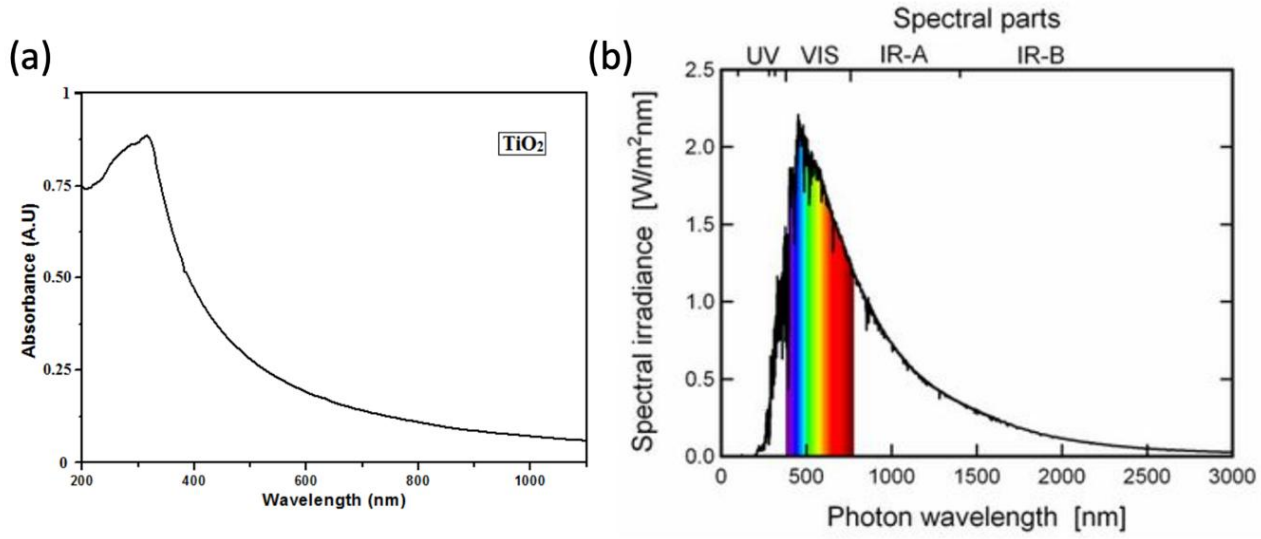

Figure 4: *(a) UV-Visible absorption spectrum of TiO_2 nanoparticles,[17] (b) Spectral irradiance at Air Mass 0 (AM0) vs photon wavelength.[18] Air Mass is explain in the* ***annex I.***

I.0.2. Electrochemical storage

The performances of battery depend on the electrode materials (at the negative and positive electrodes), the electrolyte and their association in a full device. The performance of the material can be evaluated regarding different aspects: the ability of the material to store reversibly the ions in its structure, the kinetics of the insertion/extraction reaction, and the cyclability.

The **capacity** of an electrode material (Q, in mass mAh/g or in volume Ah/L) is the amount of charge (one electron for one lithium ion) reversibly stored at a specific rate. To evaluate the experimental capacity of an electrode, a galvanostatic experiment is performed. The value of the current will dictate the rate of the discharge of the battery. It is expressed using C/n, where n stands for the theoretical capacity discharged in n hours. Rechargeable battery cycling rates can vary from an extremely high rate of 50C (theoretical capacity discharged in 72 sec) to a very slow rate of C/8 (theoretical capacity discharged in 8 hours). The kinetics of the insertion/extraction reactions must match between the two electrodes. Reaching high capacity at a specific C-rate is essential for a battery to target the most suitable technology in terms of autonomy and time of charge. Classical materials used in the battery technology are illustrated in **figure 5 a, b**.

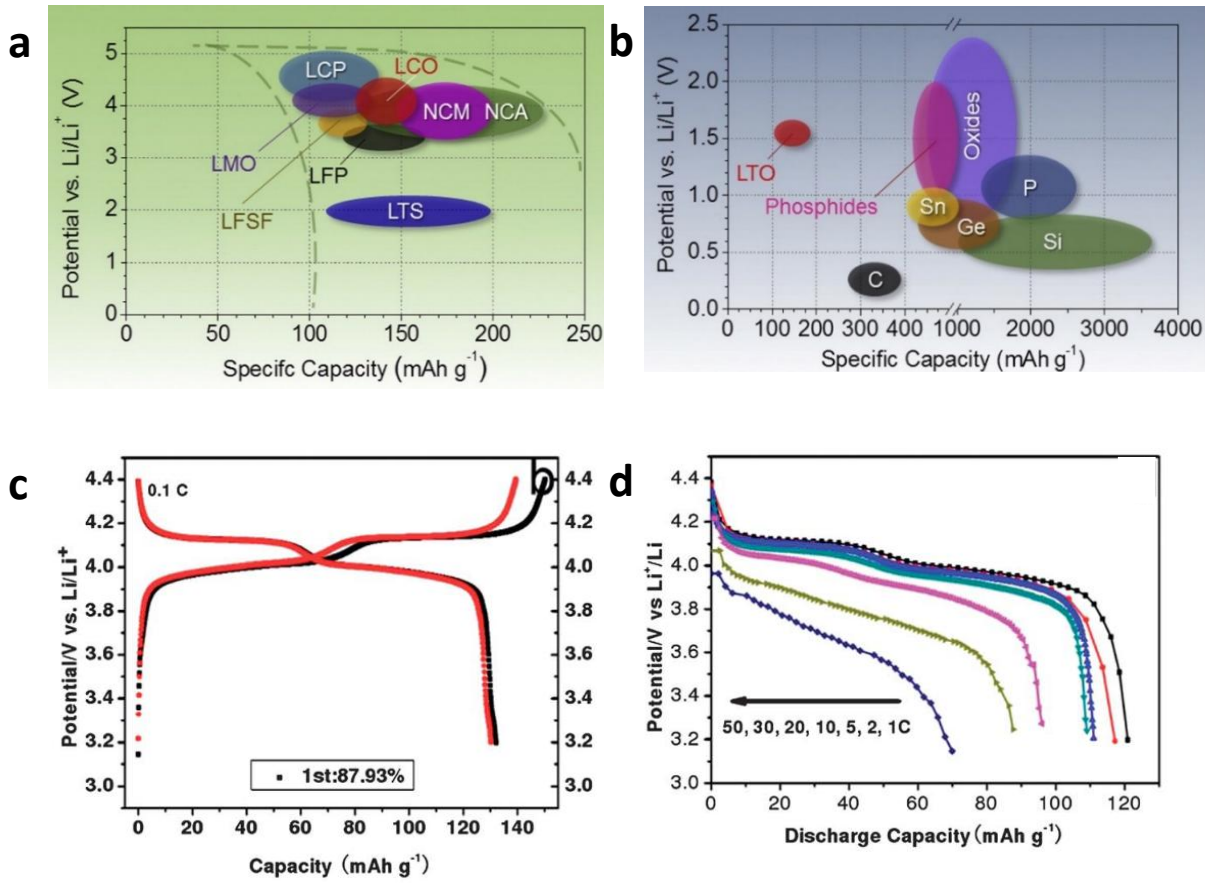

***Figure 5**: a) Approximate range of average discharge potentials and specific capacity of some of the most common (a) intercalation-type cathodes (experimental), (b) conversion type anodes (experimental) adapted from Materials Today, 18 (2015)[19]. c) discharge curves at different C-rate of an LMO (lithium manganese oxide) electrode, d) discharge–charge curves at 0.1 C.*
Adapted from J. Mater. Chem. A 1 (2013) 8170-8177.[20]

Please note that, in this thesis, the negative electrode in a rechargeable battery will sometimes be abusively called "anode". Indeed, by definition, an anode is the electrode where an oxidation reaction takes place. During a discharge, an oxidation reaction occurs at the negative electrode (= the electrode involving the redox couple with the lowest redox potential couple, E^-), it is effectively an anode. When the battery is being recharged, the opposite reaction, i.e. a reduction reaction, occurs at this negative electrode, therefore it cannot be called an anode anymore.

The material chosen for the positive and negative electrode will also dictate the **potential difference, or the voltage** of the battery ($\Delta E = E^+ - E^-$). The specific energy delivered by a battery (in Wh/kg) is the product between the potential difference and the capacity accessible for both anode and cathode material.

Another key parameter to characterize a battery is its **cyclability**. It represents the number of charge/discharge cycles that can hold a significant experimental capacity before the

degradation of the system. The **retention capacity** represents the evolution of the capacity over the number of cycle, it can be estimated as: $Q_{discharge}$ [cycle n]/ $Q_{discharge}$ [cycle 1] in %.

The **coulombic efficiency** is estimated by the ratio between the capacity of discharge and the capacity of charge, expressed in percentage ($Q_{discharge}/Q_{charge}$ in %). If the value of coulombic efficiency is different from 100 %, it indicates the presence of side reactions, including the degradation of the electrolyte with the formation of a Solid Electrolyte Interphase (SEI) and/or other irreversible reactions like the dissolution of the electrode material (**figure 5c**).

The stability of cycling upon extreme temperature[21–23] or at very high voltage needs to be also taken into account as detrimental side reactions can be favored under harsh conditions.[24–27]

I.0.3 Solar conversion & Electrochemical storage

The overall energy conversion efficiency (η, overall) of a solar rechargeable battery will mainly depend on the photo conversion efficiency (incident photon-to-current efficiency, IPCE). The coulombic efficiency of the battery is usually close to 100 %, it is therefore not the limiting factor. It is possible to evaluate how much energy is saved by the system during the photo-recharge by comparing its characteristics (applied bias, time of charge) to a regular electrochemical charge. A precise overall efficiency is calculated as the ratio of discharge energy and illumination energy for particular active areas.

Now that the basic key parameters to evaluate a photo-material and a battery material have been very briefly reviewed, we will present three possible configurations to associate a photovoltaic device and a storage device: (I.1) the tandem device, (I-2) the three-electrode set-up, and (I-3) the two-electrode set-up.

I.1. Tandem device: a photovoltaic cell coupled with a storage device

The easiest way to couple two mature technologies, namely the Si-based solar cell and the Li-ion battery is to plug them together. However, one challenge of the tandem is to cope for the voltage mismatch between a Li-ion battery and a solar panel. A solar cell open circuit voltage is usually around 0.6 to 1.0 V, while commercial Li-ion battery presents a voltage around 3.5 V. One solution to overcome this issue is to add in series several solar cells in order to multiply voltage, or booster of voltage also could be used.

Gibson and Kelly[28] studied how to charge a stack of lithium-ion batteries using a solar panel, which is itself composed of several cells (**figure 6a**). In this study, the Li-ion battery is composed of a lithium iron phosphate (LFP) positive electrode against a negative electrode of carbon (LFP//C): its voltage is about 3.4 V according to **figure 6a**.

The I-V curve of the solar panel is presented in **figure 6b**, together with the power curve. The maximum power point (MPP) corresponds to a voltage of 50 V (red curve).

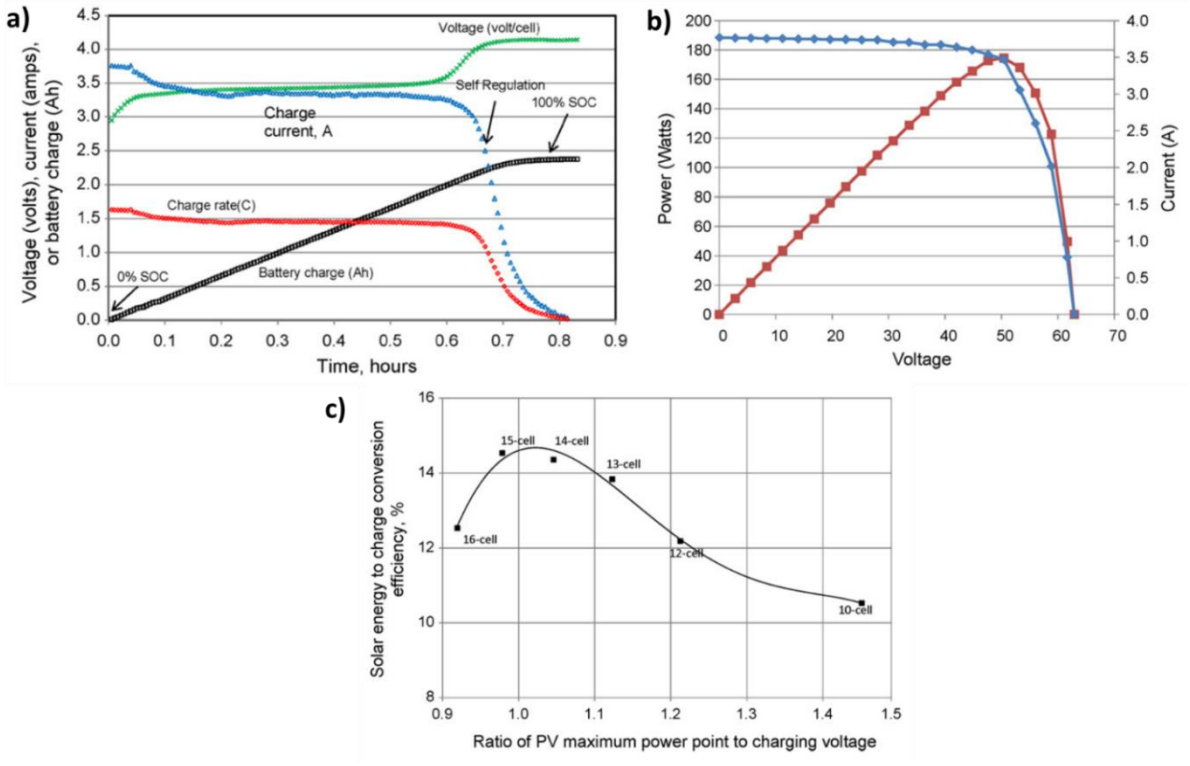

***Figure 6**: a) Solar charging of a 15-cell lithium-ion battery module—voltage per cell, current, charge rate, and battery charge capacity as a function of time, b) Current (diamonds) and power (squares) as a function of voltage for a Sanyo HIP-190BA3 module at 52 ◦C. c) Solar energy to battery charge conversion efficiency*

comparison for 10-, 12-, 13-, 14-, 15-, and 16-cell modules. The optimum efficiency was approximately 14.5 % when the battery charge voltage was equal to the PV MPP ($V_{mpp}/V_{battery\ charging}$ near unity).[28]

Given that the ratio between the solar panel voltage at MPP (about 50 V) and the charge voltage of the battery (about 3.4 V) is about 15, a solar panel could charge around 15 Li-ion cells. **Figure 6c** shows, for several number of battery cells, the solar energy to battery charge efficiency. It confirms that the 15-cell battery module powered by the solar panel exhibits the highest efficiency (14.5 %).

Gurung et al[19] used a dc-to-dc voltage boost converter. This converter allows tracking the overvoltage of the Li-ion cell and then preventing it.

In this part, we presented the tandem as the most obvious way to couple the two very advanced technologies, namely PV and batteries, in order to collect and store the solar energy. A challenge of this set-up is to match the voltage of the two devices. Also a tandem device includes the packaging of the two parts separately. To make the device more compact, many researchers are investigating all-in-one photo-electrochemical cell architectures. Three-electrode cells are under investigations, i.e. two battery electrodes plus one photo-electrode. Two-electrode configurations are also envisioned where one of the battery electrodes is also a photo-electrode. These all-in-one compact devices uses fewer components (less wires, les packaging), resulting in lighter, cheaper and less-subjected to ohmic losses. This new design targets more specifically off the grid market like nomadic application, for example for medical implants[29], lights on highways, smartphones or even electric vehicles.[30]

I.2. More compact set-ups

Leading towards more compact electrodes, we will give a few examples of reported set-ups with three and two-electrodes. Prior to discussing the examples, we would like to distinguish two main types of photo-charging mechanisms encountered in the literature, which we will call ‘photo-charge’ and ‘photo-assisted charge’.

i) ***the photo-charge*** is a charge of the battery solely by the solar energy. Please note that most of the examples reporting photo-charge in the literature refer to experiments performed at Open Circuit Voltage (OCV). This is what we illustrated **Schema 1 a and c**. Let’s however keep in mind that the term “photo-charge” is strictly speaking abusive in this case:

the photo-electron cannot go through the circuit to recharge the counter electrode. We should better talk about electrode **photo-*regeneration***; only one electrode of the battery is being regenerated, not the second one.

ii) *the* ***photo-assisted charge*** is a photo-charge of the battery supported by an additional current **(Schema 1 b and c).**

The two mechanisms will be exposed for the three- and two-electrode set-ups. In this scheme, we chose to illustrate the case of a Li-ion technology. However, the same mechanisms can be extended to other storage technologies (Li-S, redox-flow), as we will see in the examples in **section I.2.1** and **I.2.2**.

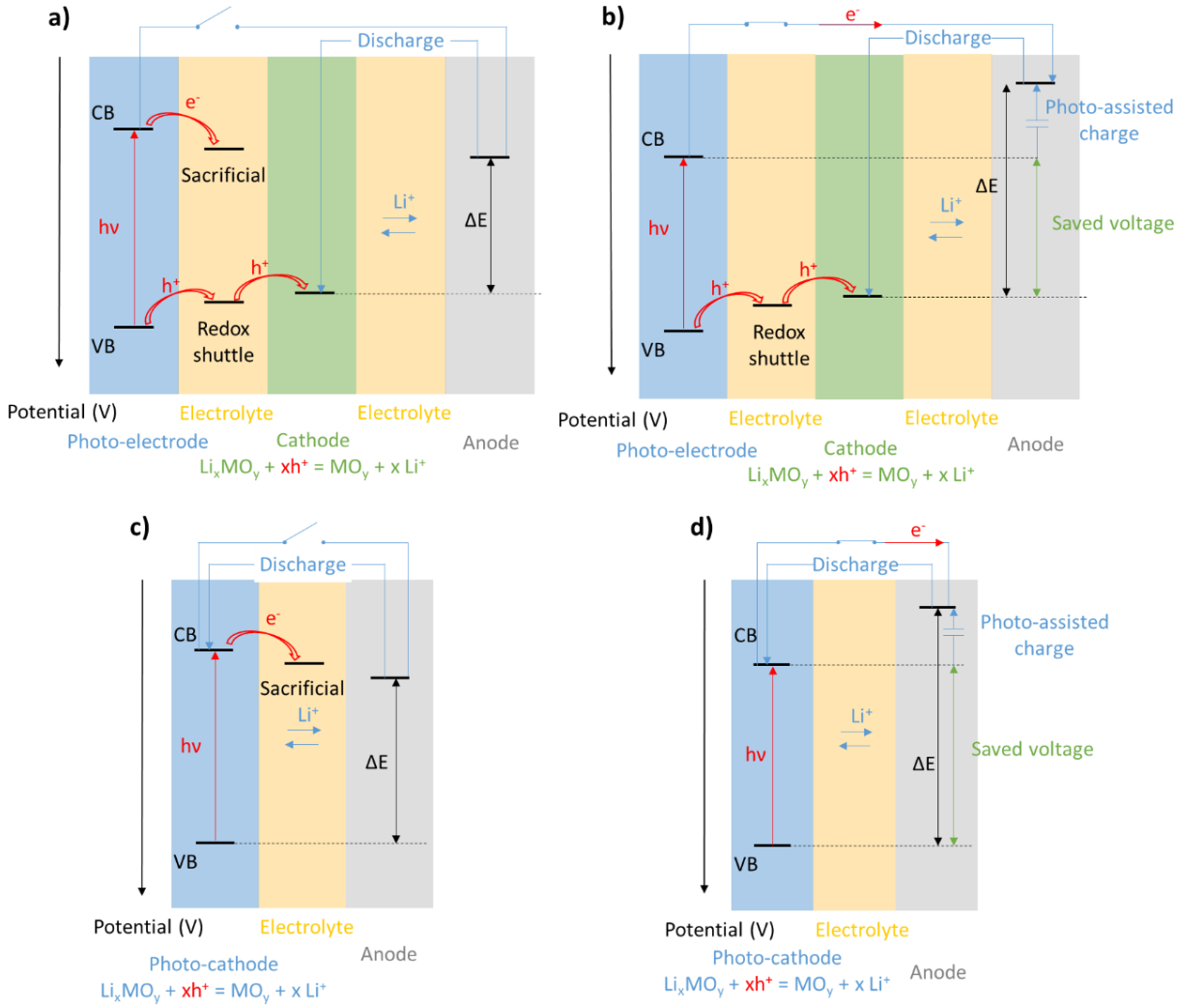

Schema 1*: (a) Illustration of a photo-charge (OCV under illumination) of a 3 electrode-set-up, (b) Illustration of a photo-assisted charge (galvanostatic experiment under illumination) of a 3 electrode-set-up, (c) illustration of a photo-charge (OCV under illumination) of a 2 electrode-set-up, (d) illustration of a photo-assisted charge (galvanostatic experiment under illumination) of a 2 electrode-set-up.*

The *first configuration* proposed is the photo-charge with a 3 electrode-set-up (**Schema 1a**). The absorption of the light with an energy *hv* generates an exciton at the photo-electrode which could be separated in two charges, the electron and the hole. The hole can travel through the electrolyte thanks to a redox-shuttle and can oxidize the lithiated material of the cathode resulting in the "photo-extraction" of the lithium from the cathode. In this scheme, we choose to only represent a photo-extraction of the lithium ion from the cathode by the hole but it is also possible to photo-insert lithium ion during a photo-charge with the photo-electron.[31]

The discharge of the battery can then operate and reform the lithiated material. The photo-electron is here in general not valued since the photo-charge is performed at OCV. The photo-electron can therefore not go through the external circuit to the counter electrode. Usually, it reacts with the electrolyte to form SEI or a sacrificial acceptor present in the electrolyte in order to avoid these side reactions.[32–34]

The *second configuration* is the photo-assisted charge with a three-electrode set-up (**schema 1b**). After the generation of the electron and hole, the hole can travel through the electrolyte thanks to a redox-shuttle and can oxidize the lithiated material of the negative electrode. Here, the external circuit is closed and the photo-electron reaches the anode and where lithium ions can be reduced. This set-up will save energy; the sun contributes partly with the photo-voltage (photo-generated bias), while the residual voltage needs the grid assistance (applied potential bias).

In **schema 1c**, a *photo-charge mechanism* in a two-electrode cell is presented. Since the photo-electrode is the cathode, the hole will directly oxidize the electrode material and so photo-extract the lithium ion from the material. Here, the photo-electron cannot pass through the external circuit (OCV) but still need to be used in order to avoid recombination with the hole, therefore the use of a sacrificial agent is needed.

In **schema 1d**, a *photo-assisted charge* in a two-electrode cell is shown. The hole will photo-extract the lithium ions, while the photo-electron, helped by the potential bias, passes through the external circuit to reduce the anode.

The presentation of this scheme will help the follow-up presentations of some selected

recent examples from the literature.[30,35–38]

I.2.1. Three-electrode set-up

In the three-electrode set-up, the challenge is to feed the battery electrode(s) with the charge carrier created at the photo-electrode. A first option is to physically connect 'back to back' the photo-electrode and one of the battery electrode using a current collector common to both.

In this context, Guo et al[39] suggest to put together 'back to back' a TiO_2 based-dye-sensitized solar cell (DSSC) and a 'TiO_2(-)//$LiCoO_2$(+)' Li-ion battery. A titanium foil materializes the contact between the two TiO_2 electrodes: it plays the role the current collector of both the TiO_2 nanotube photo-electrode on one side, and of the TiO_2 nanotube negative electrode of the battery on the other side, as illustrated in **figure 7**. The bottom part (the battery) will then be charged by the top part of the cell (the DSSC). The overall efficiency (energy conversion and storage efficiency) for this system is 0.82 % and the efficiency for energy storage is 41 %. The efficiency might seem low. However the efficiency of the conversion of the solar energy alone, despite the considerable advances in this field, remains low: for DSSCs' optimized system, a 13 % efficiency is achieved.[4] Since the field of photo-battery is pretty new, to the best of our knowledge, the overall efficiencies already reported are all <1 %.[35] The voltage of the power pack can be charged up to 3 V in about 8 min, the discharge capacity is 38.89 µAh under the discharge density of 100 µA. Such an integrated power pack could serve as a power source for mobile electronics.

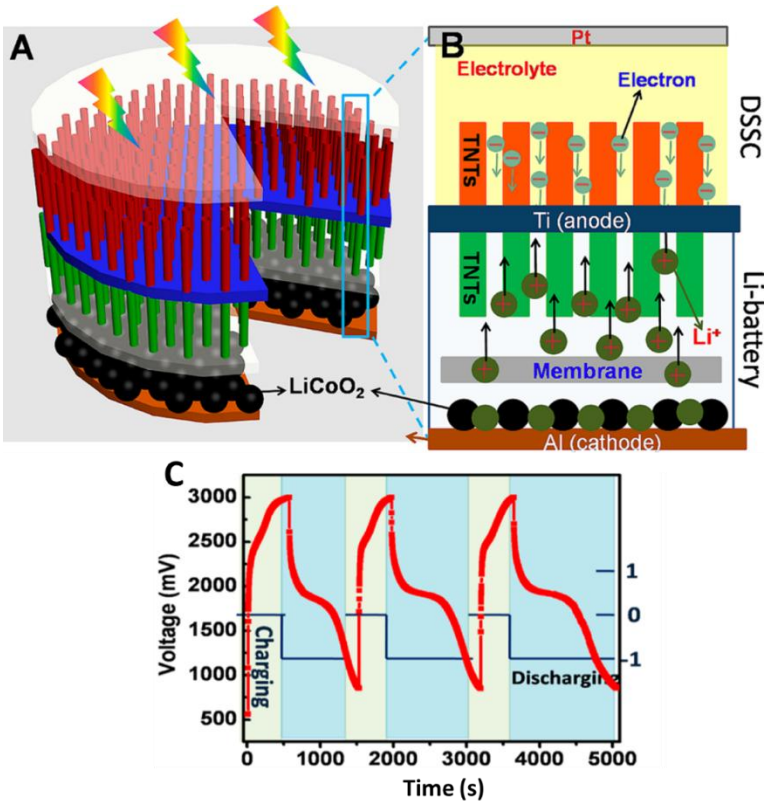

***Figure 7**: Design and principle of an integrated power pack system based on double-sided TiO_2 nanotube arrays. (A) TiO_2 nanotube arrays grown on the Ti foil substrate (B) Detailed structure and working principle of the integrated power pack system (C) Photo-charge(under open circuit voltage OCV) follow by 100 µA discharge.*[39]

A similar 'back to back' architecture was proposed, by Chen et al[40], for a lithium-sulfur (Li-S) battery technology. They combined a Li-S battery with a perovskite photo-electrode **(figure 8).** The battery has a capacity of 762 mAh/g with an overall efficiency of 5.14 % over 14 cycles.

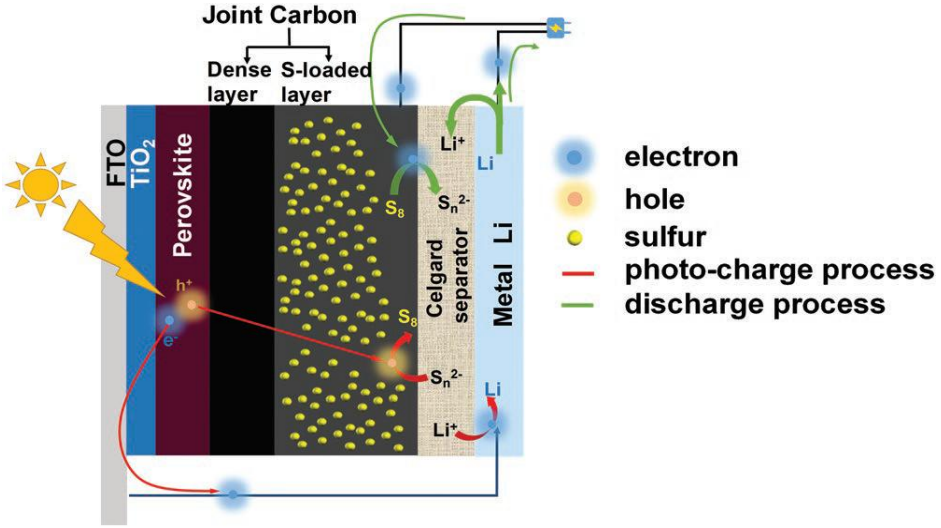

***Figure 8**: Schematic diagram of the fabricated PSC–Li–S battery FTO/ TiO_2/perovskite/C/C-S/Celgard/ Li°.*[40]

Numerous works report the three electrodes well separated in the electrolyte. In order for the charge carrier (usually the holes) to react with the electrode material, two main situations are reported.

(i) The redox active material is soluble in the electrolyte; it can travel from the battery electrode to the photo-electrode to be recharged/regenerated. That is typically the case with redox flow batteries, it has also been reported with soluble sulfur species in Li-S batteries.

(ii) The redox active material is solid, typically in a rocking chair Li-ion battery. Redox shuttles in the electrolyte are then necessary to bridge the photo-electrode and the electrode material.

To illustrate the second situation, the work of Li et al[41] present a Li°(-)//$LiFePO_4$(+) battery combined with a TiO_2 photo-electrode where they used the triiodide/iodide (I_3^-/I^-) redox shuttle **(figure 9)**. After illumination of the TiO_2 semiconductor, the hole oxidizes the I^- into I_3^-, which migrates to the positive electrode where it is reduced back into I^-, while extracting Li^+ from $LiFePO_4$ and oxidizing the positive electrode material. Here the photo-electron generated needs the application of an external applied potential bias to reach the negative electrode where it will reduce the lithium ion into lithium metal to complete the recharge. In this case, on a total voltage of 3.4 V, 0.8 V will be covered by light and the extra 2.6 V will require electricity from the grid. It is a typical example of photo-assisted charge. It allows to save 20 % of the energy during the 10 presented cycles, because of the reduction of the charged voltage at 2.78 V.

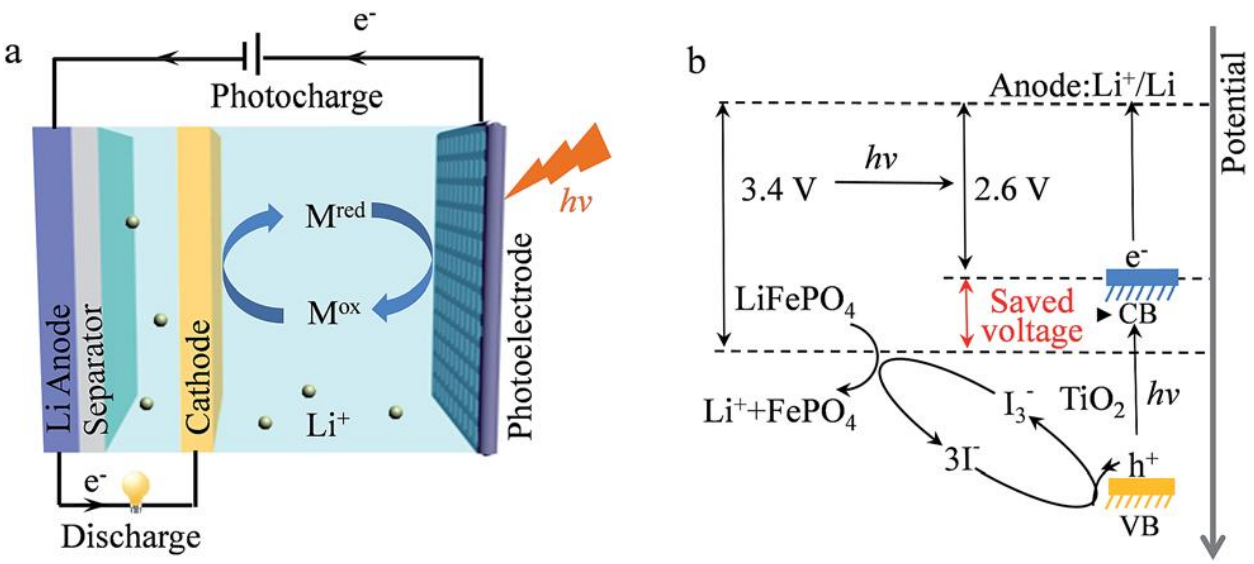

***Figure 9**: (a) Schematic illustration of a photo-assisted chargeable LIB with a three electrode system. Upon charging under illumination, the photo-electrode and anode are connected to the outside circuit. The redox shuttle M_{red} on this electrode is first oxidized to M_{ox} and then diffuses to the $LiFePO_4$ cathode. By oxidizing the $LiFePO_4$ into $FePO_4$ and Li^+, the M_{ox} gets reduced back to M_{red}. While upon discharging, the cathode and anode are connected to the outside circuit, and the intercalation of Li^+ makes $FePO_4$ reduce back to $LiFePO_4$. (b) The energy diagram of the photo-chargeable LIB. The saved voltage is determined by the energy difference between the charging voltage of the LIB and the quasi-Fermi level of electrons in the semiconductor (near to its CB).*[41]

In the work of Li et al[42], the couple I_3^-/I^- is one the redox active material. They combine a sodium-ion aqueous redox battery using iodide (I^-) as catholyte and S_4^{2-} as anolyte, plus a rutile TiO_2 nanorod-based electrode as a photo-electrode **(figure 10 a, b).** It exhibits a moderate 110 mAh/g capacity during 20 cycles, the big highlight of this system is that 90 % of the energy used to recharge the battery comes from the solar energy. The charging voltage of photo-assisted chargeable sodium polysulfide/iodine battery has been reduced to 0.08 V which is much lower than the discharging voltage (0.83 V). The low-cost and high-safety photo-assisted chargeable SPIB promises the practical application of the devices for efficient conversion and storage of solar energy into electrical power.

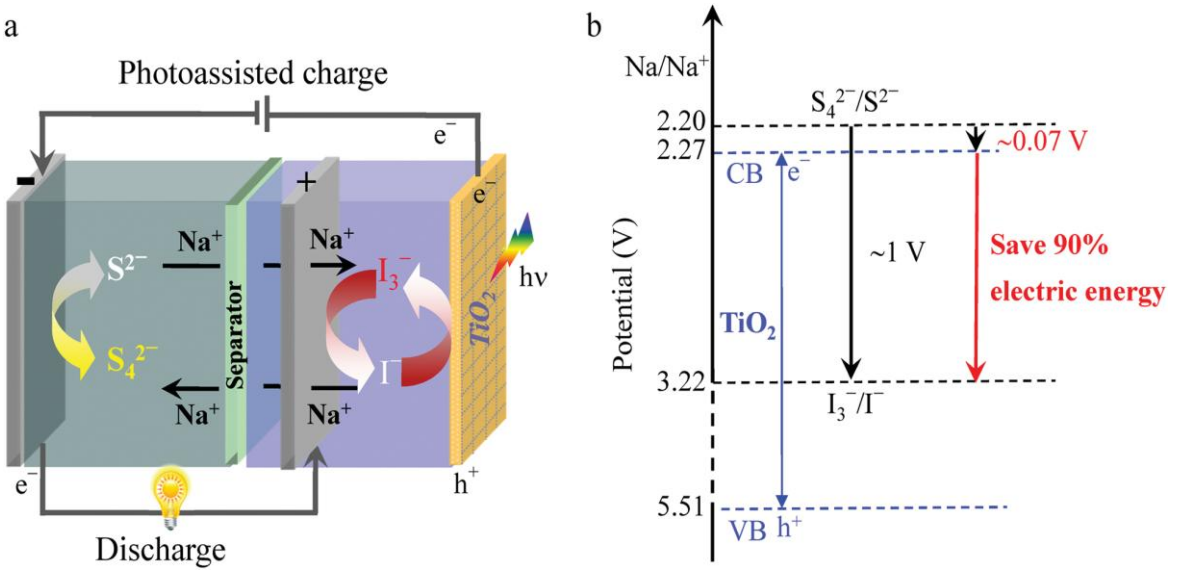

***Figure 10**: a) Schematic of a photo-assisted chargeable sodium polysulfi de/iodine battery (SPIB) with a three electrode system. b) Potential diagram for the photo-assisted charging process. The saved voltage is determined by the energy difference between the charging voltage of SPIB and the quasi-Fermi level of electrons in the TiO_2 photo-electrode (near to its CB).*[42]

Given their redox species soluble in solution, the redox-flow battery in general seems appropriate to allow photo-charge. In their work on classical pure vanadium-based redox-flow battery combined with a TiO_2 photo-electrode (**figure 11)**, Wei et al[43] argued that a key to achieve high photocurrent and elevated photo-charging depth is to avoid static electrolyte. Using forced convecting flow, they could achieve a full photo-charge (without any external bias) under AM 1.5 illumination in 1.7 h, compared to 25 h photo-charge with stagnant electrolyte.

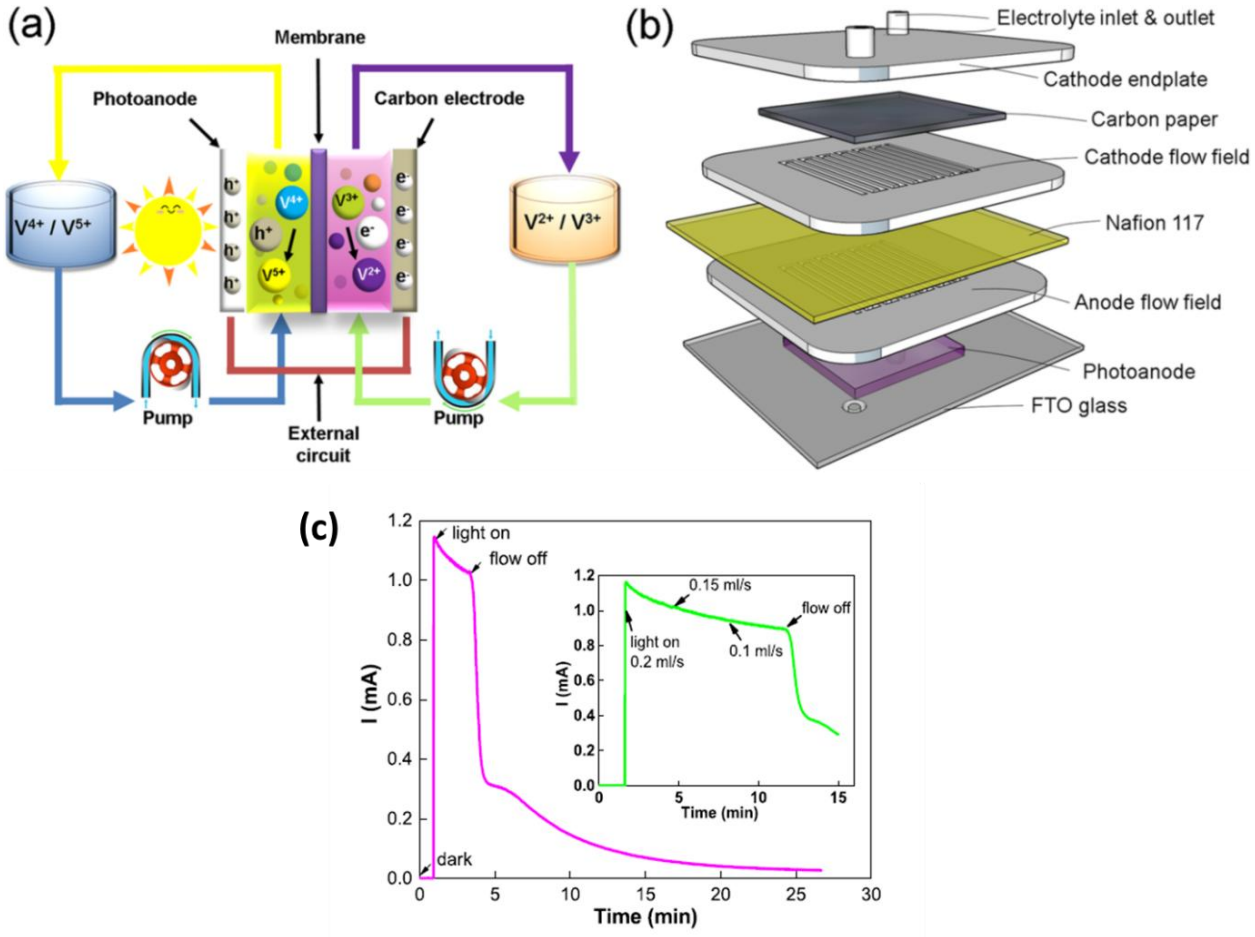

Figure 11: *(a) Schematic representation of the all-V continuous-flow setup, including the cell, pumps, and electrolyte storage tanks. (b) Exploded view of the all-V continuous-flow storage cell. V^{4+} and V^{5+} denote vanadium species of VO^{2+} and VO_2^+, respectively. During operation, two different vanadium redox electrolytes, i.e., VO^{2+} and V^{3+} (balanced with 3 M H_2SO_4 and separated by an ion-conducting membrane), are used as the anolyte (in contact with the photo-anode) and catholyte (in contact with a carbon-paper cathode), respectively. Under photo-charge, reactions at the photo-anode and cathode are $VO^{2+} + H_2O \rightarrow VO_2^+ + e^- + 2H^+$ and $V^{3+} + e^- \rightarrow V^{2+}$, respectively. (c) Photo-electrochemical response of the all-V continuous-flow PESC to flow of vanadium electrolytes. The anolyte and catholyte are 0.01 M VO^{2+} and 0.01 M V^{3+} (balanced with 3 M H_2SO_4), respectively. The photo-anode is a TiO_2 electrode. The flow rates of the anolyte and catholyte were varied simultaneously.*[43]

In their approach, Li et al[34] imagined a specific and interesting fate for the photo-electron produced during illumination at OCV: H_2, an ideal clean fuel with the largest heating value (120 $MJ.kg^{-1}$). They combined a CdS/Pt-based photo-electrode with a lithium-sulfur battery (**figure 12)**. Their cell presents two compartments**,** one containing the lithium anode in an organic electrolyte, another with the cathode and the photo-electrode in an aqueous electrolyte. In this system, the redox species to photo-regenerate are in solution and do not require any additional redox shuttle.

The discharge releases soluble S^{2-} ions that can migrate from the positive electrode to the photo-electrode where they will be oxidized to polysulfide ion by the photo-excited holes during illumination. The photo-electrons generated at the same time are here used to reduce water (from the aqueous electrolyte) into hydrogen. The cathode is photo-regenerated and hydrogen is produced. The cycling is not however sustainable regarding various aspects: the anode material is not regenerated during illumination and the cell design doesn't account for water loss.

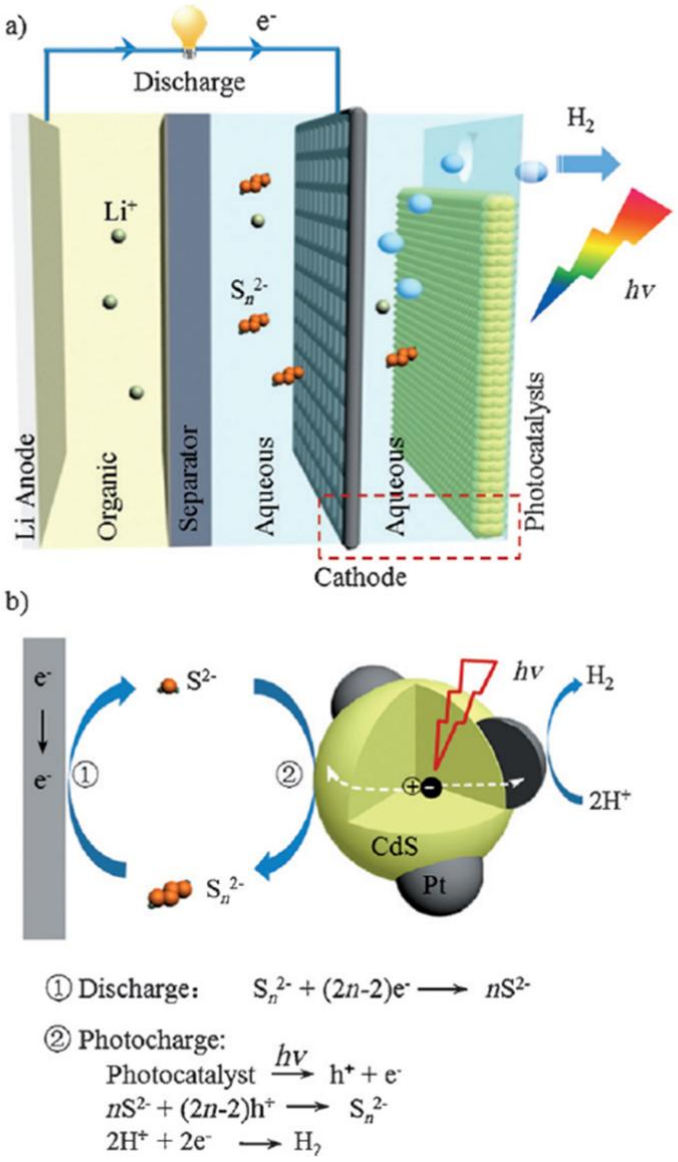

***Figure 12**: a) The battery consists of a Li anode with organic electrolyte, a Li-ion conductive LATP glass ceramic separator, and an aqueous Li_2S_n (1‹n‹4) alkalic catholyte containing the Pt/CdS photocatalysts (coated on Ti mesh). b) The discharging process is the same as that of a common aqueous Li-S battery. However, the charging process is different, the discharge product S^{2-} ions are oxidized to polysulfide ions by photo-excited holes from the CdS photocatalyst driven by light irradiation. Meanwhile the photo-excited electron, freed from the Coulomb attraction of the hole, transfers to the Pt particle, where it then reduces protons to hydrogen.*[34]

However, this technology is promising in many ways. The theoretical capacity of a Li-S battery is 1672 mAh/g. In this example, the experimental capacity is about 800 mAh/g, with 2 hours of photo-charge at OCV. The work shows only 10 cycles, which exhibit a good capacity retention of 92.5 %. The corresponding hydrogen generation rate during the photo-charging is determined to be 1.02 $mmol.g^{-1}.h^{-1}$. This example is the first example where solar energy was simultaneously beneficial for: regenerating a discharged electrode and producing a highly-value energy storage vector. It opened new perspectives for the direct and large-scale storage of solar energy.

In this part, we presented some technologies that use a three-electrode set-up. This design has the characteristic to separate the photo-phenomenon from the battery one. Different approaches were tested to use the best advantages of photo-charges towards battery charging/electrode regenerating: a specific cell design,[39] making profit of a usable by product,[34] using a soluble active storage redox couple or redox shuttle,[40–43] using both photo-charge to properly recharge the battery.[42] The main characteristics of the systems presented here are summarized in **Table 1**.

In order to reduce even more the number of elements, the weight, the cost and so improve the energy density, the researchers started to look at the two-electrode set-ups. In this technology, one electrode is able to both absorb and store the solar energy. In this configuration, no strategy needs to be developed to bridge the photo-electrode and one of the battery electrodes since they are one. The next paragraph will discuss some work reported in the literature, involving this design.

Table 1: *Summary of recent three electrode set up.*

Technology	Positive (+)	Negative (-)	Photo-electrode	Electrolyte	Mechanism	Avantages	Limitations	References
Li-ion	$LiCoO_2$	TiO_2	Dye adsorbed onto TiO_2	LP30	photo-charge	overall yield 0.82 %	3 cycles shown	39
Li-S	Li_2Sn	Li°	Pt/CdS	organic // aqueous Li_2Sn	photo-charge	2h photo-charge : 792 mAh/g, 10min photo-charge 201 mAh/g		34
Li-ion	$LiFePO_4$	Li°	TiO_2	aqueous I^-/I_3^-	photo-assisted	save 20 % energy compared to LIB	3 cycles	41
Redox-flow /Na-ion	NaI	Na_2S_4	nanorods rutile TiO_2	aqueous $S_4^{2-}/S_2^-$and I_3^-/I^-	photo-assisted	190% conversion efficiency, 90 % energy saved, 110 mAh/g, 20 cycles, Na-ion	many elements, nafion	42
Li-S	C loaded in S	Li°	perovskite on TiO_2	LiTFSI organic	photo-charge	5,14% overall efficiency, 762 mAh/g, 14 cycles	3h30 for 1 cycle, conversion material (increase of volume in a quasi solide Photo-battery)	40
Redox-flow	V^{3+} / V^{2+}	VO_2^+ and VO^{2+}	TiO_2	3 M H_2SO_4	photo-charge	95% faradic efficiency, IPCE 45 %, better compared to stagnant electrolytes	no cyclability test	43

I.2.2. Two-electrode set-up

In the two-electrode set-up, two main electrode architectures have been reported.[31,32,44–46]

In *the first architecture*, the electrode is composed of two materials: the host material for reversibly inserting/extracting lithium ions (storage material) and the photosensitive material (conversion material). The photo-charges generated at the photo-sensitizer are used to reduce/oxidize the transition metal of the electrode material while hosting/extracting the ions (Li^+ for example). In *the second architecture*, the electrode is made of one material (typically a semiconducting and host material) that is able to both collect/convert and store solar energy. They are called bi-functional materials.

In this section, we will review some of the latest examples of both types of architecture.

I.2.2.1. Photo-sensitized electrodes

In the previous part, we mentioned that different photo-sensitizers that can be used to collect the solar energy. We can find many dyes able to collect solar energy in the literature thanks to several fields of research like DSSC[47–50] or artificial photo-synthesis.[51–54]

The combination of dyes with battery material to solar assist the recharge of a battery is pretty recent. In 2017, Paolella et al[32] deposited a ruthenium dye (N719) on a lithium iron phosphate (LFP) electrode and combined this electrode with a lithium metal negative electrode to fabricate a photo-battery (**figure 13**).

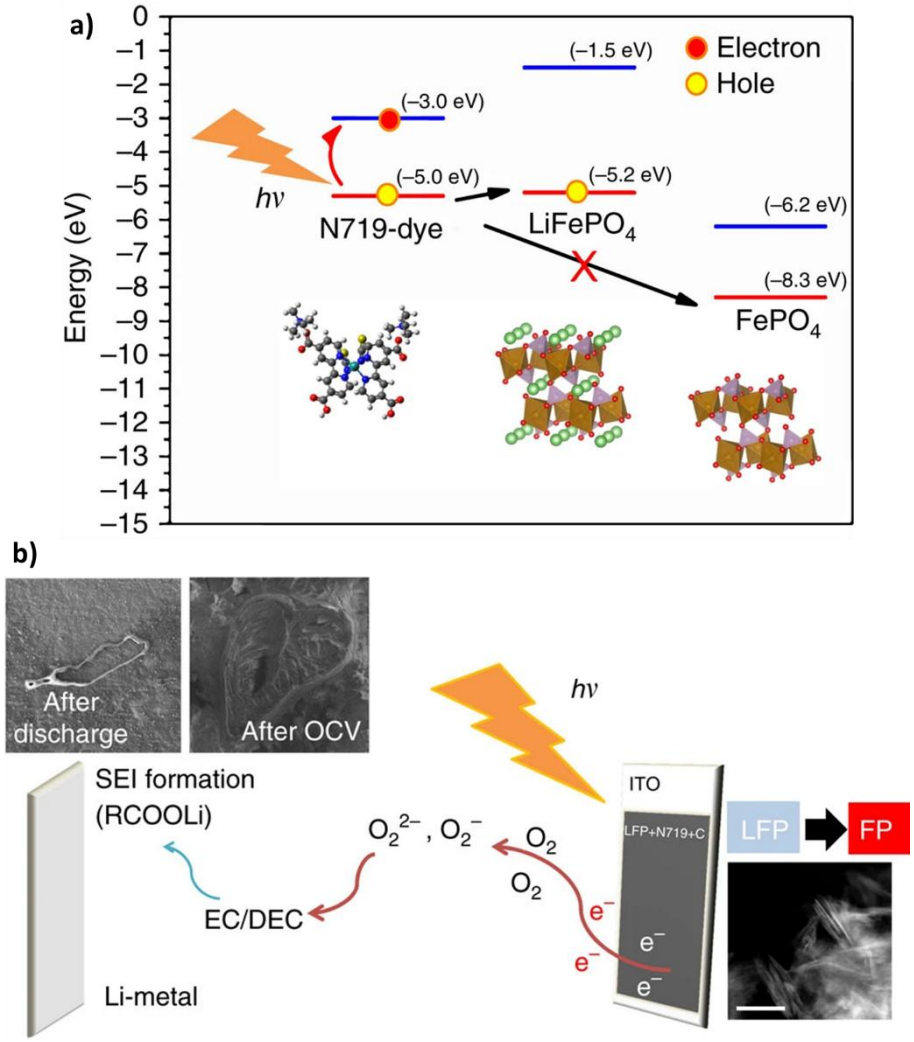

Figure 13: *(a) Representation of the photo-mechanism, the arrows illustrate the desired process: the absorption of photons excites the dye, that leads to hole injection into $LiFePO_4$ particles; the injection of holes into the charged phase of $FePO_4$ is forbidden, b) LFP photo-oxidation by holes injected by the excited dye and formation of SEI via reduction of oxygen by photoelectrons in the LFP(dye)/electrolyte/Li cell. Organic carbonate-based electrolyte is decomposed by reaction with peroxide/superoxide generated by the photo-generated electrons and oxygen. The scale bar of TEM image is 200 nm.*

In this configuration, the dye-modified electrode plays both roles: the dye allows the solar collection while LFP insures Li^+ hosting. The work suggests that the transfer of the hole from the dye to the LFP results in the oxidation of the electrode coupled with the extraction of lithium ion during the photo-charge. During the photo-charge, the system is at open circuit voltage (OCV) meaning that the photo-electron cannot be collected at the lithium electrode. The proposed mechanism is the photo-electron reduces the oxygen dissolved in the electrolyte to form a photo-SEI. They also notice during their discharge under illumination an excess capacity (about 2 times the theoretical value of LFP).

It is attributed to the fact that the photo-cathode continues undergoing partial charge during galvanostatic discharge because of its exposure to light that induces LFP to delithiate, hence creating vacancies for extra charge storage. A 0.06-0.08 % of overall efficiency is attained over 5 cycles. These very low values are attributed to the fact that the dye is not well fixed to the surface resulting of its dissolution in the electrolyte.

Molecular dyes can be replaced by semiconductor nanoparticles including CdS. In 2019, Wang et al[31] combined in an electrode WO_3 with CdS nanoparticles. A TiO_2 layer was used at the interface of WO_3 and CdS NPs, to facilitate the transfer of the photo-electron to the tungsten. When W^{6+} gets reduced to W^{5+}, the insertion of Li^+ in the WO_3 material occurs to insure the charge balance in the solid material. In the meantime, the hole is consumed by the I^- from the redox shuttle (**figure 14**). Wang et al. showed a photo-anode capable of photo-insertion.

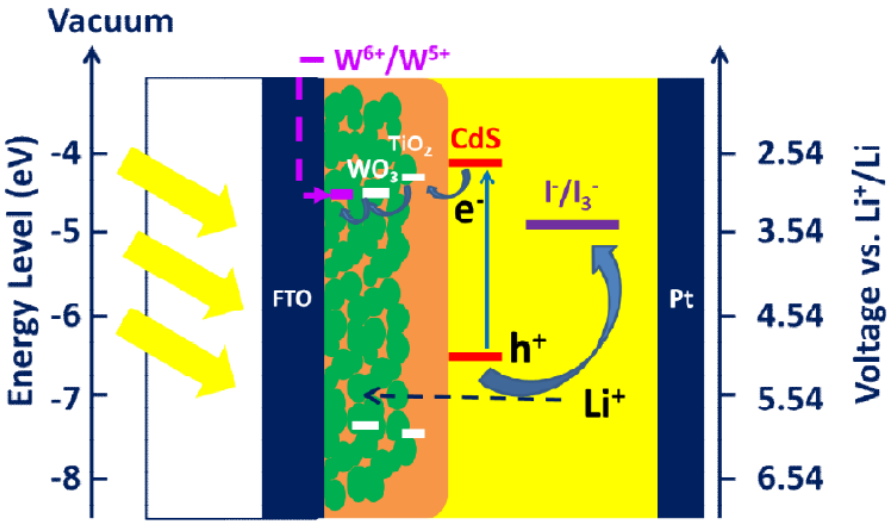

***Figure 14**: Schematic depiction of the photoelectrochemical system of CdS-sensitized WO_3 nanocomposite // LiI in propylene carbonate (PC) electrolyte // Pt cathode during photo-charging process.*[31]

In this example, the photo-corrosion of CdS induces the collapse of the system explaining the only 10 photo-charge cycles shown.

Another domain of research that deals with similar problematics (sun absorption and redox inside solid materials) is photochromic materials. They use sunlight to induce a change of color of the material. In order to access better light absorption efficiency, some of them use dye to collect the solar energy and then transfer the charge to a semi-conductor like WO_3 or

TiO_2 which can switch from transparent to blue- dark blue when the metallic center is reduced.[55,56] Usually to compensate the change of oxidation state and thereby insuring the neutral charge of the material, the insertion of a cation occurs. In 2020, Dokouzis et al[56] used an organic dye on a WO_3 electrode in a lithium perchlorate electrolyte. In the photochromic context, the important characteristics to look at are the rate of coloration and the stability of the coloration over time. Their ability to switch from one color to another, thereby to reversibly insert cations, make them good candidate for photo-battery materials, we can assimilate this ability to a self (dis)charge of a battery. Since the photochromic phenomena are similar to the photo-battery we should keep an eye on this field of research for more inspiration.

Usually, the dyes that have been developed for dye sensitized photovoltaic cells are not chemically stable under the battery environment, causing for example, the formation of SEI or byproducts. Moreover, the photo-charges created by the dye need to be controlled to avoid the same problems. To circumvent these difficulties, an alternative way is to use bi-functional materials. They are able to harvest the solar energy and use the photo-charges to insert or extract reversibly ions. They act as both photo- and battery material. The next part will discuss some literature data on these materials.

Table 2: Summary of recent photo-sensitized electrodes in two electrode set up.

Technology	Positive (+)	Negative (-)	Electrolyte	Mechanism	Avantages	Limitations	References
Li-ion	$LiFePO_4$, N719	Li°	$LiPF_6$ organic solvent	photo-charge	overall efficiency 0.06-0.08 %	O_2 photo-reduced forming SEI, 5 cycles	32
Li-ion	Pt (counter)	WO_3/TiO_2/CdS	LiI in propylene carbonate	photo-charge	photo-anode, 10 cycles	photo-corrosion of CdS	31
Li-air	C_3N_4/C	Li°	Organic solvent , I^-	photo-assisted	140 % energy efficacity, 50 cycles		57

I.2.2.2. Bi-functional material

In this work, we will call "bi-functional" a material that is able to both collect/convert and store the solar energy, typically, a semiconductor that can harvest solar energy and store it in chemical bonds. As a matter of fact, this material has a 'dynamic' composition upon battery cycling. Different phases coexist upon insertion of ions[58] The electronic properties of the electrode material are modified due to the band diagram evolution[59]. Both electronic and ionic conductivity may be impacted. We expect the solar absorption to be modified, together with the exciton transport. All of these "dynamic" properties make the understanding of the system difficult but also make it attractive. In the literature, only few examples are reported but the interest for 'dynamic' inserting material is growing.

In the 80s, Tributsch et al.[60–64] introduced the concept of photo-(de)insertion. They used semiconductors (SCs) zirconium and hafnium dichalcogenides in $HCl_{(aq)}$ or in $LiClO_{4(orga)}$. As these two SCs are p-type (meaning that the positive charges have a good mobility in these materials) a cathodic photo-current is observed under illumination, due to cation intercalation. Layer-type transition metal from the groups IV.B and V.B accept to intercalate ions following the reaction:

$$MX_2 + e^-(h\nu) + Li^+ \leftrightarrow LiMX_2$$

In parallel, they also observe the irreversible co-intercalation of water that leads to corrosion. Moreover, since these SCs are p-type (high mobility of the hole) their conductivities are low, limiting the storage of charges[60], that's why, to the best of our knowledge, the metal dichalcogenides are not used anymore for photo-intercalation of cations.

Several semiconductors with similar properties have been studied by Tributsch for this application and the results are summed up in the following **table 3**.[64]

Table 3: *Semiconducting materials used for photo-intercalation and photo-deintercalation experiments. Adapted from* [64]

Compound (Host material)	Energy gap (eV)	Conduction type	Intercalated (guest) species	Electrolyte	Observed photo-reaction	Reference
$ZrSe_2$	1.05-1.22	p	Li	Acetonitrile	Photo-intercalation	65
$HfSe_2$	1.13	n	Na	Acetonitrile	Photo-deintercalation	66
ZrS_2	1.68	n	Na	Acetonitrile	Photo-deintercalation	67
$FePS_3$	1.5	p	Li	Acetonitrile	Photo-intercalation	68
InSe	2	n, p	Cu	Propylene carbonate	Photo-(de)intercalation	69, 70
TiO_2(B)	3	n	H	Water	Photo-deintercalation	63
Cu_3PS_4	2	p	Cu	Acetonitrile	Photo-intercalation	71
$Cu_{6-x}PS_5I$	2.05	p	Cu, Ag	Acetonitrile	Photo-intercalation	72
$(CH)_n$	1.5	p	$HCLO_4$	Acetonitrile	Photo-deintercalation	73

This table suggests that if the SC is a p-type, the photo-reaction will be a photo-intercalation of cation, and if it is a n-type the reaction will be a photo-deintercalation. In the next section, the discussion will be focused on $TiO_2(B)$[63] which is a n-type SC and can absorb in the UV region (~3.2 eV) and can then photo-deintercalate protons in acidic solution. Tributsch used TiO_2 as a proton "membrane" in electrochemical cell, **see figure 15a.** In this configuration, if a current is applied on the right part of the set-up, they observed the intercalation of proton in the $TiO_2(B)$. This intercalation is accompanied by the creation of some electronic states in the band gap as shown in the energy band scheme in **figure 15b**, according to them. This indicates that electrons can be excited with visible light into the TiO_2 conducting band. Then, the protons are released into the electrolyte through a deintercalation reaction with holes created by UV-photons in the valence band. They will recombine with the electrons from the intercalation states which also lead to deintercalation of proton. During the intercalation of protons, the TiO_2 (B), the electrode turned from white to blue and according to them the only explanation is the creation of the electronic states in the forbidden energy gap. Nowadays, there is still no consensus on the origin of this change of color. Among the various hypotheses, the formation of Ti^{3+} center during proton insertion (H_xTiO_2) seems to be favor to explain the color change. During the photo-extraction of the protons, the Ti^{3+} will go back into Ti^{4+} with the white color. The coloration of the reduced phase could allow the absorption in the visible range thus increasing the absorbance of the material.

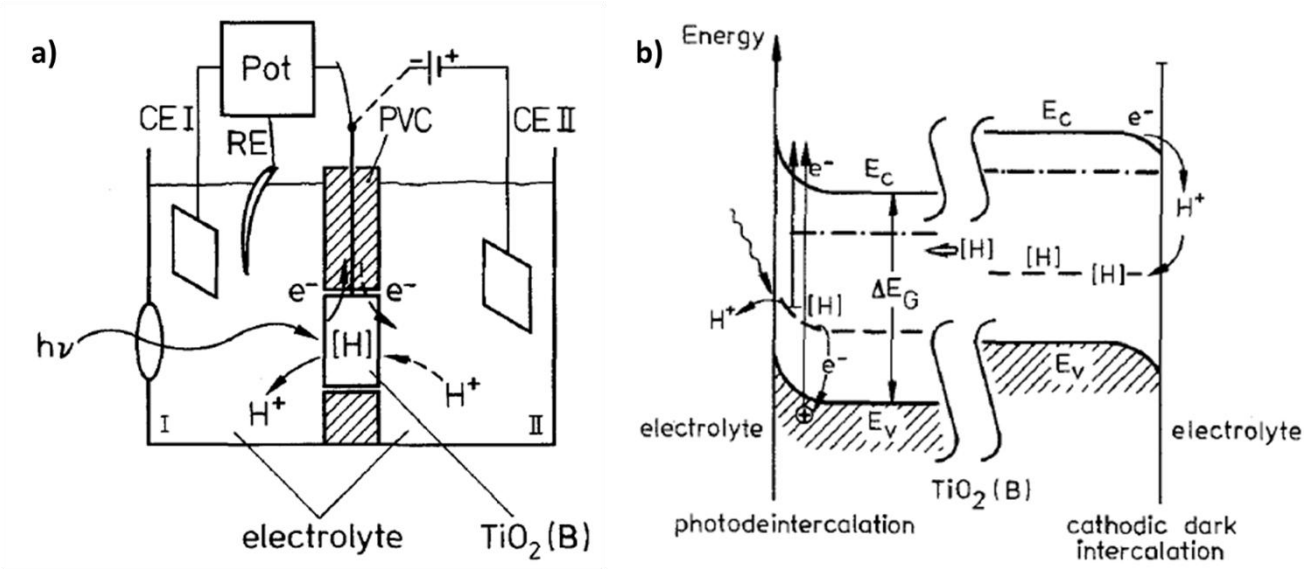

***Figure 15**: a) Two compartment electrochemical set-up. Both compartments are separated with a PVC plate, have a Pt counter electrode immerged in an acidic aqueous electrolyte. The TiO_2 (B) electrode is mounted onto a hole in the center of the plate. b) The energy band scheme of the set-up presented in a).*[63]

Few researches followed this aspect of photo-intercalation made by Tributsch et al. for the benefit of tandem devices like photovoltaic coupled with a battery. During the last 10 years the number of publication about this topic have significantly increased (**figure 16**).

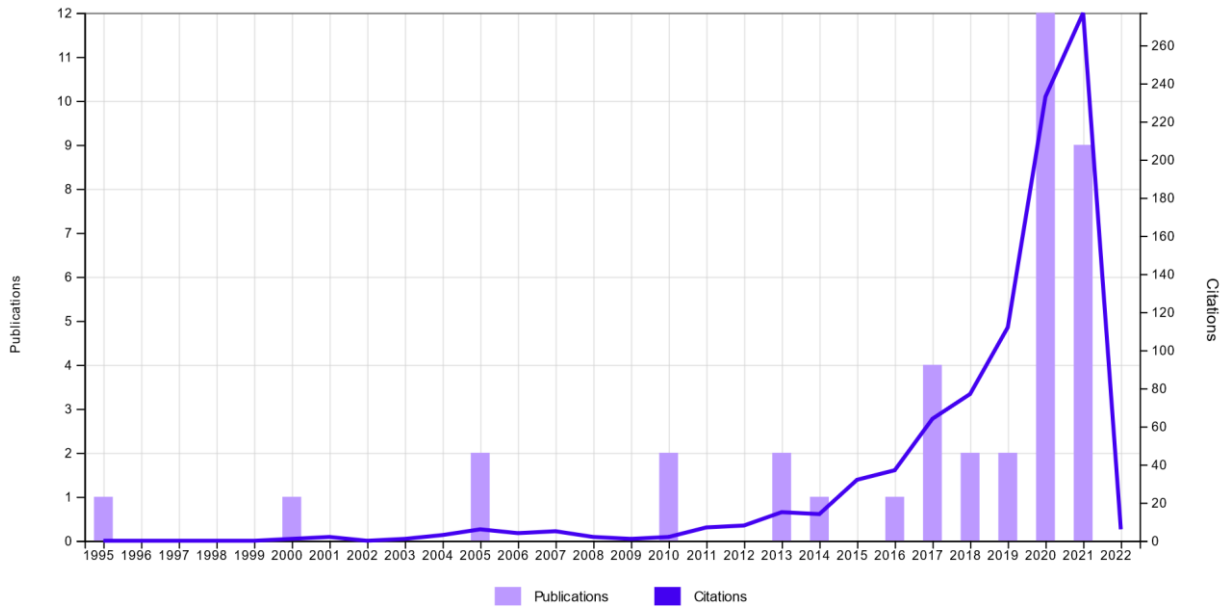

***Figure 16:** Number of publications and citations over the last decades. Reported from Web of Science with the key words "photo-rechargeable battery".*

Ahmad et al.[74] in 2018, reported a perovskite that can convert and store the solar energy. Perovskite has been selected for its good solar conversion (~25 %) but it also has the ability to insert cations. The photo-battery is then composed of perovskite (CHPI) as positive electrode and photo-electrode, versus a lithium metal negative electrode in an organic electrolyte (**figure 17**). During a photo-charge, holes will repulse the lithium-ion out of the perovskite matrix while the photo-electrons pass through the external circuit to the counter electrode and reduce the lithium ions. But since the photo-charge occurs at OCV, this mechanism seems unlikely.

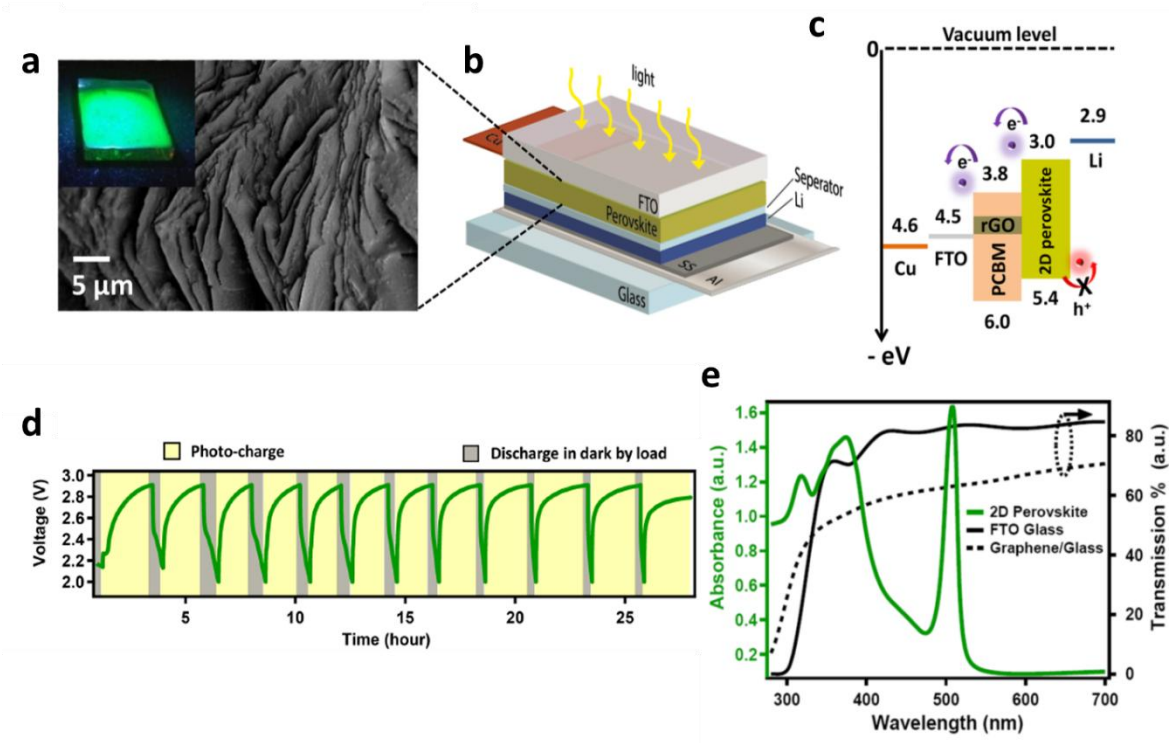

***Figure 17**: (a) SEM image of drop-cast 2D perovskite electrodes taken at 45° tilt. The inset shows a photo luminescence (PL) image of the corresponding perovskite film (λex ~ 300 nm LED source). (b) Schematic and (e) energy level diagram of perovskite photo-batteries. (d) Galvanostatic cycling discharge / photo-charge. (e) Optical absorption spectra of CHPI thin films and transmission of FTO glass and graphene substrates.*[74]

They explained the capacity fading in **figure 17d** by a deterioration of the material morphology during cycling, SEI formation and a possible formation of lead metal coming from the degradation of the perovskite. A capacity of 100 mAh/g and an overall efficiency of 0.034 % have been reported. To the best of our knowledge, this was the first time that a perovskite material was used as a bi-functional electrode. It opens perspectives since the perovskite is apparently one of the brightest future of solar cells.[4]

Other materials have been reported as a bi-functional like the germanium selenide (GeSe) nanoparticles.[75] GeSe has a low bandgap of 1.14 eV and a large absorption coefficient, moreover, it is a conversion material so it can store "multiple" cations. It appears to be a good candidate as bi-functional material. The authors performed the solar and battery tests separately and in different conditions. In dark condition, the GeSe electrode achieves a capacity of 670 mAh/g after 100 cycles. Under light, the holes allow the extraction of lithium ions from the converted GeSe material while according to them the photo-electrons reduce the lithium ions at the lithium metal electrode even though the experiments are conducted at OCV. The lack of reversibility between the charge and discharge was explained by the formation of a SEI. The GeSe seems to be a promising material since its high capacity, cyclability and its good solar absorption properties.

Another bi-functional material that has been studied is $LiMn_2O_4$ (LMO). This oxide is a common battery material (148 mAh/g), which is also a semiconductor with a bandgap in the visible range (2-3 eV). Lee et al[76] used mixed LMO nanoparticles with a conductive carbon and Teflon as cathode electrode versus lithium in an organic electrolyte (**figure 18 a,b**).

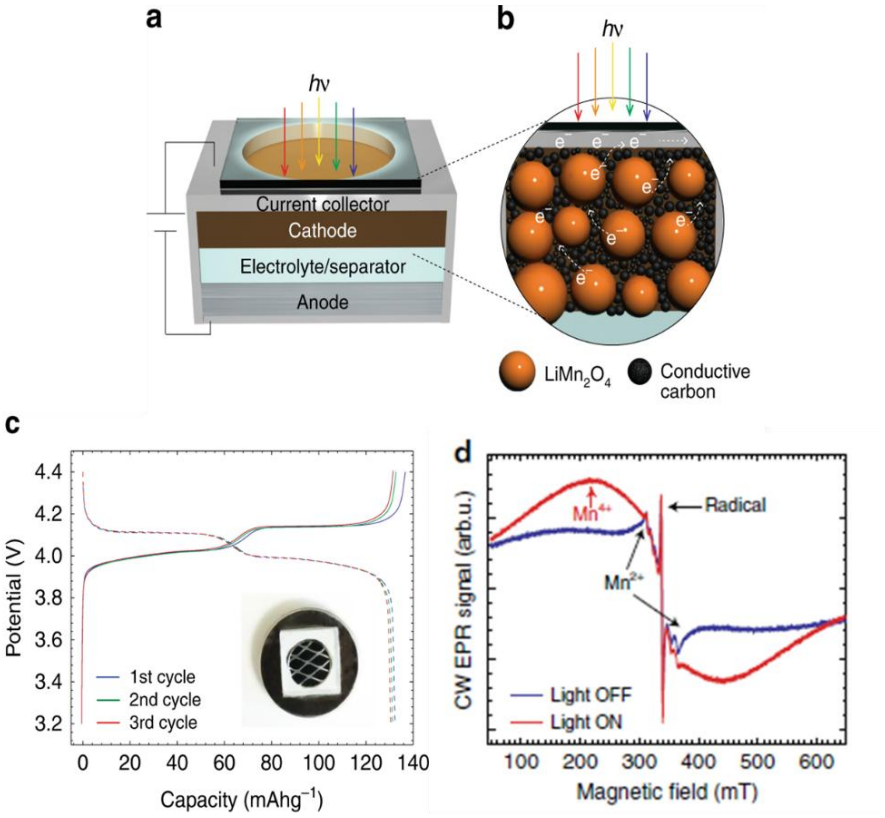

***Figure 18**: The principle of a photo-accelerated lithium-ion battery cell. The cell consists of a transparent window, current collector, cathode, electrolyte, separator, and anode. The broadband white light is used with an IR filter to avoid undesired heating of the cell. b) Magnified view of the composite LMO cathode consisting of a Teflon binder, carbon particles as conductive diluent (e.g. acetylene carbon black), and active oxide powder. c) Galvanostatic cycling voltage profile of a Li||1.2M LiPF6; EC: EMC 3:7 (w:w)||LMO (EC =ethylene carbonate; EMC = ethyl methyl carbonate). Three cycles of charging (indicated in solid lines) and discharging (in dash lines) profiles between 3.2 and 4.4 V at a C/10 rate are shown. A photograph of a fabricated 'open' cell is shown in the inset. d) Continuous wave (CW) X-band EPR spectra of a charged LMO battery cathode in the 'light-off' state (i.e., before illumination shown in blue spectrum) and 'light-on' state (i.e., during illumination in red spectrum) with white light. T =10 K. The CW EPR results in a derivative-type lineshape.*[76]

To probe the photo-mechanism in LMO, transient absorption (TA) spectroscopy, electron paramagnetic resonance (EPR) (**figure 18d**), and density functional theory (DFT) calculations were used. The TA experiments proved that the exciton comes from the irradiation of the gap of the LMO and that the excited state has a long live time. The EPR showed that the active photo-center is the Mn^{3+} and the photo-generated species are Mn^{4+}. The mechanism proposed is the following:

$$Mn^{3+} \rightarrow [Mn^{3+}]^* \rightarrow Mn^{4+}\,(\text{hole}) + e^- \quad \textit{photo-oxidation} \quad \sim\ LiMn_2O_4 + h^+ \rightarrow Mn_2O_4 + Li^+$$

The photo-extraction of the lithium is a part of the mechanism but the EPR also indicates the formation of Mn^{2+}, which could come from the disproportionation of the Mn^{3+} under

illumination into Mn^{4+} and Mn^{2+}. The DFT suggests that this photo-disproportionation is beneficial to the photo-extraction of the lithium ion.

In this configuration, according to them, the photo-electron pass through the external circuit when a potential bias is applied. But, the photo-assisted charge experiment is different from previous experiments, moving from galvanostatic experiment to potentiostatic ones. The photo-assisted charge is actually a potentiostatic experiment under illumination starting from an initial state of charge (SOC) of 50 % (4.07 V cf **figure 18c**); in these conditions, the LMO have a certain amount of lithium and the current delivered should be modest. They compared the potentiostatic under dark condition and under illumination and saw a difference in current and in capacity, as well. They confirmed these capacities with a galvanostatic experiment and concluded that the light increases the charging rate by a factor of 3.4. This study highlights the complexity of the photo-mechanism.

Recently, Boruah et al.[77] proposed a photo-cathode made of V_2O_5 nanofibers versus lithium negative electrode. Multiple layers of materials allow to drive the photo-electrons towards the current collector while blocking the holes, forcing them to extract the lithium by reacting with the $Li_xV_2O_5$ (**figure 19f**). It results in an increased capacity of 57 % under illumination.

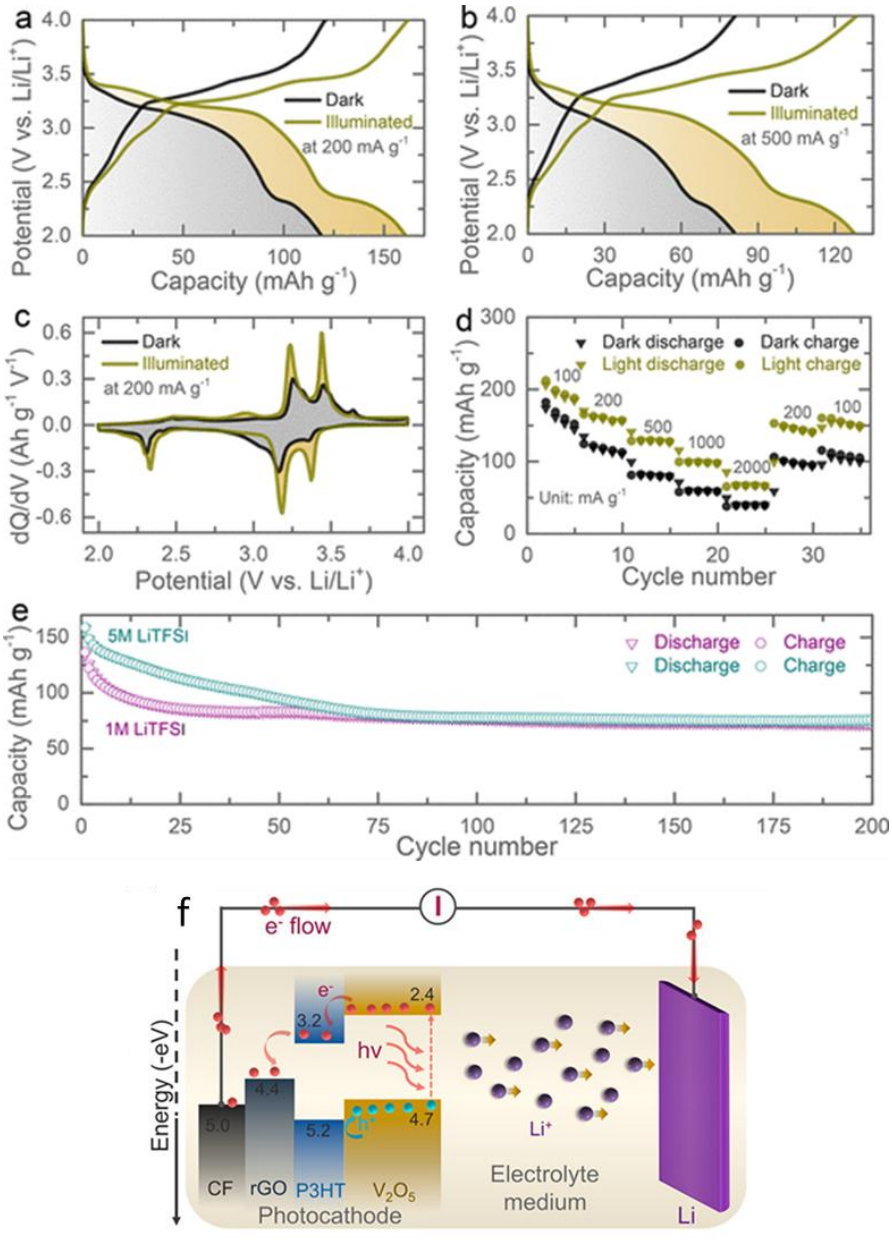

***Figure 19**: (a,b) Galvanostatic discharge–charge curves at 200 mA g^{-1} (7th cycle) and 500 mA g^{-1} (12th cycle) in dark and illuminated conditions. (c) dQ/dV curves of the respective discharge–charge curves at 200 mA g^{-1}. (d) Rate performance tests of the Photo-LIBs in dark and illuminated conditions. (e) Cycling stability (at 300 mA g^{-1}) of the Photo-LIBs tested in 1 and 5 M LiTFSI electrolytes in dark conditions. (f) Schematic representing the photo-charging mechanism of Photo-LIB.*[77]

This study shows how with an arrangement of the materials (**figure 19f**) the photo-electron could be driven towards the lithium counter electrode.

Table 4: Summary of recent bi-functional electrodes in two electrode set up.

Technology	Positive (+)	Negative (-)	Electrolyte	Mechanism	Avantages	Limitations	References
Li-ion	perovskite (CHPI)	Li°	$LiPF_6$ organic carbonate solvent	photo-charge	overall efficiency of 0.034 %, 10 cycles, SEI	100 mAh/g	74
Li-ion	GeSe	Li°	organic or aqueous	photo-charge	500 mAh/g at 2C, 100 cycles (dark)	SEI, 2 studies 1 for battery tests 1 for photo-tests	75
Li-ion	$LiMn_2O_4$	Li°	$LiPF_6$ organic carbonate solvent	photo-charge	148 mAh/g	dissolution of the active material, no cycling test	76
Li-ion	V_2O_5 nanofibers	Li°	LiTFSI in organic solvent	photo charge	0.22% overall efficiency, +57 % of capacity under light (161 mAh/g reversible)	no cyclibility under illumination	77
Li-ion	TiO_2	Li°	LP30	photo-assisted charge	33% extra capacity under light	Important SEI formation	44

Recently, Nguyen et al[44,45] used an anatase TiO_2 mesoporous thin film as photo-cathode versus lithium in a common battery organic electrolyte (LP30, 1 M $LiPF_6$ in 1:1 (v:v) of ethylene carbonate : dimethyl carbonate). A comparison of the galvanostatic cycles in the dark versus under illumination at a 2C-rate is shown in **figure 20a**. An increase of the capacity of about 33 % is observed for both charge and discharge under illumination. Two potentiostatic chopped experiments were performed using one-minute illumination periods, followed by one-minute dark (**figure 20b)**. One experiment starts from a non lithiated state (TiO_2) and the potential is set to 1.72 V vs $Li^+/Li°$, which corresponds to the potential of the reduction plateau (Li^+ insertion) on the previous discharge curve. The second one starts from a lithiated state ($Li_{0.5}TiO_2$), for a potential of 1.95 V vs $Li^+/Li°$, which is the potential of the oxidative plateau (Li^+ extraction) of the charge curve.

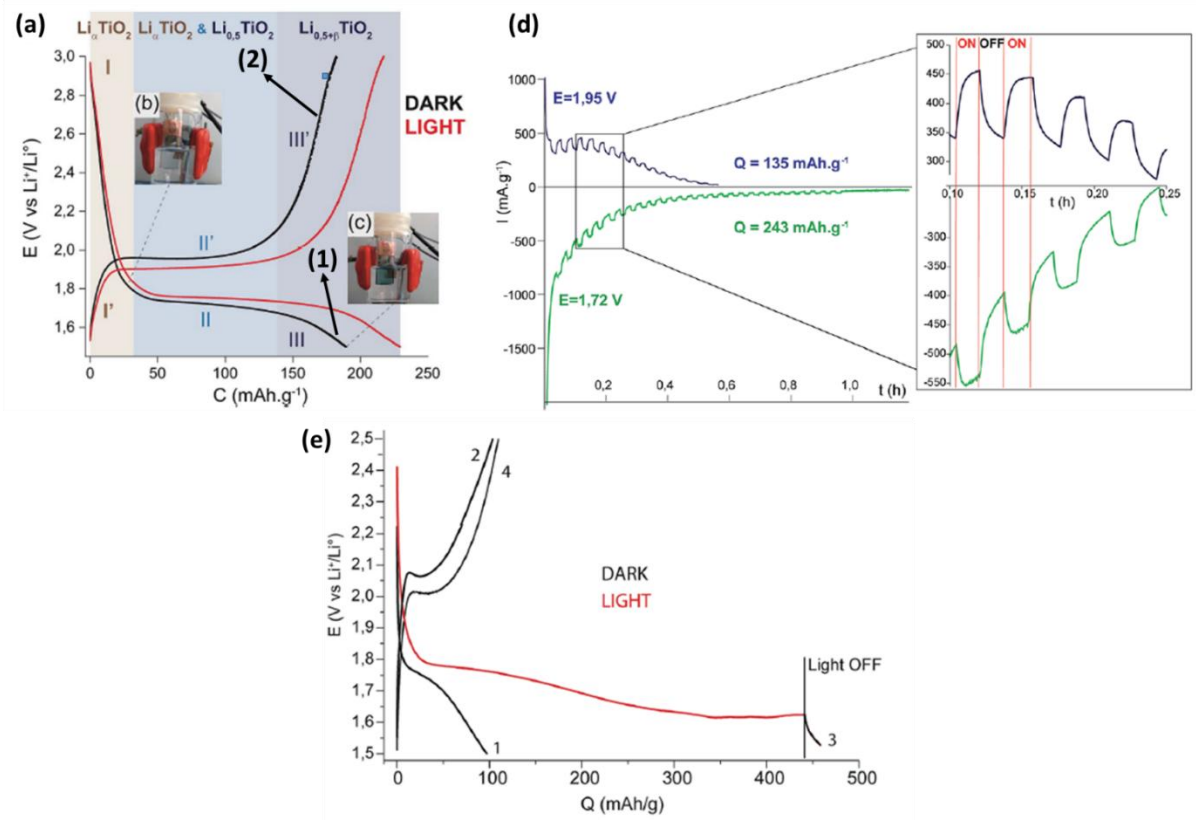

***Figure 20**: a) Potential versus capacity evolution (discharge(1)–charge(2) at 2C-rate) of TiO_2 mesoporous films (230 nm-thick, PB-PEO, 1M $TiCl_4$) under dark conditions and under light. Pictures of the cell at the beginning of zone II and at the end of zone III. $Li_{0.5}TiO_2$ corresponds to a capacity of 168 mA h/g. b) picture of the Li-poor TiO_2 anatase (transparent electrode), c) picture of the Li-rich TiO_2 anatase (blue electrode), d) Potentiostatic experiments, light ON/OFF every 1 min for E set at 1.95 V and 1.72 V. e) Illustration of the potential for "infinite" capacity of the mesoporousTiO_2-based battery. The experiment was realized in a water cooled cell (ESI 2(b)): glass/FTO/TiO_2//$LiPF_6$ 1 M in EC: DMC (1: 1 in vol)//Li°, ref. Li°. Two successive discharge–charge curves (1–2, 3–4/ i = 47 mA/g, C/7-rate if the theoretical capacity is set to 335 mA h/g) under dark (black) or light (red) conditions. The discharge no. 3 was performed under light; the light had to be turned off after 8 hours.*[44]

As in Tributsch's work, the proposed mechanism is the photo-extraction of Li^+ as a consequence of the oxidation of the Ti^{3+} to Ti^{4+} by the holes. At 1.95 V, a decrease of the photo-current is observed with time, suggesting that when lithiated TiO_2 have no longer lithium the photo-extraction of lithium logically stopped. At 1.72 V, the photo-current remains constant. Since lithium ions are supplied by the electro-insertion and light encourages the photo-extraction of Li, the photo-extraction frees space for more lithium ions to be electro-inserted, and the possibility for them to be photo-extracted during illumination, resulting in a small but never vanishing photo-current (called informally "*parking phenomena"*).

Charge:

(1) $Li_xTiO_2 \rightarrow TiO_2 + x\ Li^+ + x\ e^-$

Charge under illumination:

(1) $Li_xTiO_2 \rightarrow TiO_2 + x\ Li^+ + x\ e^-$

(2) $Li_xTiO_2 + x\ h^+ \rightarrow TiO_2 + x\ Li^+$

Discharge:

(3) $TiO_2 + x\ Li^+ + x\ e^- \rightarrow Li_xTiO_2$

Discharge under illumination:

(3) $TiO_2 + x\ Li^+ + x\ e^- \rightarrow Li_xTiO_2$

(2) $Li_xTiO_2 + x\ h^+ \rightarrow TiO_2 + x\ Li^+$

They also demonstrated that through the control of the scan rates, during galvanostatic experiment, the kinetics of the electrochemical insertion could be adjusted at the same rate of the photo-extraction. This resulted in an "infinite" capacity (**figure 20e**). Indeed, if the kinetics of the electro-insertion, equation (3), is equal to the kinetic of the photo-extraction, equation (2), an apparent infinite capacity could be achieved, given the *so-called parking phenomena*. The capacity achieved in such conditions is 440 mAh/g, exceeding the theoretical capacity of $LiTiO_2$ (335 mAh/g). This tends to prove that lithium has to be photo-extracted in order for more to come in. If the fate of the hole seems to be settled, the fate of the photo-electron remains unclear; one hypothesis was that the extra capacity is due to solvent (LP30) reduction by this photo-electron.

To summarize, different configurations of tandem, three or two-electrode, have been reported. They have pros and cons. The tandem one takes the advantage of the mature technology like Li-ion battery and Si-based photovoltaic panel but require space and resources to compose a viable module. The three-electrode configuration is highly inspired by their parent technology but requires to separate them to each other because of their medium. Indeed, the battery technology is mostly in organic electrolyte whereas the PV technology is in aqueous electrolyte. Another issue remains the collect of both photo-charges. They need to travel through the external circuit and/or through the electrolyte with the help of a redox shuttle if they are not used for SEI or other by product. The two-electrode configuration has the advantage to “store” locally one photo-charge but the other photo-charge remains not fully used for energy storage at the moment.

I.3. Thesis Introduction

In Chapter I, we selected some very recent examples of photo-rechargeable batteries. We found out that, due to this early stage of the photo-rechargeable battery development, most of the mechanisms underlying the photo-recharge, or the photo-assisted recharge were not fully understood.

Nguyen et al[44] show that Li^+ could be photo-extracted from mesoporous anatase TiO_2 films (**figure 20**, glass/FTO/TiO_2// $LiPF_6$ 1 M in EC: DMC (1: 1 in vol)// Li°, ref. Li°). The suggested mechanism for this photo-extraction relies on the ability of lithiated-TiO_2 to absorb visible light and generates an electron-hole pair. The hole would oxidize Ti^{3+} to Ti^{4+} resulting in the extraction of the lithium ions, they called this phenomenon the photo-extraction of the lithium ions. However, the fate of the photo-electron was still unclear. It has been previously discussed that the photo-electron could react with the oxygen from the air[32] , or the water[34,78,79] contained in the electrolyte, or the electrolyte itself[32,44] creating a Solid Electrolyte Interface (SEI)[21,24–27,80–107]. Since we are looking at rechargeable batteries, SEI occur in both cathode[30–39] and anode[118–126] electrodes. The most common electrolyte is the LP30 and the SEI formation is reported here[127–129]. Post mortem analysis of 10 times cycled photo-electrodes, showed the presence of crystals of LiF of bigger size compared to dark-cycled sample.[45] From this observation, it was however very difficult to conclude which reaction was actually photo-catalyzed to allow the electrode regeneration. Another grey area is the fact that the light arriving to the electrode lies in the visible (VIS) range since the electrochemical cell is in glass. This suggest that the lithiated electrode is photoactive in the VIS range as opposite to pure anatase TiO_2, which would only be active in UV light.

Accordingly, the aim of the PhD was to clarify the mechanisms proposed in the O. Nguyen thesis by adding voluntary an electron acceptor, H_2O, in the electrolyte. This situation allows to use the photo-electron to a well-known reaction the reduction of water to produce H_2. The use of “photo-electron” toward this reaction presents the advantage to store energy in chemical bound.

When it comes to pure anatase TiO_2, the position of the conduction band is well-known. However, when it comes to lithiated TiO_2, the attribution of the photo-generated electron is not straightforward. Depending on the state of charge, it presents a composition that varies continuously between a lithium-poor phase (anatase-solid solution Li_xTiO_2, x<0,1) to a lithium-rich phase (orthorhombic-$Li_{0.5}TiO_2$ or tetragonal -$LiTiO_2$). The potential at which there is phase transition is 1.75 V vs $Li^+/Li°$. Since this potential reflects the electronic maximal band filling, we decide to consider that the electronic level of a photo-generated electron would at least be that one. The photo-electron acceptor, should then be placed right below this level for an efficient transfer (**Figure 21**).

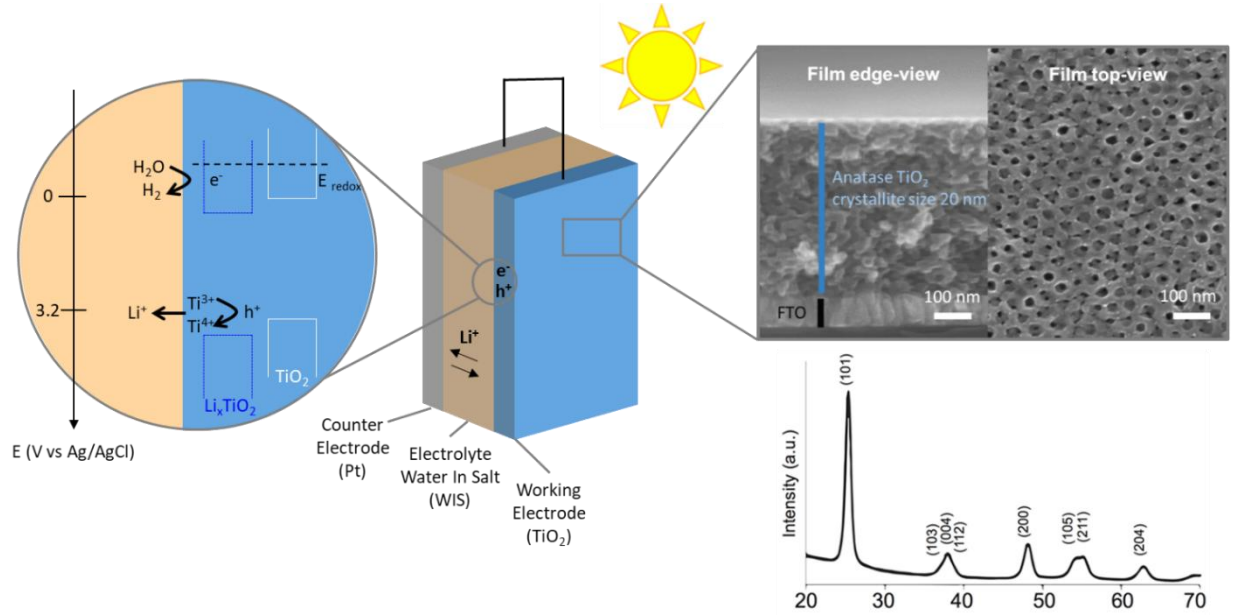

Figure 21: *Schema of the system: glass/FTO/TiO_2// Water In Salt (WIS) 20 M of LiTFSI // AgAgCl (KCl saturated)/ Pt. With a schema of the band diagram of TiO_2 and Li_xTiO_2 on the left and on the right SEM-FEG images of the TiO_2 film with an edge-view and a top-view, XRD of the TiO_2 anatase thin film.*

To do so, we changed the electrolyte, going from organic-LP30 electrolyte to H_2O-based Water-In-Salt electrolyte (WIS). The Water In Salt (WIS) electrolyte composed of 20 mol/kg (M, molality) of lithium bis (trifluoromethanesulfonyl) imide (LiTFSI) in water. We choose this electrolyte because the water will be used as a photo-electron acceptor. In very concentrated electrolyte the potential of hydrogen evolution reaction (HER) is 1.9 V vs Li^+/Li and oxygen evolution reaction (OER) is 4.9 V vs Li^+/Li[130] instead of the common thermodynamic 1.23 V potential window of the water in aqueous solvent. Abusively the stability windows are represented in **figure 22a**. Indeed, the stability windows could be

modulate depending on the medium and are then not fixed; unlike the standard potential of the water.

This has been attributed to the fact that the water molecules are less accessible due to the "solvation" shell of the salt[131] and the formation of a small SEI[132] (**figure 22b**). If H_2 is actually observed when a photo-charge is performed, it would give us an information on the minimal level of the photo-electron.

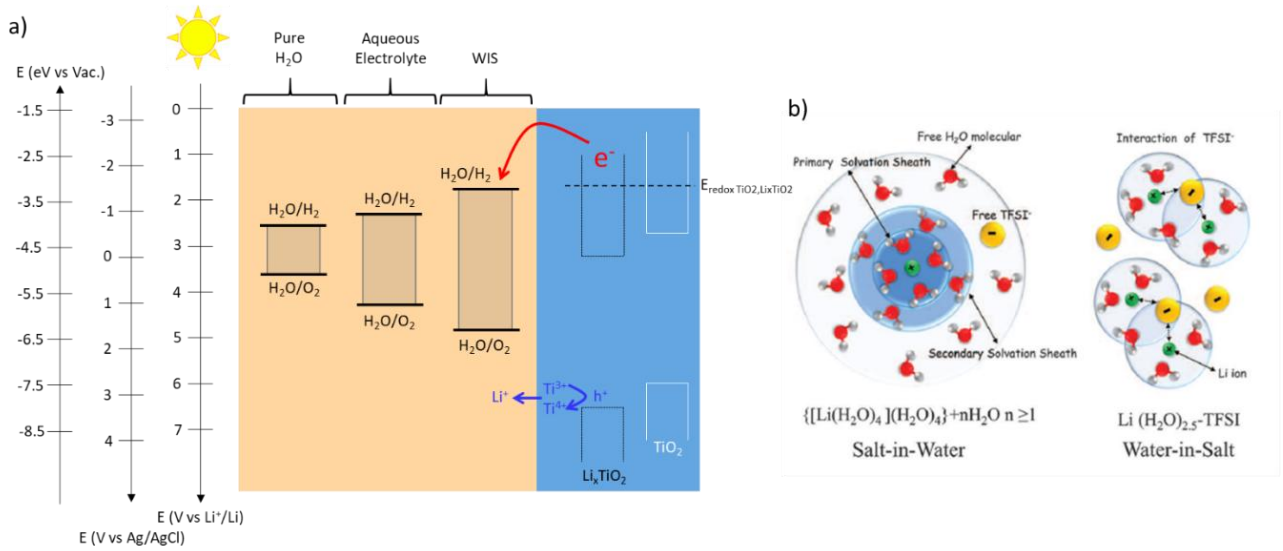

Figure 22: *a) Stability window of pure water, aqueous electrolyte and water in salt electrolyte[131] regarding the band diagram of TiO_2 and lithiated TiO_2[89]. b) Illustration of the evolution of the Li^+ primary solvation sheath in diluted and water-in-salt solutions.[131]*

This WIS electrolyte has been used as in lithium-ion batteries to enhance the stability window of the water in order to reach an acceptable capacity of lithium insertion. The TiO_2 mesoporous films used as (photo-)electrodes exhibit a high surface area exposed to the electrolyte to favor all redox reactions including the lithium insertion/extraction. Relatively small TiO_2 crystallites (20 nm) are composing the walls of the film, which reduce the travelling distance of the Li-ions, theoretically allowing for high rate cycling. An intimate contact between the nanoparticles is created by sintering the film at 500°C, which results in the creation of necks between the particles. Such a high-quality connection is important to ensure efficient electronic conductivity across this carbon-free material towards the Fluorine doped Tin Oxide (FTO) transparent conducting substrate. A 500 nm-thickness[45] has shown to be the best compromise to achieve the best capacities vs kinetic of 'photo-rechargeability'. The idea was to have in priority the lithium insertion with a small HER

during reductions but the strategy was during the photo-charge to use the water as photo-electron acceptor to avoid the recombination between the electron and the hole and so increase the photo-extraction of the lithium.

Accordingly, the aim of the PhD was to clarify the mechanisms proposed in the O. Nguyen thesis by adding voluntary an electron acceptor, H_2O, in the electrolyte. This situation allows to use the photo-electron to a well-known reaction the reduction of water to produce H_2. The use of “photo-electron” toward this reaction presents the advantage to store energy in chemical bound.

In this context, after a brief literature review of the different electrochemical devices combining light and storage (**chapter I**). **Chapter II** will gather the synthesis protocol for the synthesis of mesoporous TiO_2 and the characterization tools used during the PhD.

we studied in **chapter III**, the intercalation of Li in the presence of water. Since the composition of the material is changing with the lithiation, its activity toward the ElectroCatalysis hydrogen Evolution Reaction (EC-HER) may be impacted and will be investigated in the context of using inserting material as HER catalyst promising candidates. To do so, the HER will be studied as function of the quantity of Li inserted/de-inserted in the electrode. To better understand light harvesting and mechanisms involved in this “dual” electrode (light harvester and energy storage), we will investigate the impact of light in two different configurations: photo-charge (at OCV) and photo-assisted charge (under polarization) (**chapter IV**). We expected that both photo-recharge will have its own mechanism that we will discuss. For the photo-charge mechanism, we will study at different State of (dis)Charge (SOC) the influence on the rate of photo-charge i.e the rate of photo-extraction of the lithium ions. For the photo-assisted charge the mechanism will be studied through galvanostatic, potentiostatic and cyclic voltammetry experiment but also thanks to the evolution upon cycling.

Bibliography

(1) Yun, S.; Qin, Y.; Uhl, A. R.; Vlachopoulos, N.; Yin, M.; Li, D.; Han, X.; Hagfeldt, A. New-Generation Integrated Devices Based on Dye-Sensitized and Perovskite Solar Cells. *Energy & Environmental Science* **2018**, *11* (3), 476–526.

(2) Perez, M.; Perez, R. A Fundamental Look at Supply Side Energy Reserves for the Planet. **2015**, *62*, 4.

(3) Le solaire thermique (accessed 2021 -12 -04).

(4) Laboratory, N. R. E. *English: Conversion Efficiencies of Best Research Solar Cells Worldwide for Various Photovoltaic Technologies since 1976.*; 2017.

(5) Parida, B.; Iniyan, S.; Goic, R. A Review of Solar Photovoltaic Technologies. *Renewable and Sustainable Energy Reviews* **2011**, *15* (3), 1625–1636.

(6) Williams, J. Why It Pays to Reduce Energy Demand at Peak Times. *The Earthbound Report*, 2018.

(7) Tarascon, J.-M.; Dunn, B. Electrical Energy Storage for the Grid: A Battery of Choices. *SCIENCE* **2011**.

(8) Le recyclage des batteries Li-ion https://culturesciences.chimie.ens.fr/thematiques/chimie-physique/electrochimie/le-recyclage-des-batteries-li-ion (accessed **2021** -04 -29).

(9) Combien y-a-t-il de voitures dans le monde? https://www.transitionsenergies.com/combien-voitures-monde/. *Transitions & Energies*, **2020**.

(10) Aptera Motors | Efficient Electric Vehicles https://www.aptera.us https://www.aptera.us (accessed **2021** -03 -22).

(11) Podjaski, F.; Kröger, J.; Lotsch, B. V. Toward an Aqueous Solar Battery: Direct Electrochemical Storage of Solar Energy in Carbon Nitrides. *Advanced Materials* **2018**, *30* (9), 1705477.

(12) An, C.; Wang, Z.; Xi, W.; Wang, K.; Liu, X.; Ding, Y. Nanoporous Cu@Cu_2O Hybrid Arrays Enable Photo-Assisted Supercapacitor with Enhanced Capacities. *Journal of Materials Chemistry A* **2019**, *7* (26), 15691–15697.

(13) Gong, J.; Liang, J.; Sumathy, K. Review on Dye-Sensitized Solar Cells (DSSCs): Fundamental Concepts and Novel Materials. *Renewable and Sustainable Energy Reviews* **2012**, *16* (8), 5848–5860.

(14) Hou, W.; Cronin, S. B. A Review of Surface Plasmon Resonance-Enhanced Photocatalysis. *Advanced Functional Materials* **2013**, *23* (13), 1612–1619.

(15) Amendola, V.; Pilot, R.; Frasconi, M.; Maragò, O. M.; Iatì, M. A. Surface Plasmon Resonance in Gold Nanoparticles: A Review. *J. Phys.: Condens. Matter* **2017**, *29* (20), 203002.

(16) Quantum Efficiency. *HiSoUR - Hi So You Are*, **2018**.

(17) Rao, K. G.; Ashok, C.; Rao, K. V.; Rajendar, V.; Chakra, C. S. Green Synthesis of TiO_2 Nanoparticles Using Hibiscus Flower Extract. 5.

(18) The extraterrestrial (AM0) solar spectrum https://www2.pvlighthouse.com.au/resources/courses/altermatt/The%20Solar%20Spe

ctrum/The%20extraterrestrial%20(AM0)%20solar%20spectrum.aspx (accessed **2021** -05 -09).

(19) Gurung, A.; Chen, K.; Khan, R.; Abdulkarim, S. S.; Varnekar, G.; Pathak, R.; Naderi, R.; Qiao, Q. Highly Efficient Perovskite Solar Cell Photocharging of Lithium Ion Battery Using DC–DC Booster. *Advanced Energy Materials* **2017**, *7* (11), 1602105.

(20) Deng, Y.; Zhou, Y.; Shi, Z.; Zhou, X.; Quan, X.; Chen, G. Porous $LiMn_2O_4$ Microspheres as Durable High Power Cathode Materials for Lithium Ion Batteries. *Journal of Materials Chemistry A* **2013**, *1* (28), 8170.

(21) Campion, C. L.; Li, W.; Euler, W. B.; Lucht, B. L.; Ravdel, B.; DiCarlo, J. F.; Gitzendanner, R.; Abraham, K. M. Suppression of Toxic Compounds Produced in the Decomposition of Lithium-Ion Battery Electrolytes. *Electrochem. Solid-State Lett.* **2004**, *7* (7), A194.

(22) Li, W.; Campion, C.; Lucht, B. L.; Ravdel, B.; DiCarlo, J.; Abraham, K. M. Additives for Stabilizing LiPF6-Based Electrolytes Against Thermal Decomposition. *J. Electrochem. Soc.* **2005**, *152* (7), A1361.

(23) Larush-Asraf, L.; Biton, M.; Teller, H.; Zinigrad, E.; Aurbach, D. On the Electrochemical and Thermal Behavior of Lithium Bis(Oxalato)Borate (LiBOB) Solutions. *Journal of Power Sources* **2007**, *174* (2), 400–407.

(24) Zhuang, G. V.; Xu, K.; Yang, H.; Jow, T. R.; Ross, P. N. Lithium Ethylene Dicarbonate Identified as the Primary Product of Chemical and Electrochemical Reduction of EC in 1.2 M $LiPF_6$ /EC:EMC Electrolyte. *J. Phys. Chem. B* **2005**, *109* (37), 17567–17573.

(25) Aurbach, D.; Markovsky, B.; Levi, M. .; Levi, E.; Schechter, A.; Moshkovich, M.; Cohen, Y. New Insights into the Interactions between Electrode Materials and Electrolyte Solutions for Advanced Nonaqueous Batteries. *Journal of Power Sources* **1999**, *81–82*, 95–111.

(26) Shkrob, I. A.; Zhu, Y.; Marin, T. W.; Abraham, D. Reduction of Carbonate Electrolytes and the Formation of Solid-Electrolyte Interface (SEI) in Lithium-Ion Batteries. 1. Spectroscopic Observations of Radical Intermediates Generated in One-Electron Reduction of Carbonates. *J. Phys. Chem. C* **2013**, *117* (38), 19255–19269.

(27) Aurbach, D. Review of Selected Electrode–Solution Interactions Which Determine the Performance of Li and Li Ion Batteries. *Journal of Power Sources* **2000**, *89* (2), 206–218.

(28) Gibson, T. L.; Kelly, N. A. Solar Photovoltaic Charging of Lithium-Ion Batteries. *Journal of Power Sources* **2010**, *195* (12), 3928–3932.

(29) Moon, E.; Blaauw, D.; Phillips, J. D. Subcutaneous Photovoltaic Infrared Energy Harvesting for Bio-implantable Devices. *IEEE Transactions on Electron Devices* **2017**, *64* (5), 2432–2437.

(30) Fang, Z.; Hu, X.; Yu, D. Integrated Photo-Responsive Batteries for Solar Energy Harnessing: Recent Advances, Challenges, and Opportunities. *ChemPlusChem* **2020**, *85* (4), 600–612.

(31) Wang, Z.; Chiu, H.; Paolella, A.; Zaghib, K.; Demopoulos, G. P. Lithium Photo-intercalation of CdS-Sensitized WO_3 Anode for Energy Storage and Photoelectrochromic Applications. *ChemSusChem* **2019**, *12* (10), 2220–2230.

(32) Paolella, A.; Faure, C.; Bertoni, G.; Marras, S.; Guerfi, A.; Darwiche, A.; Hovington, P.; Commarieu, B.; Wang, Z.; Prato, M.; Colombo, M.; Monaco, S.; Zhu, W.; Feng, Z.; Vijh, A.; George, C.; Demopoulos, G. P.; Armand, M.; Zaghib, K. Light-Assisted Delithiation of Lithium Iron Phosphate Nanocrystals towards Photo-Rechargeable Lithium Ion Batteries. *Nature Communications* **2017**, *8*, 14643.

(33) Ben M'Barek, Y.; Rosser, T.; Sum, J.; Blanchard, S.; Volatron, F.; Izzet, G.; Salles, R.; Fize, J.; Koepf, M.; Chavarot-Kerlidou, M.; Artero, V.; Proust, A. Dye-Sensitized Photocathodes: Boosting Photoelectrochemical Performances with Polyoxometalate Electron Transfer Mediators. *ACS Applied Energy Materials* **2020**, *3* (1), 163–169.
(34) Li, N.; Wang, Y.; Tang, D.; Zhou, H. Integrating a Photocatalyst into a Hybrid Lithium–Sulfur Battery for Direct Storage of Solar Energy. *Angewandte Chemie* **2015**, *127* (32), 9403–9406.
(35) Paolella, A.; Vijh, A.; Guerfi, A.; Zaghib, K.; Faure, C. Review—Li-Ion Photo-Batteries: Challenges and Opportunities. *Journal of The Electrochemical Society* **2020**, *167* (12), 120545.
(36) Lau, D.; Song, N.; Hall, C.; Jiang, Y.; Lim, S.; Perez-Wurfl, I.; Ouyang, Z.; Lennon, A. Hybrid Solar Energy Harvesting and Storage Devices: The Promises and Challenges. *Materials Today Energy* **2019**, *13*, 22–44.
(37) Zeng, Q.; Lai, Y.; Jiang, L.; Liu, F.; Hao, X.; Wang, L.; Green, M. A. Integrated Photorechargeable Energy Storage System: Next-Generation Power Source Driving the Future. *Advanced Energy Materials* **2020**, *10* (14), 1903930.
(38) Li, Q.; Liu, Y.; Guo, S.; Zhou, H. Solar Energy Storage in the Rechargeable Batteries. *nano today* **2017**, *16*, 46–60.
(39) Guo, W.; Xue, X.; Wang, S.; Lin, C.; Wang, Z. L. An Integrated Power Pack of Dye-Sensitized Solar Cell and Li Battery Based on Double-Sided TiO_2 Nanotube Arrays. *Nano Lett.* **2012**, *12* (5), 2520–2523.
(40) Chen, P.; Li, G.-R.; Li, T.-T.; Gao, X.-P. Solar-Driven Rechargeable Lithium–Sulfur Battery. *Advanced Science* **2019**, *6* (15), 1900620.
(41) Li, Q.; Li, N.; Ishida, M.; Zhou, H. Saving Electric Energy by Integrating a Photoelectrode into a Li-Ion Battery. *Journal of Materials Chemistry* **2015**, *3*, 20903.
(42) Li, Q.; Li, N.; Liu, Y.; Wang, Y.; Zhou, H. High-Safety and Low-Cost Photoassisted Chargeable Aqueous Sodium-Ion Batteries with 90% Input Electric Energy Savings. *Advanced Energy Materials* **2016**, *6* (18), 1600632.
(43) Wei, Z.; Shen, Y.; Liu, D.; Liu, F. An All-Vanadium Continuous-Flow Photoelectrochemical Cell for Extending State-of-Charge in Solar Energy Storage. *Scientific Reports* **2017**, *7* (1), 629.
(44) Nguyen, O.; Courtin, E.; Sauvage, F.; Krins, N.; Sanchez, C.; Laberty-Robert, C. Shedding Light on the Light-Driven Lithium Ion de-Insertion Reaction: Towards the Design of a Photo-Rechargeable Battery. *Journal of Materials Chemistry A* **2017**, *5* (12), 5927–5933.
(45) Nguyen, O. Towards a Li-Ion Photo-Rechargeable Battery. thesis, Sorbonne Université, 7 place Jussieu, **2018**.
(46) Nguyen, O.; Krins, N.; Laberty-Robert, C. Harvesting Light with Semiconductor: Role of Interface in the Processes of Charge Transfer. *Materials Science in Semiconductor Processing* **2018**, *73*, 2–12.
(47) Richhariya, G.; Kumar, A.; Tekasakul, P.; Gupta, B. Natural Dyes for Dye Sensitized Solar Cell: A Review. *Renewable and Sustainable Energy Reviews* **2017**, *69*, 705–718.
(48) Kong, F.-T.; Dai, S.-Y.; Wang, K.-J. Review of Recent Progress in Dye-Sensitized Solar Cells. *Advances in OptoElectronics* **2007**, *2007*, 1–13.
(49) Shalini, S.; Balasundaraprabhu, R.; Kumar, T. S.; Prabavathy, N.; Senthilarasu, S.; Prasanna, S. Status and Outlook of Sensitizers/Dyes Used in Dye Sensitized Solar Cells (DSSC): A Review. *International Journal of Energy Research* **2016**, *40* (10), 1303–1320.

(50) Ludin, N. A.; Al-Alwani Mahmoud, A. M.; Bakar Mohamad, A.; Kadhum, A. A. H.; Sopian, K.; Abdul Karim, N. S. Review on the Development of Natural Dye Photosensitizer for Dye-Sensitized Solar Cells. *Renewable and Sustainable Energy Reviews* **2014**, *31*, 386–396.
(51) Andreiadis, E. S.; Chavarot-Kerlidou, M.; Fontecave, M.; Artero, V. Artificial Photosynthesis: From Molecular Catalysts for Light-Driven Water Splitting to Photoelectrochemical Cells. *Photochemistry and Photobiology* **2011**, *87* (5), 946–964.
(52) Zhang, B.; Sun, L. Artificial Photosynthesis: Opportunities and Challenges of Molecular Catalysts. *Chemical Society Reviews* **2019**, *48* (7), 2216–2264.
(53) Berardi, S.; Drouet, S.; Francàs, L.; Gimbert-Suriñach, C.; Guttentag, M.; Richmond, C.; Stoll, T.; Llobet, A. Molecular Artificial Photosynthesis. *Chem. Soc. Rev.* **2014**, *43* (22), 7501–7519.
(54) Frischmann, P. D.; Mahata, K.; Würthner, F. Powering the Future of Molecular Artificial Photosynthesis with Light-Harvesting Metallosupramolecular Dye Assemblies. *Chem. Soc. Rev.* **2013**, *42* (4), 1847–1870.
(55) Bogati, S.; Georg, A.; Graf, W. Photoelectrochromic Devices Based on Sputtered WO_3 and TiO2 Films. *Solar Energy Materials and Solar Cells* **2017**, *163*, 170–177.
(56) Dokouzis, A.; Bella, F.; Theodosiou, K.; Gerbaldi, C.; Leftheriotis, G. Photoelectrochromic Devices with Cobalt Redox Electrolytes. *Materials Today Energy* **2020**, *15*, 100365.
(57) Liu, Y.; Li, N.; Wu, S.; Liao, K.; Zhu, K.; Yi, J.; Zhou, H. Reducing the Charging Voltage of a Li–O_2 Battery to 1.9 V by Incorporating a Photocatalyst. *Energy & Environmental Science* **2015**, *8* (9), 2664–2667.
(58) Zhou, C.; Sanders-Bellis, Z.; Smart, T. J.; Zhang, W.; Zhang, L.; Ping, Y.; Liu, M. Interstitial Lithium Doping in $BiVO_4$ Thin Film Photoanode for Enhanced Solar Water Splitting Activity. *Chem. Mater.* **2020**, *32* (15), 6401–6409.
(59) Andriamiadamanana, C.; Sagaidak, I.; Bouteau, G.; Davoisne, C.; Laberty-Robert, C.; Sauvage, F. Light-Induced Charge Separation in Mixed Electronic/Ionic Semiconductor Driving Lithium-Ion Transfer for Photo-Rechargeable Electrode. *Advanced Sustainable Systems* **2018**, *2* (5), 1700166.
(60) Tributsch, H. Photo-Intercalation: Possible Application in Solar Energy Devices. *Appl. Phys.* **1980**, *23* (1), 61–71.
(61) Tributsch, H. Photoelectrochemical Energy Conversion Involving Transition Metal D-States and Intercalation of Layer Compounds. In *Solar Energy Materials*; Springer Berlin Heidelberg: Berlin, Heidelberg, 1982; Vol. 49, pp 127–175.
(62) Tributsch, H. Photo-Electrochemical Studies on Intercalation and Semiconducting Intercalation Compounds. *Solid State Ionics* **1983**, *9–10*, 41–57.
(63) Betz, G.; Tributsch, H.; Marchand, R. Hydrogen Insertion (Intercalation) and Light Induced Proton Exchange at TiO_2(B) -Electrodes. *J Appl Electrochem* **1984**, *14* (3), 315–322.
(64) Tributsch, H. Interfacial Processes Involving Strong Electronic Interactions in Solar Energy Conversion and Storage. *Journal of Photochemistry* **1985**, *29* (1), 89–113.
(65) Tributsch, H. Photo-Intercalation: Possible Application in Solar Energy Devices. *Appl. Phys.* **1980**, *23* (1), 61–71.
(66) Abramovich, M.; Gorochov, O.; Tributsch, H. Photo-deintercalation phenomena studied with layer-type hafnium diselenide, J. Electroanal. Chem. **1983**.
(67) Gorochov, O.; Schleich, D.; Tributsch, H. ZrS_2 to Be Published.
(68) H. Tributsch, Solid State Ioncs, 9 - 10 (**1983**) 41.

(69) D. Schleich. H.-M. Kiihne and H. Tributsch, to Be Published.
(70) Levy-Clement, C.; Theys, B. Photointercalation and Photodeposition of Copper in P-Type Lamellar InSe. *J. Electrochem. Soc.* **1984**, *131* (6), 1300.
(71) Betz, G.; Fiechter, S.; Tributsch, H. Photon Energy Conversion and Storage with a Light-driven Insertion Reaction. *Journal of Applied Physics* **1987**, *62* (11), 4597–4605.
(72) Betz, B.; Tributsch, H.; Fiechter, S. Photointercalation and Optical Information Storage Using $Cu_{6-x}PS_5$ I, ECS, **1984**.
(73) G. Betz, M. Kiinst, J. G. Rabe and H. Tributsch, to Be Published.
(74) Ahmad, S.; George, C.; Beesley, D. J.; Baumberg, J. J.; De Volder, M. Photo-Rechargeable Organo-Halide Perovskite Batteries. *Nano Lett.* **2018**, *18* (3), 1856–1862.
(75) Ren, C.; Zhou, Q.; Jiang, W.; Li, J.; Guo, C.; Zhang, L.; Su, J. Investigation of Germanium Selenide Electrodes for the Integrated Photo-Rechargeable Battery. *International Journal of Energy Research* **2020**, *44* (7), 6015–6022.
(76) Lee, A.; Vörös, M.; Dose, W. M.; Niklas, J.; Poluektov, O.; Schaller, R. D.; Iddir, H.; Maroni, V. A.; Lee, E.; Ingram, B.; Curtiss, L. A.; Johnson, C. S. Photo-Accelerated Fast Charging of Lithium-Ion Batteries. *Nat Commun* **2019**, *10* (1), 1–7.
(77) Boruah, B. D.; Wen, B.; De Volder, M. Light Rechargeable Lithium-Ion Batteries Using V_2O_5 Cathodes. *Nano Letters* **2021**, *21* (8), 3527–3532.
(78) Wei, Z.; Liu, D.; Hsu, C.; Liu, F. All-Vanadium Redox Photoelectrochemical Cell: An Approach to Store Solar Energy. *Electrochemistry Communications* **2014**, *45*, 79–82.
(79) Podjaski, F.; Kröger, J.; Lotsch, B. V. Toward an Aqueous Solar Battery: Direct Electrochemical Storage of Solar Energy in Carbon Nitrides. *Advanced Materials* **2018**, *30* (9), 1705477.
(80) Vetter, J.; Novák, P.; Wagner, M. R.; Veit, C.; Möller, K.-C.; Besenhard, J. O.; Winter, M.; Wohlfahrt-Mehrens, M.; Vogler, C.; Hammouche, A. Ageing Mechanisms in Lithium-Ion Batteries. *Journal of Power Sources* **2005**, *147* (1–2), 269–281.
(81) Castro, L.; Dedryvère, R.; Ledeuil, J.-B.; Bréger, J.; Tessier, C.; Gonbeau, D. Aging Mechanisms of $LiFePO_4$ // Graphite Cells Studied by XPS: Redox Reaction and Electrode/Electrolyte Interfaces. *J. Electrochem. Soc.* **2012**, *159* (4), A357–A363.
(82) Menkin, S.; Golodnitsky, D.; Peled, E. Artificial Solid-Electrolyte Interphase (SEI) for Improved Cycleability and Safety of Lithium–Ion Cells for EV Applications. *Electrochemistry Communications* **2009**, *11* (9), 1789–1791.
(83) Azcarate, I.; Yin, W.; Méthivier, C.; Ribot, F.; Laberty, C.; Grimaud, A. Assessing the Oxidation Behavior of EC: DMC Based Electrolyte on Non-Catalytically Active Surface. 30.
(84) Characterization of Lithium Alkyl Carbonates by X-ray Photoelectron Spectroscopy: Experimental and Theoretical Study | The Journal of Physical Chemistry B
(85) Kawamura, T.; Okada, S.; Yamaki, J. Decomposition Reaction of $LiPF_6$-Based Electrolytes for Lithium Ion Cells. *Journal of Power Sources* **2006**, *156* (2), 547–554.
(86) Yoshida, T.; Takahashi, M.; Morikawa, S.; Ihara, C.; Katsukawa, H.; Shiratsuchi, T.; Yamaki, J. Degradation Mechanism and Life Prediction of Lithium-Ion Batteries. *J. Electrochem. Soc.* **2006**, *153* (3), A576.
(87) Murakami, M.; Yamashige, H.; Arai, H.; Uchimoto, Y.; Ogumi, Z. Direct Evidence of LiF Formation at Electrode/Electrolyte Interface by ^{7}Li and ^{19}F Double-Resonance Solid-State NMR Spectroscopy. *Electrochemical and Solid-State Letters* **2011**, *14* (9), A134.
(88) Sasaki, T.; Jeong, S.-K.; Abe, T.; Iriyama, Y.; Inaba, M.; Ogumi, Z. Effect of an Alkyl Dicarbonate on Li-Ion Cell Performance. *J. Electrochem. Soc.* **2005**, *152* (10), A1963.

(89) Bouteau, G.; Van-Nhien, A. N.; Sliwa, M.; Sergent, N.; Lepretre, J.-C.; Gachot, G.; Sagaidak, I.; Sauvage, F. Effect of Standard Light Illumination on Electrolyte's Stability of Lithium-Ion Batteries Based on Ethylene and Di-Methyl Carbonates. *Scientific Reports* **2019**, *9* (1), 135.

(90) Strmcnik, D.; Castelli, I. E.; Connell, J. G.; Haering, D.; Zorko, M.; Martins, P.; Lopes, P. P.; Genorio, B.; Østergaard, T.; Gasteiger, H. A.; Maglia, F.; Antonopoulos, B. K.; Stamenkovic, V. R.; Rossmeisl, J.; Markovic, N. M. Electrocatalytic Transformation of HF Impurity to H_2 and LiF in Lithium-Ion Batteries. *Nat Catal* **2018**, *1* (4), 255–262.

(91) Dedryvère, R.; Foix, D.; Franger, S.; Patoux, S.; Daniel, L.; Gonbeau, D. Electrode/Electrolyte Interface Reactivity in High-Voltage Spinel $LiMn_{1.6}Ni_{0.4}O_4$/$Li_4Ti_5O_{12}$ Lithium-Ion Battery. *J. Phys. Chem. C* **2010**, *114* (24), 10999–11008.

(92) Huang, C.; Zhuang, S.; Tu, F. Electrode/Electrolyte Interfacial Behaviors of $LiCoO_2$/Mixed Graphite Li-Ion Cells during Operation and Storage. *J. Electrochem. Soc.* **2012**, *160* (2), A376.

(93) Xu, K. Electrolytes and Interphases in Li-Ion Batteries and Beyond. *Chem. Rev.* **2014**, *114* (23), 11503–11618.

(94) Electrolytes and Interphases in Li-Ion Batteries and Beyond | Chemical Reviews.

(95) Lu, D.; Xu, M.; Zhou, L.; Garsuch, A.; Lucht, B. L. Failure Mechanism of Graphite/$LiNi_{0.5}Mn_{1.5}O_4$ Cells at High Voltage and Elevated Temperature. *J. Electrochem. Soc.* **2013**, *160* (5), A3138.

(96) Sasaki, T.; Abe, T.; Iriyama, Y.; Inaba, M.; Ogumi, Z. Formation Mechanism of Alkyl Dicarbonates in Li-Ion Cells. *Journal of Power Sources* **2005**, *150*, 208–215.

(97) Gireaud, L.; Grugeon, S.; Laruelle, S.; Pilard, S.; Tarascon, J.-M. Identification of Li Battery Electrolyte Degradation Products Through Direct Synthesis and Characterization of Alkyl Carbonate Salts. *J. Electrochem. Soc.* **2005**, *152* (5), A850.

(98) Jeong, S.-K.; Inaba, M.; Iriyama, Y.; Abe, T.; Ogumi, Z. Interfacial Reactions between Graphite Electrodes and Propylene Carbonate-Based Solutions: Electrolyte-Concentration Dependence of Electrochemical Lithium Intercalation Reaction. *Journal of Power Sources* **2008**, *175* (1), 540–546.

(99) Xu, K. Nonaqueous Liquid Electrolytes for Lithium-Based Rechargeable Batteries. *Chem. Rev.* **2004**, *104* (10), 4303–4418.

(100) Shkrob, I. A.; Zhu, Y.; Marin, T. W.; Abraham, D. Reduction of Carbonate Electrolytes and the Formation of Solid-Electrolyte Interface (SEI) in Lithium-Ion Batteries. 2. Radiolytically Induced Polymerization of Ethylene Carbonate. *The Journal of Physical Chemistry C* **2013**, *117* (38), 19270–19279.

(101) Marom, R.; Haik, O.; Aurbach, D.; Halalay, I. C. Revisiting $LiClO_4$ as an Electrolyte for Rechargeable Lithium-Ion Batteries. *Journal of The Electrochemical Society* **2010**, *157* (8), A972.

(102) Nie, M.; Abraham, D. P.; Chen, Y.; Bose, A.; Lucht, B. L. Silicon Solid Electrolyte Interphase (SEI) of Lithium Ion Battery Characterized by Microscopy and Spectroscopy. *J. Phys. Chem. C* **2013**, *117* (26), 13403–13412.

(103) Xu, K.; Zhuang, G. V.; Allen, J. L.; Lee, U.; Zhang, S. S.; Ross, P. N.; Jow, T. R. Syntheses and Characterization of Lithium Alkyl Mono- and Dicarbonates as Components of Surface Films in Li-Ion Batteries. *The Journal of Physical Chemistry B* **2006**, *110* (15), 7708–7719.

(104) Li, S. R.; Chen, C. H.; Xia, X.; Dahn, J. R. The Impact of Electrolyte Oxidation Products in $LiNi_{0.5}Mn_{1.5}O_4$ /$Li_4Ti_5O_{12}$ Cells. *J. Electrochem. Soc.* **2013**, *160* (9), A1524–A1528.

(105) Xing, L.; Li, W.; Wang, C.; Gu, F.; Xu, M.; Tan, C.; Yi, J. Theoretical Investigations on Oxidative Stability of Solvents and Oxidative Decomposition Mechanism of Ethylene Carbonate for Lithium Ion Battery Use. *The Journal of Physical Chemistry B* **2009**, *113* (52), 16596–16602.

(106) Yamada, Y.; Furukawa, K.; Sodeyama, K.; Kikuchi, K.; Yaegashi, M.; Tateyama, Y.; Yamada, A. Unusual Stability of Acetonitrile-Based Superconcentrated Electrolytes for Fast-Charging Lithium-Ion Batteries. *J. Am. Chem. Soc.* **2014**, *136* (13), 5039–5046.

(107) Dedryvère, R.; Leroy, S.; Martinez, H.; Blanchard, F.; Lemordant, D.; Gonbeau, D. XPS Valence Characterization of Lithium Salts as a Tool to Study Electrode/Electrolyte Interfaces of Li-Ion Batteries. *J. Phys. Chem. B* **2006**, *110* (26), 12986–12992.

(108) Liu, H.; Tong, Y.; Kuwata, N.; Osawa, M.; Kawamura, J.; Ye, S. Adsorption of Propylene Carbonate (PC) on the $LiCoO_2$ Surface Investigated by Nonlinear Vibrational Spectroscopy. *J. Phys. Chem. C* **2009**, *113* (48), 20531–20534.

(109) Lei, J.; Li, L.; Kostecki, R.; Muller, R.; McLarnon, F. *Characterization of SEI Layers on $LiMn_2O_4$ Cathodes with In-Situ Spectroscopic Ellipsometry*; LBNL--55939, 837416; **2004**; p LBNL--55939, 837416.

(110) Wang, Z.; Sun, Y.; Chen, L.; Huang, X. Electrochemical Characterization of Positive Electrode Material Li $Ni_{1/3}$ $Co_{1/3}$ $Mn_{1/3}$ O_2 and Compatibility with Electrolyte for Lithium-Ion Batteries. *J. Electrochem. Soc.* **2004**, *151* (6), A914.

(111) Yang, L.; Ravdel, B.; Lucht, B. L. Electrolyte Reactions with the Surface of High Voltage $LiNi_{0.5}Mn_{1.5}O_4$ Cathodes for Lithium-Ion Batteries. *Electrochem. Solid-State Lett.* **2010**, *13* (8), A95.

(112) Norberg, N. S.; Lux, S. F.; Kostecki, R. Interfacial Side-Reactions at a $LiNi_{0.5}Mn_{1.5}O_4$ Electrode in Organic Carbonate-Based Electrolytes. *Electrochemistry Communications* **2013**, *34*, 29–32.

(113) Liu, N.; Li, H.; Wang, Z.; Huang, X.; Chen, L. Origin of Solid Electrolyte Interphase on Nanosized $LiCoO_2$. *Electrochem. Solid-State Lett.* **2006**, *9* (7), A328.

(114) Wang, Z.; Huang, X.; Chen, L. Performance Improvement of Surface-Modified $LiCoO_2$ Cathode Materials: An Infrared Absorption and X-Ray Photoelectron Spectroscopic Investigation. *J. Electrochem. Soc.* **2003**, *150* (2), A199.

(115) Yu, L.; Liu, H.; Wang, Y.; Kuwata, N.; Osawa, M.; Kawamura, J.; Ye, S. Preferential Adsorption of Solvents on the Cathode Surface of Lithium Ion Batteries. *Angew. Chem.* **2013**, *125* (22), 5865–5868.

(116) Kanamura, K.; Toriyama, S.; Shiraishi, S.; Ohashi, M.; Takehara, Z. Studies on Electrochemical Oxidation of Non-Aqueous Electrolyte on the $LiCoO_2$ Thin Film Electrode. *Journal of Electroanalytical Chemistry* **1996**, *419* (1), 77–84.

(117) Shu, J. Study of the Interface Between $Li_4Ti_5O_{12}$ Electrodes and Standard Electrolyte Solutions in 0.0–5.0 V. *Electrochem. Solid-State Lett.* **2008**, *11* (12), A238.

(118) Yamada, Y.; Koyama, Y.; Abe, T.; Ogumi, Z. Correlation between Charge−Discharge Behavior of Graphite and Solvation Structure of the Lithium Ion in Propylene Carbonate-Containing Electrolytes. *J. Phys. Chem. C* **2009**, *113* (20), 8948–8953.

(119) Soon-Ki Jeong; Minoru Inaba; Yasutoshi Iriyama; Takeshi Abe; Zempachi Ogumi. Electrochemical Intercalation of Lithium Ion within Graphite from Propylene Carbonate Solutions - IOPscience https://iopscience.iop.org/article/10.1149/1.1526781/meta (accessed **2021** -08 -17).

(120) Lithium Ion Battery Graphite Solid Electrolyte Interphase Revealed by Microscopy and Spectroscopy | The Journal of Physical Chemistry C.

(121) Liu, Y.; Lin, D.; Liang, Z.; Zhao, J.; Yan, K.; Cui, Y. Lithium-Coated Polymeric Matrix as a Minimum Volume-Change and Dendrite-Free Lithium Metal Anode. *Nat Commun* **2016**, *7* (1), 1–9.

(122) Molecular Dynamics Simulation Studies of the Structure of a Mixed Carbonate/$LiPF_6$ Electrolyte near Graphite Surface as a Function of Electrode Potential | The Journal of Physical Chemistry C https://pubs.acs.org/doi/full/10.1021/jp2101539 (accessed **2021** -08 -17).

(123) Harilal, S. S.; Allain, J. P.; Hassanein, A.; Hendricks, M. R.; Nieto-Perez, M. Reactivity of Lithium Exposed Graphite Surface. *Applied Surface Science* **2009**, *255* (20), 8539–8543.

(124) Tasaki, K.; Goldberg, A.; Lian, J.-J.; Walker, M.; Timmons, A.; Harris, S. J. Solubility of Lithium Salts Formed on the Lithium-Ion Battery Negative Electrode Surface in Organic Solvents. *J. Electrochem. Soc.* **2009**, *156* (12), A1019.

(125) Xu, K.; Lam, Y.; Zhang, S. S.; Jow, T. R.; Curtis, T. B. Solvation Sheath of Li^+ in Nonaqueous Electrolytes and Its Implication of Graphite/Electrolyte Interface Chemistry. *J. Phys. Chem. C* **2007**, *111* (20), 7411–7421.

(126) Xu, K. Whether EC and PC Differ in Interphasial Chemistry on Graphitic Anode and How. *J. Electrochem. Soc.* **2009**, *156* (9), A751.

(127) Ventosa, E.; Madej, E.; Zampardi, G.; Mei, B.; Weide, P.; Antoni, H.; La Mantia, F.; Muhler, M.; Schuhmann, W. Solid Electrolyte Interphase (SEI) at TiO_2 Electrodes in Li-Ion Batteries: Defining *Apparent* and *Effective* SEI Based on Evidence from X-Ray Photoemission Spectroscopy and Scanning Electrochemical Microscopy. *ACS Appl. Mater. Interfaces* **2017**, *9* (3), 3123–3130.

(128) Han, C.; Yang, D.; Yang, Y.; Jiang, B.; He, Y.; Wang, M.; Song, A.-Y.; He, Y.-B.; Li, B.; Lin, Z. Hollow Titanium Dioxide Spheres as Anode Material for Lithium Ion Battery with Largely Improved Rate Stability and Cycle Performance by Suppressing the Formation of Solid Electrolyte Interface Layer. *J. Mater. Chem. A* **2015**, *3* (25), 13340–13349.

(129) Parimalam, B. S.; Lucht, B. L. Reduction Reactions of Electrolyte Salts for Lithium Ion Batteries: $LiPF_6$, $LiBF_4$, LiDFOB, LiBOB, and LiTFSI. *Journal of The Electrochemical Society* **2018**, *165* (2), A251–A255.

(130) Suo, L.; Borodin, O.; Sun, W.; Fan, X.; Yang, C.; Wang, F.; Gao, T.; Ma, Z.; Schroeder, M.; von Cresce, A.; Russell, S. M.; Armand, M.; Angell, A.; Xu, K.; Wang, C. Advanced High-Voltage Aqueous Lithium-Ion Battery Enabled by "Water-in-Bisalt" Electrolyte. *Angewandte Chemie International Edition* **2016**, *55* (25), 7136–7141.

(131) Suo, L.; Borodin, O.; Gao, T.; Olguin, M.; Ho, J.; Fan, X.; Luo, C.; Wang, C.; Xu, K. "Water-in-Salt" Electrolyte Enables High-Voltage Aqueous Lithium-Ion Chemistries. *Science* **2015**, *350* (6263), 938–943.

(132) Dubouis, N.; Lemaire, P.; Mirvaux, B.; Salager, E.; Deschamps, M.; Grimaud, A. The Role of the Hydrogen Evolution Reaction in the Solid–Electrolyte Interphase Formation Mechanism for " Water-in-Salt " Electrolytes. *Energy & Environmental Science* **2018**, *11* (12), 3491–3499.

CHAPTER II: Experimental section

CHAPTER II: Experimental section

The main objective of this chapter is a description of the experimental part of the work, from the synthesis of the films, their structural characterizations to their (photo-)electrochemical characterizations, and in situ or post mortem characterizations.

II.1. Electrode preparation

II.1.1. FTO substrates

The TiO_2 material is deposited on a Fluorine-doped tin oxide (FTO) substrate purchased from SOLEMS (YSUB/ASAHI120/1: 10*30 mm / resistivity 80 $\Omega.cm^{-2}$, with an 80-100 nm of FTO on glass. Fluorine-doped tin oxide is a SnO_2-based wide band gap semiconductor with fluorine doping. The substrates are cleaned with ethanol and acetone before the dipping process.

II.1.2. Titania precursor solution

11.6 g of $TiCl_4$ (Sigma Aldrich, >99.9 % trace metals basis) is added dropwise in 14.3 g of cold absolute ethanol (VWR, AnalaR NORMAPUR® ACS, reag. Ph. Eur analytical reagent (99.9 %) with a molar ratio of 1($TiCl_4$): 5(EtOH). This solution will be referred as “precursor solution”. When stored a 4°C, the solution can be used for over 5 months.

II.1.3. Dip-coating solutions

100mg of block-copolymers PB-b-PEO (Poly(1,4-butadiene)-bpoly(ethylene oxide), PB-b-PEO:P4515-BdEO; M.W.(PB)=11800 $g.mol^{-1}$; M.W.(PEO)=13500 $g.mol^{-1}$) purchased from Polymer Source, is dissolved in 5.0 g of ethanol and 0.4 g of distilled water (18.2 MΩ.cm). The solution is stirred and heated at 70°C during 1 hour to complete the dissolution of the polymer. The solution is cooled to room temperature and the titania “precursor solution” is added dropwise into the PB-b-PEO solution. The concentration of inorganic salts in the final solution is 2 M (1.6 g of “precursor solution”). The FTO pre-cleaned is then dip-coated into this solution at a withdrawal speed of 2.5 $mm.s^{-1}$ in dry atmosphere (< 5 % relative humidity). The back side of the FTO-dipped substrate is cleaned with an ethanol soaked paper. The TiO_2 film is then heated for 1h in a furnace at 500°C in air (static atmosphere) to induce the crystallization of the anatase and decompose the block-copolymer. The thickness of one layer-film is expected to be around 120 nm. To obtain a 500 nm-thick film, a multilayer process is used.

After the cleaning of the back of the FTO an intermediate pre-heating treatment is used at 350°C during 1-3 min to start the crystallization and start the degradation of the polymer. 4 layers are needed to achieve the desired 500 nm. A final thermal treatment at 500 °C for 1 h is then necessary to complete the polymer degradation and allow the inorganic wall to crystallize. The electrode preparation process is summarized in the following **figure 23**.

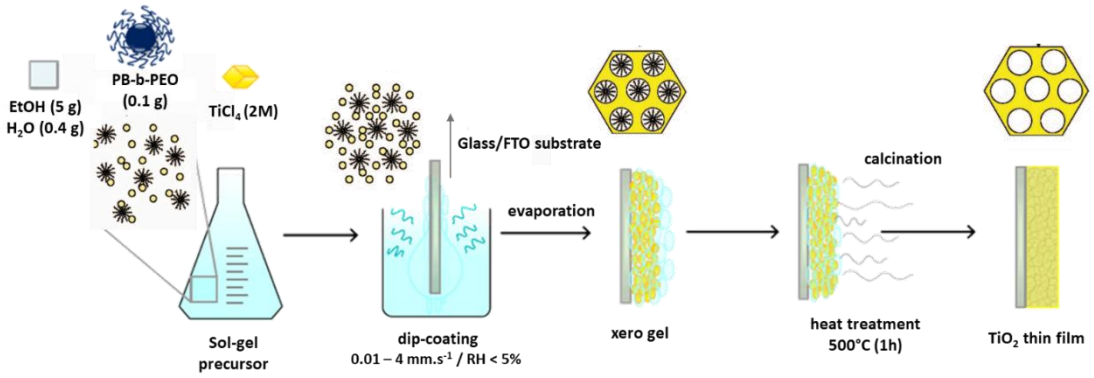

***Figure 23**: Sol-gel dip coating thin film fabrication process. Adapted from Hilliard.*[1]

II.2. Film Characterizations

II.2.1. Spectroscopic Ellipsometry

Ellipsometry measurements were used as a fast method to evaluate the thickness of the films and also to evaluate the porosity of the films. It was performed on a UV-visible (from 240 to 1000 nm) variable angle spectroscopic ellipsometer (VASE – 2000 U Woollam), and the data analyses were performed with the CompleteEASE software using Cauchy models. Environmental ellipsometric porosimetry was performed through a water adsorption/desorption isotherm using an atmospheric control chamber as described in Boissiere et al[2].

II.2.2. X-Ray Diffraction

The XRD study was performed on a Bruker D8 advance diffractometer (Bruker Corporation, Billerica, MA, USA) using Cu-Kα radiation (λ = 15,418°A at 45 KV and 40 mA, 0.05 step size, and 150.4 s step time over a range from 10 to 80°. XRD were done on the mesoporous PB-b-PEO TiO_2 (2M, 500 nm-thick), TiO_2 anatase, on the FTO substrate.

II.2.3. Scanning Electron Microscopy

The microstructure of the films and film thickness were observed by Scanning Electron Microscopy with Field Emission Gun (SEM-FEG) on a SU-70 Hitachi FEG-SEM, instruments facilitated by the IMPC (Institut des Matériaux de Paris Centre FR2482) financially supported by the C'Nano projects of the Region Ile-de-France. FEG-SEM images were collected under 10 kV tension. Measurements were performed with MONTERO David from the IMPC (Institut des Matériaux de Paris Centre FR2482). To image the edge of the sample, the sample is cut using a diamond cutter. For the electrochemical post-mortem analysis, all the samples are rinsed in order to remove the remaining salt. For the electrode film studied in LP30 electrolyte, it is rinsed in a glove box with DMC. For the one used in WIS, the sample is rinsed with deionized water. The samples are stored fort two weeks maximum prior to being analyzed.

II.3. Electrochemical and Photo-electrochemical measurements

II.3.1. Electrode contact

Contacts of the working electrode were made by placing the denuded part of a WCT30 wire (Radiospare) directly onto the FTO (top part, which is not covered by the TiO_2) with copper Radiospare tape (1 cm width, 4.5 $N.cm^{-1}$ / RS 542-5460), a Kapton tape (3 M 92, 33 m * 19 mm * 0.08 mm) purchased from Radiospare is used to delimitate 1 cm^2 of the TiO_2 in contact with the electrolyte (**figure 24**).

Figure 24: *Picture of the FTO/TiO_2 electrode as describe above. With the Kapton tape used to delimitate the TiO_2 exposed surface at 1 cm^2.*

II.3.2. Cell with LP30 electrolyte

For the counter- and reference electrodes, two lithium foils (Sigma Aldrich) are directly placed on the denuded part of a WCT30 wire (Radiospare). The three-electrode cell is made of a sealed glass container (transparent in the visible range) assembled in an argon glovebox using a silicon cap (Saint-Gobain, Versilic). LP30 (1 M $LiPF_6$ salt in ethylene carbonate: dimethyl carbonate. EC: DMC 1: 1 (v: v); <15 ppm H_2O <50 ppm HF, Sigma Aldrich) electrolyte is added in order to cover ≃ 1 cm^2 of the TiO_2 electrode. The electrolyte is used without any purification. Before any experiment, 10 CV cycles between 2.6 and 1.4 V vs Li^+/Li at 0.5 mV/s are needed to stabilize the electrode, the first and last CVs cycles are shown in **annex II**.

II.3.3. Cell with Water-in-salt (WIS) electrolyte

Water in salt (WIS) preparation:

The 20 mol/kg (m, molality) water in salt electrolyte is prepared by adding 4.74 g of distilled water (18.2 MΩ.cm) in 27.13 g of LiTFSI (Bis(trifluoromethane)sulfonamide lithium, 99.9 %, extra dry <20 ppm H_2O) purchased from solvionic.

The cell:

For the counter and the reference electrode a 23 cm platinum wire and a Ag/AgCl (A-013429: RE-1CP Reference Electrode (Ag/AgCl/Saturated KCl – length: 92 mm- OD: 6 mm)) is used respectively, purchased from Biologic.

The three-electrode cell is assembled in a glass cell, (transparent in the visible range) (A-012669: SVC-3 Oxygen-free Voltammetry cell) purchased from Biologic. The WIS electrolyte is added in order to cover $\simeq$ 1 cm^2 of the TiO_2 electrode. It is purged of the oxygen by bubbling argon inside the electrolyte to avoid reactions as in the Paolella's study[3] where the oxygen in solution reacted with the photo-electron and leading in fine to SEI.

II.3.4. Photoelectrochemical set-up

Potentiostat:

AMETEK Solartron pstat 1 MS/s, Bio-logic SP300 and Princeton 273A were used for electrochemical characterizations. AMETEK Solartron pstat 1 MS/s was used for all the photo-electrochemical measurements, Bio-logic SP300 was used for all electrochemical measurements (without light) and Princeton 263A was used for all the electrochemical UV-VIS-NIR coupled measurements.

II.3.5. Description of cyclic voltammetry experiments

Before any further experiment 7 CV cycles between -0.6 and -1.4 V vs Ag/AgCl (KCl sat) at 0.5 mV/s are needed to stabilize the electrode, the first and last CV cycles are shown in **annex II**. Indeed, at lower potential the FTO substrate is not stable anymore. During all the experiments a flow of argon is maintained on top of the solution.

The capacity of the TiO_2 material is calculated by integrating the oxidation wave. Indeed, we supposed that during the oxidation the only phenomenon is the extraction of the lithium in contrary during the reduction the HER occur and would lead to overvalue the capacity. The next equation is used to calculate the capacity:

$Q = \frac{I*t}{m}$ with Q: capacity (mAh/g), I: current (A), t: time (h), m: mass (g)

The mass of the electrode is determined by the equation: density*Surface area* thickness. The density is 0.85 since the porosity has been evaluated from ellipsoporosimetry at 15 %; the surface area has been delimitated by the Kapton tape to have 1 cm^2; and the thickness has been evaluated after each TiO_2 films after their synthesis by Spectroscopic Ellipsometry.

II.3.6. Description of galvanostatic experiments

The current applied for the 2C rate has been calculated from the same equation:

$Q = \frac{I*t}{m}$ with Q: capacity (mAh/g), I: current (A), t: time (h), m: mass (g)

Since a 2C is a galvanostatic experiment during 30 min we can calculate the current needed from the capacity evaluated during the CV and the mass of the material.

Here the so called discharge is the insertion of lithium ions so the reduction reaction from 2.2 V to 1.6 V vs Li^+/Li for the LP30 and -0.8 V to -1.3 V vs Ag/AgCl KCl saturated for the WIS electrolyte since we are considering the half-cells WE: TiO_2//electrolyte//Ref/ CE. The charge corresponds to the extraction of the lithium ions so the oxidation reaction from 1.6 V to 2.2 V and from -1.3 V to -0.8 V respectively.

The galvanostatic experiment is then plotted by multiplying the applied current by the time divided by the mass pre-evaluated. The calculated capacity over the cycle is then plotted versus the measured potential.

If the galvanostatic experiment is plotted versus the lithium composition a simple cross multiplication starting from the capacities measured and by taking into account that Li_1TiO_2 = 335 mAh/g.

II.3.7. Description of chopped potentiostatic experiments

From the CV, 2 potentials are interesting. The potential where the insertion of lithium starts and the potential where the extraction start. Thanks to these potential and a periodic illumination, photo-current occur and could be measured. The period of illumination is fixed at 30 seconds in order to have a high enough photo-current without changing too much the composition during the illumination.

Xenon Lamp:

A Newport xenon arc lamp was used throughout photo-electrochemical experiments (**spectrum in figure 25a**). Newport model 6258 300 W ozone free lamp working was used at 280 W for photo-electrochemical measurements in an Arc Lamp Housing enclosure, model 67001. This was powered by a Newport power supply 69911 in junction with an Oriel liquid filter 61945 (250-950 nm transmission) filled with water in order to filter the IR light and resultant heat (**spectrum in figure 25b**) an additional filter AM (Air Mass) 1.5 is added. This filter is a reference used to simulate the sun lights that need to pass through the Earth atmosphere to reach the surface of the Earth when the sun is at a zenith angle of 37°. AM 1 being the reference when the sun lights need to pass through the Earth atmosphere to reach the sea level and AM 0 the extraterrestrial reference (**annex I**)[4]. All photo-electrochemical measurements were done at 1 SUN, the light output was verified by a calibrator Newport model 91150V.

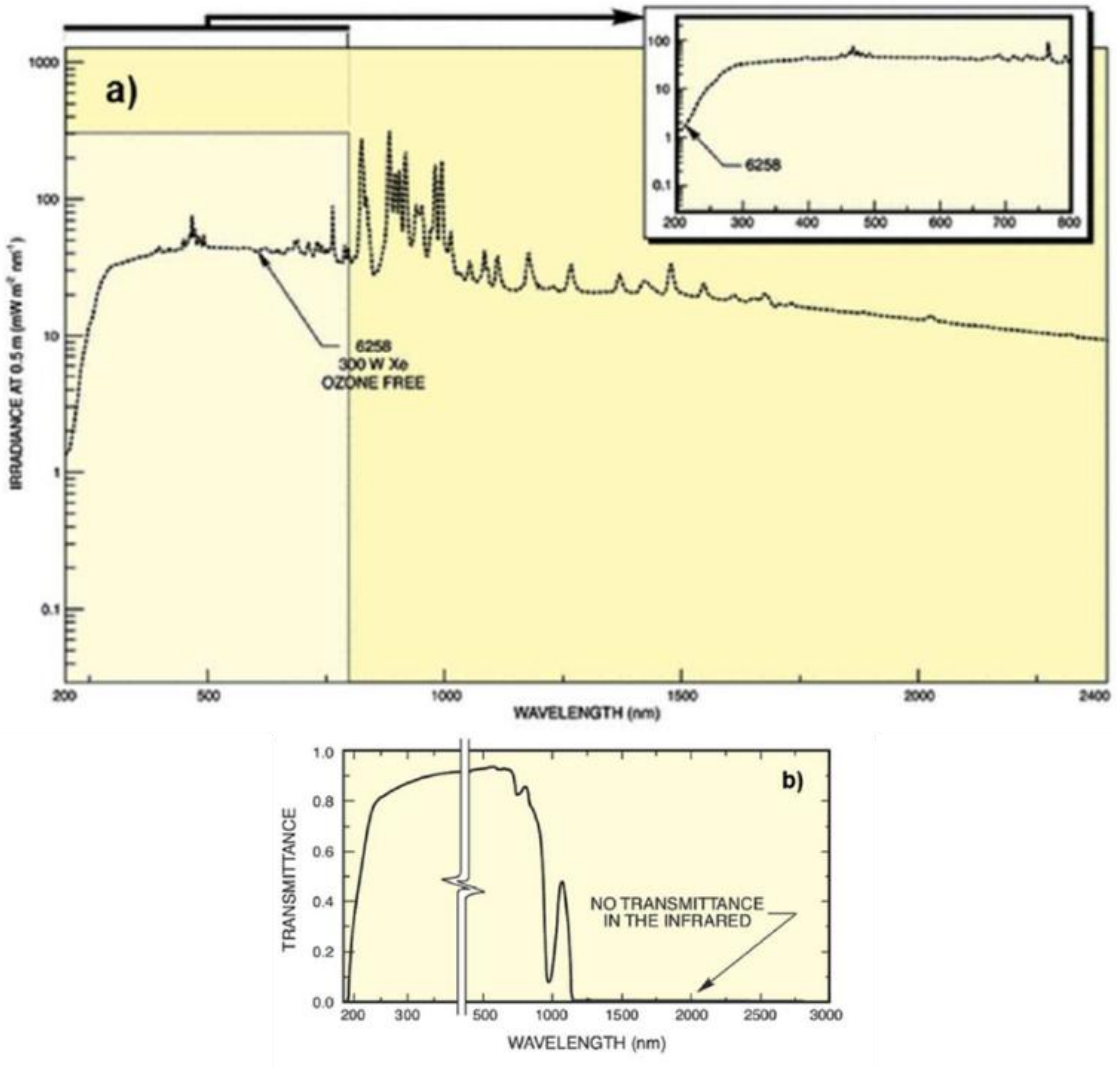

***Figure 25**: Newport 300 W Xe arc lamp ozone free spectrum (model 6258) (a) and Oriel liquid filter 61945 transmission (250-950 nm) (b).*

A particular attention is made when the cell used for the experiment are in glass. Indeed, a part of the UV lights will be cut by the glass. According to the International Ultraviolet Association (IUVA) most of the glasses are transparent until 330 nm and below they are blocking (Transparent for UVA, blocking for UV B-C)[5]: UVA 320 - 400 nm; UVB 280 - 320 nm; UVC <280 nm.

To sum up, we irradiate the electrode with a spectrum window of 330-950 nm by taking into account the lamp spectrum an all the filters.

II.4. In-situ UV-VIS-NIR spectroscopy

The TiO_2 absorption is measure by UV-VIS-NIR spectroscopy using a spectrophotometer Carry 5000 purchased from Agilent with 200-3300 nm of range is used. For the operando measurement during galvanostatic cycle, a large liquid quartz cell is used. A 3-electrodes set up is used with FTO/TiO_2 //WIS (20 m) //Pt /Ag, AgCl (KCl sat). A particular attention is made to aligning the TiO_2 active part of the electrode with the spectrophotometer beam, without the counter or the references electrodes in the way of the beam. Another cell with FTO//WIS (20 m) without the TiO_2 is used as a reference.

II.5. Gas Chromatography

The H_2 formation has been characterized by a gas chromatograph (GC) (SRI 8610C) equipped with a packed Molecular Sieve 5 Å column for permanent gases separation and a packed Haysep-D column for light hydrocarbons separation was used. Argon was used as carrier gas. A flame ionization detector (FID) coupled to a methanizer was used to quantify CO, methane and hydrocarbons while a thermal conductivity detector (TCD) was used to quantify H_2. The GC has been calibrated for H_2 by measuring different but well known amount of H_2/CO_2 in a vial. From these measures a calibration curve is plotted between the area of the H_2 signal and the concentration of H_2 in ppm introduced in the GC. This calibration curve allows us to deduct from the area of the H_2 signal of our sample the concentration in ppm of H_2 contained inside the sample.

GC were used to confirm the formation of hydrogen at the working electrode. We used a two compartment (**figure 26**) cell in order to separate the counter electrode from the working electrode. Indeed, the hydrogen could be formed at the counter. The system needs also to be removed from any trace of oxygen, so argon was bubbled in both compartments during 30 minutes and then sealed. Knowing the estimated volume of our electrochemical cell and the volume of WIS added in the cell the remaining gas volume could be deduced. The gas from the working electrode could be then analyzed using a precision syringe and introducing in the GC. The signal between 0.9- 1 min of retention time is attributed to the H_2.

Normally thanks to the area of the signal and the calibration data it is possible to evaluate the amount of H_2 in the syringe by adding the factor of dilution the amount in the cell and so the amount produced by the TiO_2. Unfortunately, the amount produced is to small (< 1 ppm) so the calibration data is not accurate in this range.

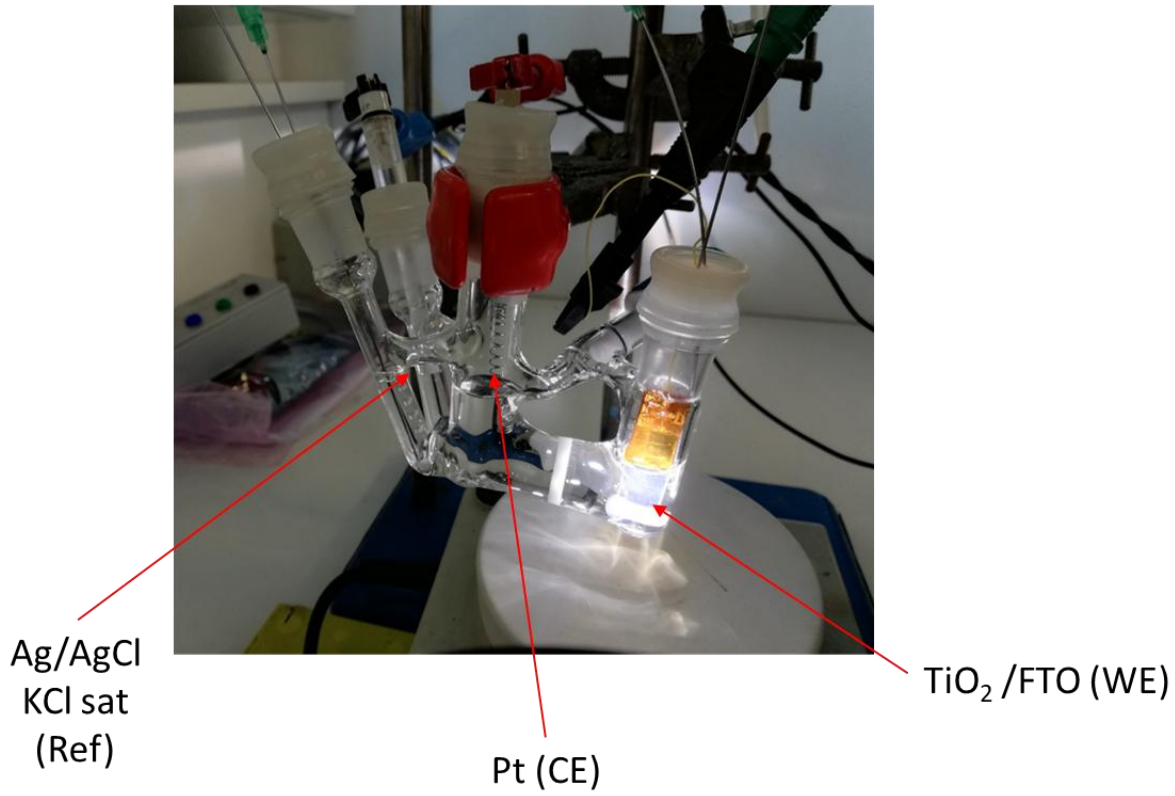

***Figure 26**: Picture of the 2 compartment set up. In the left compartment a platinum and a Ag/AgCl KCl saturated reference electrode are immerged in LiTFSI water in salt (WIS) 20 m. The right compartment is only composed of the TiO_2 working electrode. Both compartments are separated by a ceramic membrane and gas tight.*

Bibliography

(1) Hilliard, S. Water Splitting Photoelectrocatalysis: The Conception and Construction of a Photoelectrocatalytic Water Splitting Cell. 220.
(2) Boissiere, C.; Grosso, D.; Lepoutre, S.; Nicole, L.; Bruneau, A. B.; Sanchez, C. Porosity and Mechanical Properties of Mesoporous Thin Films Assessed by Environmental Ellipsometric Porosimetry. *Langmuir* **2005**, *21* (26), 12362–12371.
(3) Paolella, A.; Faure, C.; Bertoni, G.; Marras, S.; Guerfi, A.; Darwiche, A.; Hovington, P.; Commarieu, B.; Wang, Z.; Prato, M.; Colombo, M.; Monaco, S.; Zhu, W.; Feng, Z.; Vijh, A.; George, C.; Demopoulos, G. P.; Armand, M.; Zaghib, K. Light-Assisted Delithiation of Lithium Iron Phosphate Nanocrystals towards Photo-Rechargeable Lithium Ion Batteries. *Nature Communications* **2017**, *8*, 14643.
(4) Solar Simulation. Oriel Newport https://www.newport.com/p/81094.
(5) International Ultraviolet Association Inc - UV FAQs https://iuva.org/UV-FAQs/ (accessed **2021** -09 -02).

CHAPTER III: Structure Driven Electrocatalysis

TABLE of CONTENTS

CHAPTER III: Structure Driven Electrocatalysis

Introduction

In order to understand the mechanism under illumination a preliminary step is need. This chapter will investigate the mechanism under dark condition. Indeed, since we added water in the system, under reductive conditions the formation of dihydrogen (H_2) is expected even without light. The vision of utilizing hydrogen as a future energy carrier requires cost-effective, sustainable, and efficient H_2 production. While Pt and other precious metals are the best catalysts for the hydrogen evolution reaction (HER) in acidic media replacing rare and expensive electrocatalysts with earth-abundant materials would represent a significant step toward making H_2 a competitive alternative energy source and facilitate the transition to a hydrogen economy.[1] Although traditionally used as a (photo) electrocatalyst, TiO_2 is an exciting HER catalyst[2] that exhibits promising HER activity in crystalline[3] or amorphous materials.[4] However, its catalytic HER performance is currently limited by the density and reactivity of active sites, poor electrical transport.

TiO_2 is described as n-type semiconductor[5] and as insertion material.[6,7] The **figure 27 a and b** summarizes the evolution of TiO_2 nanoparticles (around 7 nm) over a discharge in a lithium battery cell as function of the phase composition distribution (a) and the electrochemical response (b).

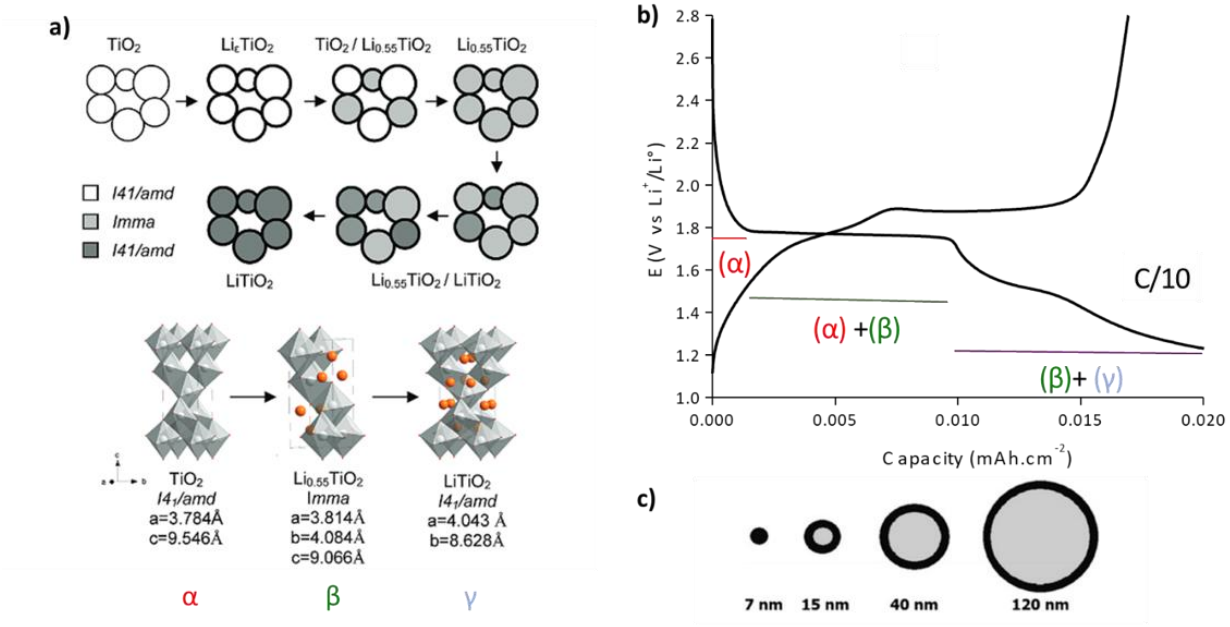

***Figure 27**: a) Phase transition upon Li insertion in anatase TiO_2 (gray) Ti, red = O, orange = Li)[8], b) distribution of the phases over a galvanostatic cycle at C/10 of a TiO_2 anatase, c) spatial distribution of $LiTiO_2$ phase in a lithium poor phase.*[9]

The Li insertion process in region (α) is attributed to the formation of a solid solution. This means that the insertion of Li ions into the anatase structure will happen without any phase transition, leading to a Li-poor phase denoted as $Li_{0.05\ to\ 0,1}TiO_2$ or $Li_\varepsilon TiO_2$. It presents the same space group as the anatase TiO_2 phase, namely, I41 /amd. Decreasing the size of the crystallites induces the extension of the solid solution domain[10]. Then a second phase appears, the Li-titanate *Imma* (β) phase or $Li_{0.55}TiO_2$, leading to a bi-phasic domain (α+β) (first plateau). After this biphasic domain, a second pseudo plateau is distinguished with the formation of a new phase, the tetragonal $LiTiO_2$ I41 /amd (γ) phase.

This demonstrates that the lithium phases distribution within the particles depends on its size (**figure 28**). [8,9,11] Furthermore, the use of nanoparticles within the electrode allows shortening the diffusion path of the lithium ion. This increases the accessible capacity of the nanoparticle at high cycling rate (typically 2C)[12]. Below 7 nm and at low speed (around C/10), one particle corresponds to one phase (alpha, beta or gamma). Above 7 nm, the nanoparticle exhibits a core-shell structure with a gradient of lithium composition (**figure 28c**).

Klerk et al[13] used modeling to study the lithiation of TiO_2 anatase with different radius (5, 20 and 50 nm) at 2 C-rate (0.5C and 2C). In this theoretical model, the cut-off is 5 nm (**figure 28**).

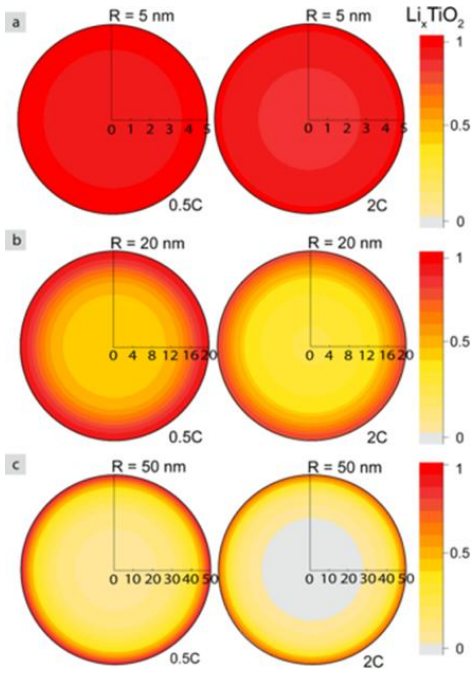

***Figure 28**: Final concentration profiles at the end of a simulation at 0.5C and 2C for particles with a radius of (a) 5, (b) 20, and (c) 50 nm.*[13]

Interestingly, the optical and semiconducting properties of Li_xTiO_2 seems to be driven by the quantity of lithium inserted in the structure, according to the mechanism described above. Although the TiO_2 structure was extensively characterized for the Li-ion insertion, the catalytic HER properties of lithiated TiO_2 remains unexplored. In this chapter, we were able to overcome the challenges limiting the catalytic performance of TiO_2 by controlling the synthesis of its nanostructures and structural polymorphs using simple intercalation chemistry to make TiO_2 nanostructures a highly competitive earth-abundant catalyst for the HER. The intercalation of Li^+ will be investigated in the presence of water for mesoporous nanostructured TiO_2 film. To do so, new electrolyte such as water in salt is used. Since the composition of the material is evolving with the lithiation, its activity toward the ElectroCatalysis hydrogen Evolution Reaction (EC-HER) may be impacted and needs to be investigated. To do so, the HER will be studied as function of the quantity of Li inserted/de-inserted in the Li_xTiO_2 electrodes.

III.1. Comparaison between LP30 and WIS electrolyte

In order to test the H_2O (in WIS) as photo-electron acceptor, we decided to compare the experiments in WIS to the ones in LP30. First step, the mesoporous anatase TiO_2 electrode was cycled at 0.5 mV/s in WIS in the dark (**figure 29**).

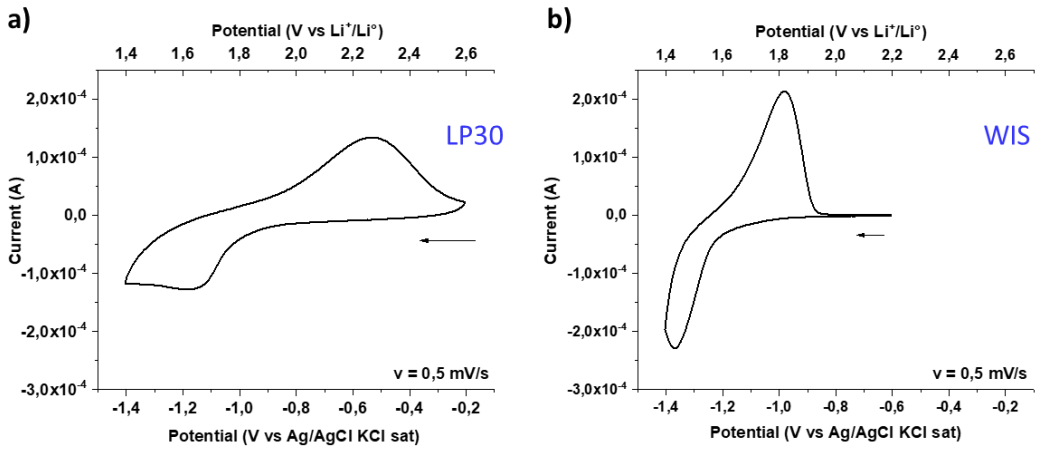

***Figure 29**: Comparison between liquid electrolyte for cyclic voltammetry (CV) at 0.5 mV/s (a) starting from 2.6 V to 1.4 V vs $Li^+/Li°$ in LP30 electrolyte ($TiO_2/LiPF_6$ 1 M in EC: DMC (1: 1 vol) (LP30) // Li°/Li°), (b) starting from -0.6 V to -1.4 V vs Ag/AgCl KCl saturated in WIS electrolyte (TiO_2// LiTFSI water in salt 20 m (WIS) //AgAgCl KCl sat/ Pt).The current measure is in A/cm^2 since the dipped area of the TiO_2 is 1 cm^2 thanks to the Kapton tape.*

The CV exhibit an oxidation wave at $E_{1/2}$= -1.0 V vs Ag/AgCl (KCl saturated) and a reduction wave at $E_{1/2}$= -1.37 V vs Ag/AgCl (KCl saturated) that represent the extraction and the insertion of the lithium ions respectively. These waves are separated by around 0.3 V ($dE_{1/2}$) in WIS against 0.4 V for the LP30. A comparison with literature indicates that reduction wave is associated to the reaction: $TiO_2 + xLi^+ + xe^-$ ➔ Li_xTiO_2 while the oxidation wave represents the following reaction: Li_xTiO_2 ➔ $TiO_2 + xLi^+ + xe^-$. Additionally, the waves are well defined in WIS so that the titanium couple seems to be more reversible than in LP30. The change in area of the wave between LP30 and WIS suggests that more lithium inserted/extracted from the TiO_2.

Galvanostatic experiments at 2C in WIS were performed and compared to the same experiments in LP30 (**figure 30**).

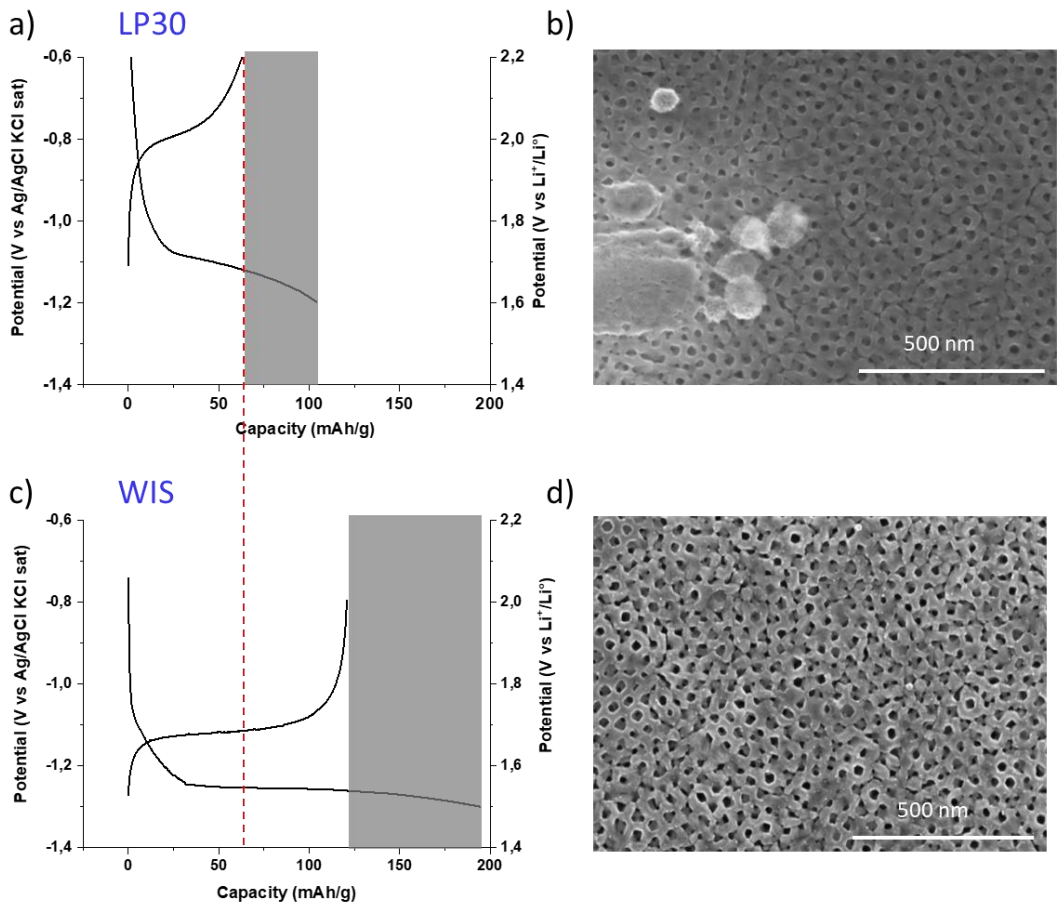

***Figure 30**: Comparison between liquid electrolyte for galvanostatic charge/discharge experiment at 2C in a) TiO_2 $LiPF_6$ 1 M in EC: DMC (1: 1 vol) (LP30) // Li°/Li°, first cycle after the 10 CV of stabilization with b) post mortem SEM-FEG image of the TiO_2 surface, (c) TiO_2// LiTFSI water in salt 20 m (WIS) //AgAgCl KCl sat/ Pt, first cycle after the 7 CV of stabilization, with d) post mortem SEM-FEG image of the TiO_2 surface.*

The behavior of curves is similar. The comparison of the charge-discharge curves shows that higher capacity could be achieved in water-in-salt (180 mAh/g vs. 120 mAh/g for LP30 for the discharge). Several factors could explain this improvement: a better wetting of the electrolyte because of a greater affinity for water-based electrolyte with respect to sol-gel synthesized films (therefore highly hydrophilic).

Both galvanostatic responses exhibit a large irreversibility between the discharge and the charge. In LP30, it was not clearly attributed.

The coulombic efficiency is equivalent for both electrolytes 61 % and 62 % for LP30 and WIS respectively. In the case of WIS, the low coulombic efficiency can be linked to the electrocatalysed reduction of H^+ to H_2 (EC-HER).

Using Gas Chromatography, we were able to highlight its presence (<1 ppm), although we could not access qualitative results given the small quantity of H_2 produced and actually collected. In LP30, the presence of particles on top of the mesoporous film is observed, which were assigned with EDX to LiF salt.[7] This salt is usually observed as a main component of SEIs. In WIS, the surface of the film appears "clean" ie. particle-free (**figure 30d**). The irreversible capacity between the charge and the discharge for the WIS is mostly attributed to H_2 production.

Those experiments show that WIS is a good electrolyte as it allows reversible insertion-extraction of Li^+ within mesoporous anatase TiO_2. We will call 'EC-HER', the HER induced electrochemically during discharge while using WIS electrolyte. If we make the plausible hypothesis that it represents the main source of irreversibility between discharge and charge, it will be estimated as the following difference in mAh/g (Capacity of discharge – Capacity of charge). The capacity reached during the charge is around 125 mAh/g whereas the capacity reached during the discharge is around 200 mAh/g, we would have 75 mAh/g used for HER. The relative production of H_2 might also be reflected by the Coulombic Efficiency in % ((Capacity of Charge)/(Capacity of discharge)).

III.2. Impact of the rate on the ratio HER/ lithium insertion

To identify the impact of the rate on the proportion (1) EC-HER and (2) lithium insertion capacity, different galvanostatic rates were tested, from 4C to C/2 C-rate (**Figure 31a**).

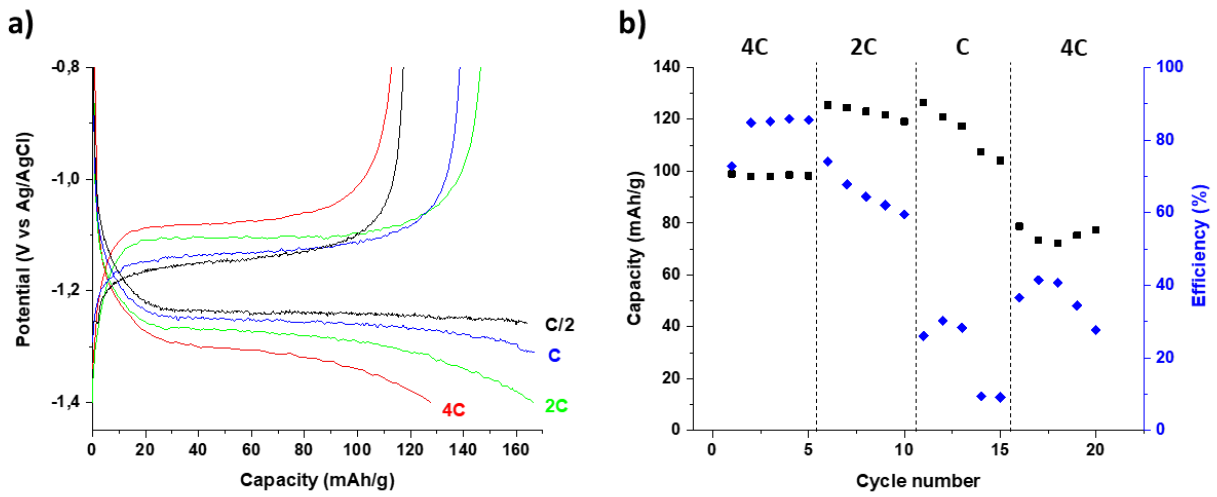

***Figure 31**: (a) Galvanostatic cycle at different C-rate from 4C to C/2. (b) Study of the evolution of the charge capacity (black) and the coulombic efficiency (blue) over cycling and C-rate. Cut-off in discharge: -1.4 V and in time. Cut-off in charge: -0.8 V.*

From this figure, we can see that if we reduce the rate from 4C to 2C an increase of both capacities of charge and discharge is observed. However, if the rate is decreased down to C/2 the capacity of discharge does not change much and the charge capacity decreases resulting in an increased irreversible capacity at low C-rate. Another set of measures with 5 galvanostatic cycles confirm this trend (**figure 31b**). The resulting charge capacity and the coulombic efficiencies are shown in blue**.** Since we made the hypothesis of EC-HER as the main source of irreversible capacity, we can deduce that at low C-rate EC-HER is promoted. Another possible contribution could also be the "self-charge" of the material

$$Li_xTiO_2 + x\ H_2O \rightarrow TiO_2 + x\ Li^+ + {}^{x}/_{2}\ H_2 + x\ HO^-$$

We can see that the "best" coulombic efficiency is obtained for 4C-rate, meaning that the fastest we try to induce the reduction of TiO_2 (corresponding to the insertion of Li^+), the less EC-HER is produced. This may result from a large overpotential for HER at this speed. The highest and most stable capacity is obtained for 2C-rate. We saw that at low rate the production of EC-HER occur but at high C-rate (like at 4C) it is probable that the insertion is kinetically to slow to reached a good enough capacity. Indeed, the highest capacities achieved for 5 cycles is at 2C but the coulombic efficiency is not the best of the series. At 4C the coulombic efficiency is higher.

As a compromise, we decided to do our experiment at the C-rate of 2C. For battery application, HER should be prevented, but still H_2 is a valuable product also considered as a chemical storage.

It is actually interesting to bring up at this point that there are a few examples in the literature[14] (some very recent) where insertion materials have been considered as promising catalyst for proton-coupled electron transfer reactions like HER[15–20] and OER[79]. The origin of the catalytic effect is not fully understood yet. Inserting cations in a material implies complex (yet very interesting) material modifications, which include: introducing defects, filling their electronic band, achieving thereby higher carrier densities, building up an internal electric field, causing polaron absorption.

III.3. Structure driven electrocatalysis

Furthermore, we have decided to investigate the evolution of the electrocatalytic properties of TiO_2 at various state of charge (SOC). First, we propose to develop an original technique to determine the SOC of TiO_2 lithiated by following the change in color of TiO_2 upon the insertion of cations via UV-VIS-NIR spectroscopy to track *in situ* the lithiation state of the film. Indeed, the reduction of Ti^{4+} to Ti^{3+} states in TiO_2 is accompanied by a change in color from transparent to a dark blue. Furthermore, the structure of TiO_2 evolves with the SOC and this is also dependent on the particle size. In our electrodes, TiO_2 particles are around 20 nm. According to de KIerk et al[13], they can present gradient between the poor-lithium phase and the rich one. We suggest the following schema to illustrate the lithiation around a hole of the here-studied mesoporous films (**figure 32**). This schema highlights the complexity of this material in terms of transport path to only cite this one.

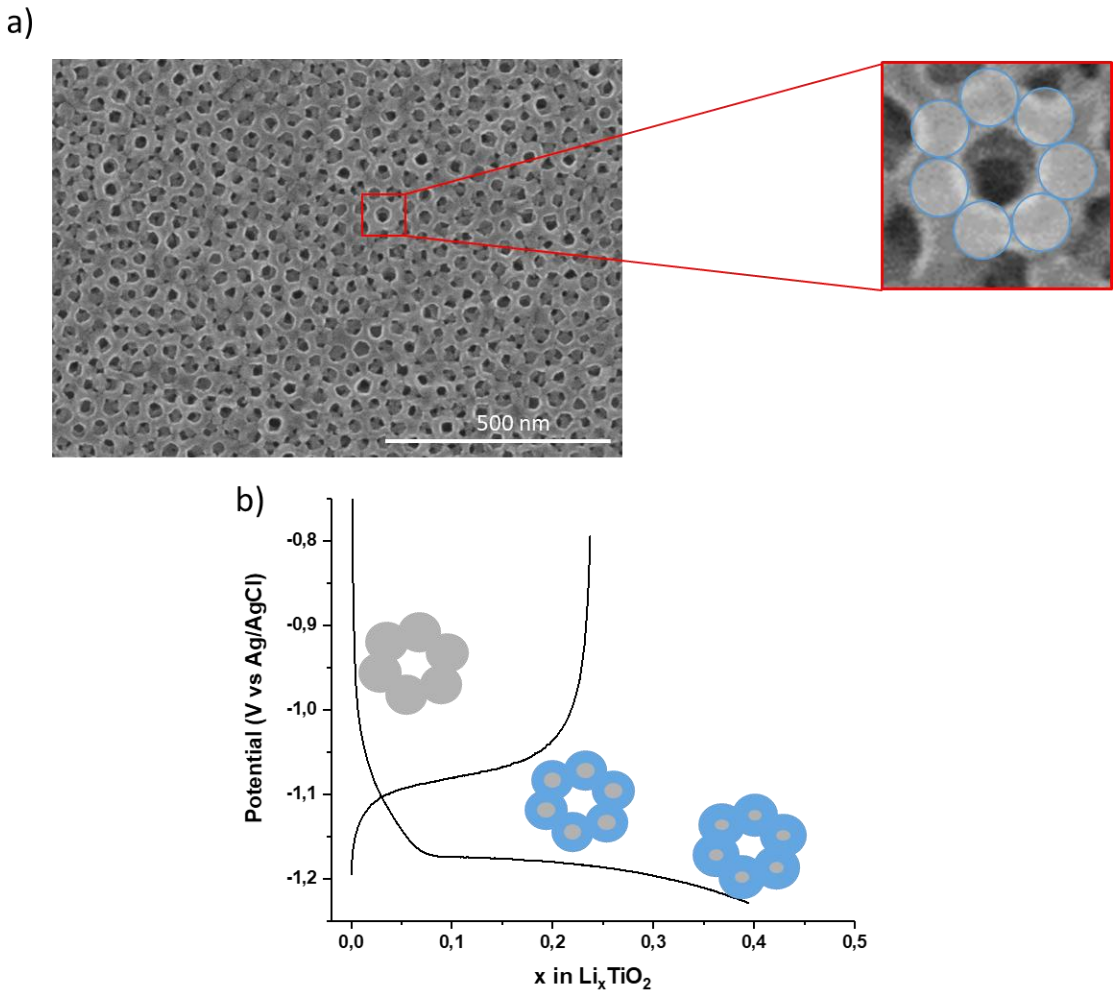

***Figure 32**: (a) SEM-FEG image of the surface of the TiO_2 with a zoom and a visualization of the crystallite materialized by blue circles, (b) galvanostatic cycle at a 2C rate with the evolution of the composition over a discharge schematized by circles with in grey the lithium poor and in blue the titanate phase.*

Electrochemical experiments (**figure 31**) show that (1) the gamma phase was not accessible (no second plateau), and (2) the films exhibit limited capacities at 2C (120 mAh/g, with respect to 175 mAh/g for $Li_{0.5}TiO_2$). The absence of gamma phase mainly results from the fact that at low potential the FTO substrate was starting to reduce. The reduced capacity that we do observe can be explained by several factors: the absence of carbon additives in our electrodes that leads to poorer electronic conductivity since the TiO_2 have a conductivity between 10^{-12}–10^{-7} S/cm), the size of the nanoparticles (bigger than 5-7 nm). This will slow down the Li^+ diffusion rate, between 10^{-15}–10^{-9} cm^2/s for the TiO_2.[6]

The absorbance of the electrode is followed using *operando* UV-VIS-NIR spectroscopy during a galvanostatic cycle (at 2C-rate). A spectrum is recorded every 2 minutes (a little bit longer than scanning time of one spectrum) allowing a very precise tracking of the evolution of the absorbance along the cycling. Only six spectra are shown in **figure 33** for the sake of clarity.

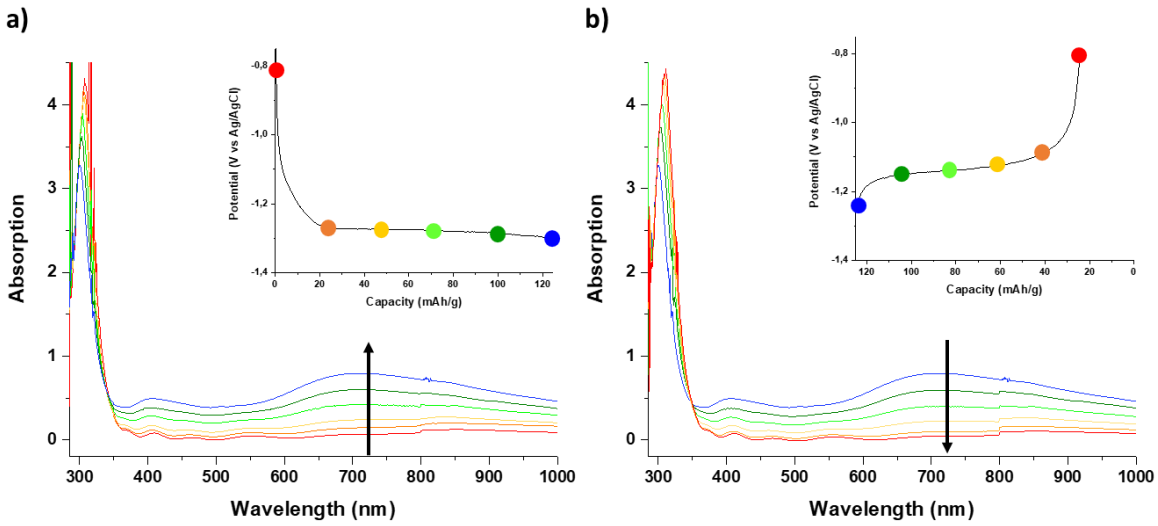

***Figure 33**: Operando UV-VIS-NIR spectroscopy (300-1000 nm ~2 min for 1 spectrum) during (a) a 2C discharge and (b) a 2C charge of the TiO_2.*

As the potential of the electrode is decreasing (**figure 33a**), we observe (1) broad absorption band around 300 nm, (2) a global increase of the absorption in the visible range, and (3) the appearance of a broad band centered at 720 nm. These changes in the absorption band at around 720 nm represent a reduction of Ti^{4+} sites to Ti^{3+} sites and the accompanying intercalation of cations. The phenomenon (2) is linked to the improvement of the conductivity of the electrode: the semi-conductor became conductor. This process is accompanied by the injection of electrons, which pushed the Fermi level toward the conduction band. When the quantity of injected electrons is significant enough, the Fermi level completely shifts into the conduction band. Consistent with electron injection and n-type doping, the oxidation state of Ti is reduced. As a result, we expect a continuous increase of electronic conductivity with increasing lithiation level in Li_xTiO_2[22,23] which is seen on the absorption band. In parallel to the increase in carrier density, the lithiation of TiO_2 results in an increase in the mobility of the charge carriers, that may arise from the increase in hybridation of Ti-O bonds.

The inverse trend is seen when Li^+ ions are extracted, i.e. the intensity of band at 720 nm decreases and Ti^{3+} oxidizes in Ti^{4+}, impacting the carrier density and mobility (**figure 33b**). A decrease of the global absorption in the visible range is observed. From the analysis of absorption spectra during charge and discharge, we can conclude that, the band at 720 nm can be used as a mean to follow the SOC.

In **figure 34b**, we have plotted the evolution of the intensity of the band at 720 nm and at 300 nm, as function of the SOC. We notice that during the lithium insertion, the 720 nm absorbance increases when the 300 nm one decreases. During the extraction of the lithium, the reverse phenomenon occurs. This result highlights that, with the insertion of Li^+ into the Li_xTiO_2, a change of the band structure is observed and eventually the conductive behavior, through an increase of the concentration of electronic charge in TiO_2, namely Ti^{4+}/Ti^{3+} polarons.

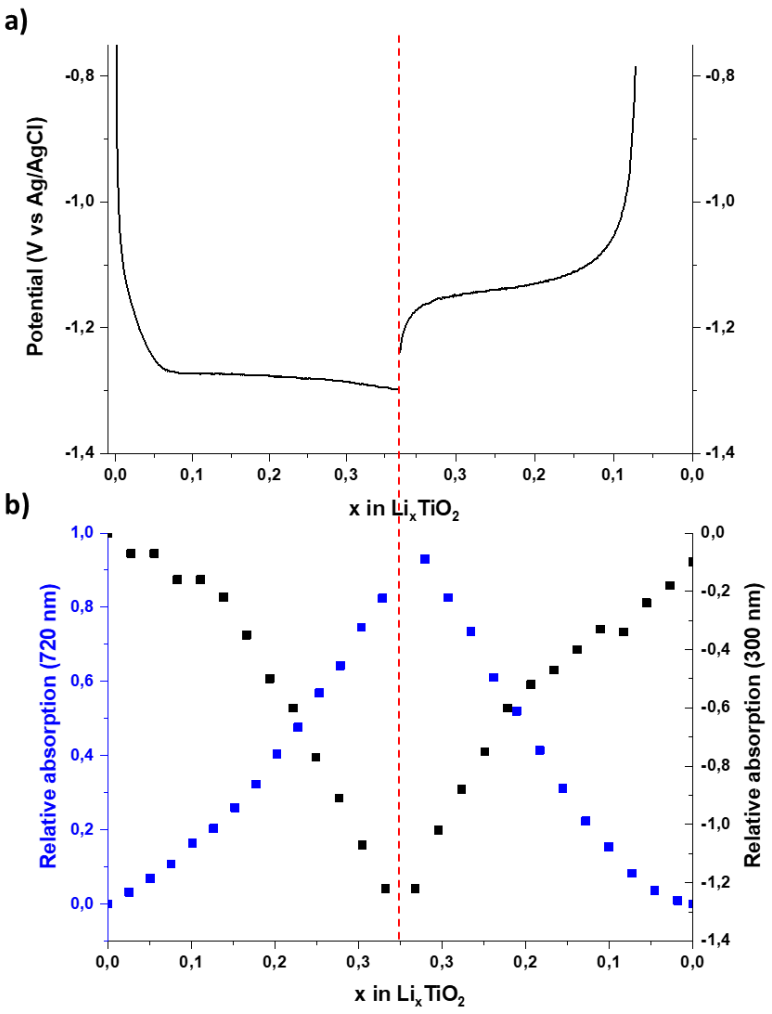

***Figure 34**: (a) Galvanostatic charge and discharge at a 2C rate potted with the lithium composition, (b) evolution of the 720 nm band (blue scare) and the 300 nm band (black scare) over the lithium composition. The composition of lithium is determined by using the theoretical capacity of $LiTiO_2$ (335 mAh/g). FTO/TiO_2//WIS (20 m)// AgAgCl KCl saturated/ Pt in a quartz cell.*

Furthermore, we notice a shift of the 300 nm band as seen in **figure 33**. The shift of this gap is known as Moss–Burstein shift[24] and corresponds to a "virtual" increase of the gap thanks to the filling of the conductive band of the TiO_2. Indeed, during the discharge the TiO_2 is reduced and so electron will partially fill its conductive band.

To evaluate the optical gap of our material, the following equation is used: $A = \frac{B(h\nu - E_g)^m}{h\nu}$

where A is the absorption coefficient, B a constant, hν the light energy from Planck's constant (h) and frequency (ν) determined by the speed of light (3 x 10^8 m/s) over the wavelength (λ in nm) by the Planck-Einstein relation.

For direct semiconductors m = ½, whereas for indirect, m = 2. According to the literature[25] the TiO_2 have an indirect band gap so we have plotted $(Ahv)^{1/2}$ vs. hν, with hν = hc/ λ. This is called a Tauc plot and results are summarized in **figure 35**. The x-axis intercept from the linear feature of the absorption edge allows the determination of the band gap.[26]

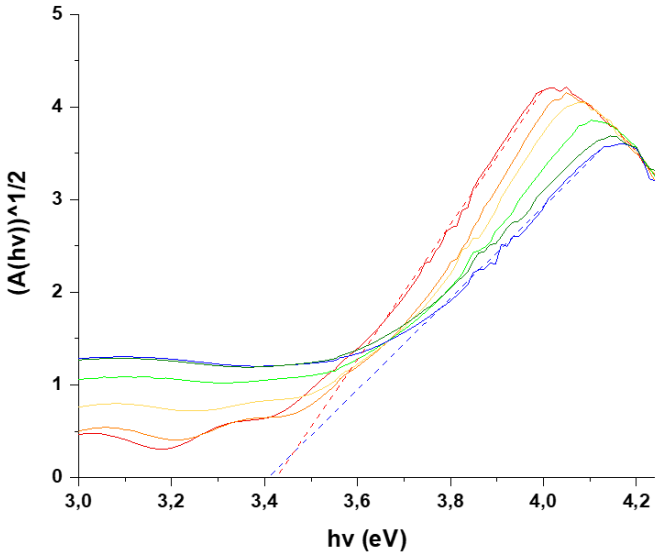

***Figure 35**: Tauc plot (~300-400 nm) of TiO_2 during operando UV-VIS-NIR spectrum with in red the TiO_2 poor phase and in blue the TiO_2 rich phase.*

The absorbance spectrum (**figure 33**) and the Tauc plot (**figure 35**) indicate a shift of the band but the determination of the gap with the Tauc method does not show any difference in the band gap value for the TiO_2 and the lithiated Li_xTiO_2 (3.4 eV).

In order to study the lithiation of Li_xTiO_2, we used the 720 nm absorption band as function of capacity as this band is solely related to the "real" capacity of Li^+ insertion/extraction. First, the absorption of the 720 nm band of the TiO_2 just before the discharge, so without lithium in it, is used as baseline. We have then followed the increase of this band during the discharge. The relative absorption at each capacity is then estimated by subtracting the absorbance at a certain capacity by the absorption of the non lithiated TiO_2 ($A_{relative} = A_x(720\ nm) - A_0(720\ nm)$). The same calculation has been performed for the charge as well. To do so, we have postulated that during the charge the only reaction occurring is the lithium extraction; the relative absorption is then associated to the real capacity. These results are plotted as function of the capacity and represented in **figure 36a**.

This figure shows that the absorbance of the discharge is smaller than the absorbance of the charge for a same capacity, confirming that the current of the discharge serves to another electrochemical reaction, ie. EC-HER.

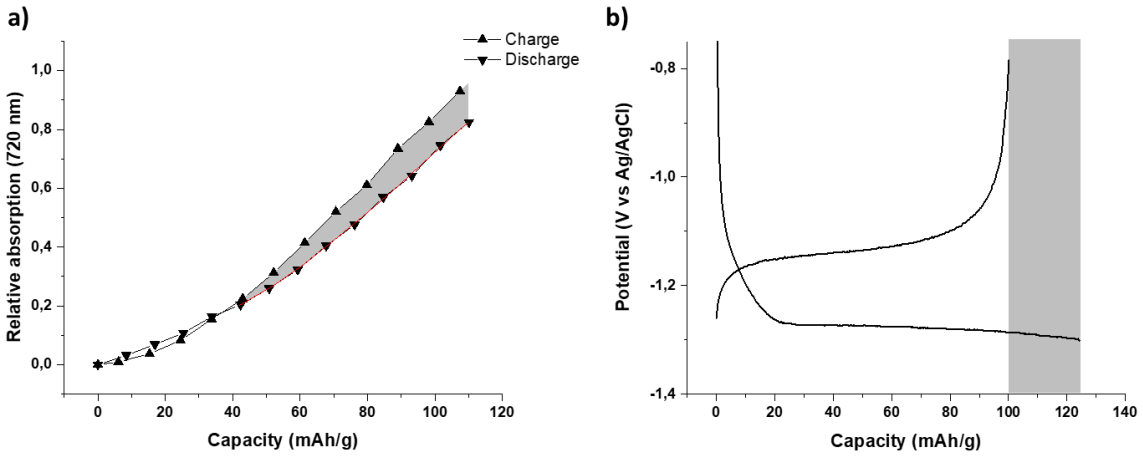

***Figure 36**: (a) Relative absorption at 720 nm over the capacity during discharge and charge, (b) visualization of the irreversible part between the galvanostatic charge and discharge at a 2C rate.*

Furthermore, the difference between the charge and the discharge absorbance increases with the capacity, meaning that the more the TiO_2 is lithiated the more EC-HER occurs. This tends to indicate that the lithiated Li_xTiO_2 seems to be a better electro-catalyst for this reaction. It could also be the consequence of a better conductivity of the lithiated phase. This observation confirms that the ion insertion changes the electron population of the host structure, changing both the electronic conductivity of the electrode and the thermodynamic electrochemical driving force of the reaction ($\eta=E_F-E_{eq}$, where E_F is the Fermi level of the electrode and E_{eq} is the Fermi level of the reactant in solution). Additional kinetic effects occur based on the stabilization of the E_{eq} of a reactive intermediate with the surface of an electrocatalyst and the overlap of electronic states between the electrode and the reactant. Furthermore, in Li-ion battery, it is assumed that ion insertion is likely the true rate- limiting step for a wide range of (dis)charging conditions. By changing the C rate, we tune “the slowest” process, and then the reaction occurring at the interface. At low C-rate, the electro-catalytic reaction (EC-HER) is preponderant to the insertion of Li^+.

The results presented in this part point out that two reactions occur during the discharge and that the Li_xTiO_2 is a better electro-catalyst for EC-HER. We also show a tunable electro-catalyst activity of our material toward HER with the insertion of lithium ions. Furthermore, galvanostatic experiments performed at various C-rate, indicate that at low C-rate the EC-HER is favored. The kinetics of reaction differ and can be used as a tool for controlling one reaction to the other.

Conclusion

In conclusion, we have demonstrated a simple and rational method to provide a significant enhancement of the electrocatalytic performance of Li_xTiO_2 by controlling the quantity of Li^+ and then the State of Charge (SOC). This new approach leads to favorable kinetics, metallic conductivity, and proliferation of active sites in Li_xTiO_2, which enable yet regeneration of catalytic activity and make Li_xTiO_2 nanostructures a highly competitive earth-abundant catalyst for HER and potentially other reactions. Furthermore, this represents the first application of the Li_xTiO_2 in catalysis, and this general approach for controlling nanostructures and SOC can be useful in modifying many insertion materials including WO_3[16,27], MoS_2[18,19] to enhance their applications in heterogeneous catalysis, solar energy, and high-performance electronics.

Accordingly, in the next chapter, we will use the ability of this lithiated TiO_2 to harvest light for Li^+ insertion/de-insertion and electrocatalysis (H_2 production). First, the impact of light at the OCV will be investigated. Then, a potential/current will be applied to the lithiated electrodes and the impact of light will be monitored.

Bibliography

(1) Le vecteur hydrogène https://www.ademe.fr/expertises/energies-renouvelables-enr-production-reseaux-stockage/passer-a-laction/vecteur-hydrogene (accessed **2021** -12 -05).

(2) Recent progress in TiO_2-based photocatalysts for hydrogen evolution reaction: A review - ScienceDirect https://www.sciencedirect.com/science/article/pii/S1878535219301868 (accessed **2021** -12 -05).

(3) Jiang, Y.; Ning, H.; Tian, C.; Jiang, B.; Li, Q.; Yan, H.; Zhang, X.; Wang, J.; Jing, L.; Fu, H. Single-Crystal TiO_2 Nanorods Assembly for Efficient and Stable Cocatalyst-Free Photocatalytic Hydrogen Evolution. *Applied Catalysis B: Environmental* **2018**, *229*, 1–7.

(4) Kaur, K.; Singh, C. V. Amorphous TiO_2 as a Photocatalyst for Hydrogen Production: A DFT Study of Structural and Electronic Properties. *Energy Procedia* **2012**, *29*, 291–299.

(5) Bard, A. J.; Faulkner, L. R. *ELECTROCHEMICAL METHODS. Fundamentals and Applications*; **1944**; Vol. 2nd edition.

(6) Monconduit, L.; Croguennec, L.; Dedryvère, R. *Electrodes de batteries Li-ion volume 2*, ISTE.; Collection Energie; **2015**; Vol. 2.

(7) Nguyen, O. Towards a Li-Ion Photo-Rechargeable Battery. thesis, Sorbonne Université, 7 place Jussieu, **2018**.

(8) Lafont, U.; Carta, D.; Mountjoy, G.; Chadwick, A. V.; Kelder, E. M. In Situ Structural Changes upon Electrochemical Lithium Insertion in Nanosized Anatase TiO_2. *J. Phys. Chem. C* **2010**, *114* (2), 1372–1378.

(9) Borghols, W. J. H.; Lützenkirchen-Hecht, D.; Haake, U.; van Eck, E. R. H.; Mulder, F. M.; Wagemaker, M. The Electronic Structure and Ionic Diffusion of Nanoscale $LiTiO_2$ Anatase. *Physical Chemistry Chemical Physics* **2009**, *11* (27), 5742.

(10) WAGEMAKER, M. Structure and Dynamics of Lithium in Anatase TiO2, Technische Universiteit Delft, 2003.

(11) Wagemaker, M.; Borghols, W. J. H.; Mulder, F. M. Large Impact of Particle Size on Insertion Reactions. A Case for Anatase Li_xTiO_2. *J. Am. Chem. Soc.* **2007**, *129* (14), 4323–4327.

(12) Rai, A. K.; Anh, L. T.; Gim, J.; Mathew, V.; Kang, J.; Paul, B. J.; Song, J.; Kim, J. Simple Synthesis and Particle Size Effects of TiO2 Nanoparticle Anodes for Rechargeable Lithium Ion Batteries. *Electrochimica Acta* **2013**, *90*, 112–118.

(13) de Klerk, N. J. J.; Vasileiadis, A.; Smith, R. B.; Bazant, M. Z.; Wagemaker, M. Explaining Key Properties of Lithiation in TiO_2 -Anatase Li-Ion Battery Electrodes Using Phase-Field Modeling. *Physical Review Materials* **2017**, *1* (2).

(14) Sood, A.; Poletayev, A. D.; Cogswell, D. A.; Csernica, P. M.; Mefford, J. T.; Fraggedakis, D.; Toney, M. F.; Lindenberg, A. M.; Bazant, M. Z.; Chueh, W. C. Electrochemical Ion Insertion from the Atomic to the Device Scale. *Nat Rev Mater* **2021**, *6* (9), 847–867.

(15) Xie, X.; Mu, W.; Li, X.; Wei, H.; Jian, Y.; Yu, Q.; Zhang, R.; Lv, K.; Tang, H.; Luo, S. Incorporation of Tantalum Ions Enhances the Electrocatalytic Activity of Hexagonal WO_3 Nanowires for Hydrogen Evolution Reaction. *Electrochimica Acta* **2014**, *134*, 201–208.

(16) Rajeswari, J.; Kishore, P.; Viswanathan, B.; Varadarajan, T. Facile Hydrogen Evolution Reaction on WO_3 Nanorods. *Nanoscale Res Lett* **2007**, *2* (10), 496–503.

(17) Wang, H.; Lu, Z.; Kong, D.; Sun, J.; Hymel, T. M.; Cui, Y. Electrochemical Tuning of MoS_2 Nanoparticles on Three-Dimensional Substrate for Efficient Hydrogen Evolution. *ACS Nano* **2014**, *8* (5), 4940–4947.
(18) Wang, H.; Lu, Z.; Xu, S.; Kong, D.; Cha, J. J.; Zheng, G.; Hsu, P.-C.; Yan, K.; Bradshaw, D.; Prinz, F. B.; Cui, Y. Electrochemical Tuning of Vertically Aligned MoS_2 Nanofilms and Its Application in Improving Hydrogen Evolution Reaction. *Proceedings of the National Academy of Sciences* **2013**, *110* (49), 19701–19706.
(19) Lukowski, M. A.; Daniel, A. S.; Meng, F.; Forticaux, A.; Li, L.; Jin, S. Enhanced Hydrogen Evolution Catalysis from Chemically Exfoliated Metallic MoS_2 Nanosheets. *J. Am. Chem. Soc.* **2013**, *135* (28), 10274–10277.
(20) Shokhen, V.; Zitoun, D. Electrochemical Intercalation of Sodium in Vertically Aligned Molybdenum Disulfide for Hydrogen Evolution Reaction. *FlatChem* **2019**, *14*, 100086.
(21) Yang, C.; Rousse, G.; Louise Svane, K.; Pearce, P. E.; Abakumov, A. M.; Deschamps, M.; Cibin, G.; Chadwick, A. V.; Dalla Corte, D. A.; Anton Hansen, H.; Vegge, T.; Tarascon, J.-M.; Grimaud, A. Cation Insertion to Break the Activity/Stability Relationship for Highly Active Oxygen Evolution Reaction Catalyst. *Nat Commun* **2020**, *11* (1), 1378.
(22) Dahlman, C. J.; Tan, Y.; Marcus, M. A.; Milliron, D. J. Spectroelectrochemical Signatures of Capacitive Charging and Ion Insertion in Doped Anatase Titania Nanocrystals. *Journal of the American Chemical Society* **2015**, *137* (28), 9160–9166.
(23) Dahlman, C. J.; Heo, S.; Zhang, Y.; Reimnitz, L. C.; He, D.; Tang, M.; Milliron, D. J. Dynamics of Lithium Insertion in Electrochromic Titanium Dioxide Nanocrystal Ensembles. 34.
(24) Kamat, P. V.; Dimitrijevic, N. M.; Nozik, A. J. Dynamic Burstein-Moss shift in semiconductor colloids https://pubs.acs.org/doi/pdf/10.1021/j100345a003 (accessed **2021** -12 -12).
(25) Ardo, S.; J. Meyer, G. Photodriven Heterogeneous Charge Transfer with Transition-Metal Compounds Anchored to TiO 2 Semiconductor Surfaces. *Chemical Society Reviews* **2009**, *38* (1), 115–164.
(26) Tauc, J.; Grigorovici, R.; Vancu, A. Optical Properties and Electronic Structure of Amorphous Germanium. *physica status solidi (b)* **1966**, *15* (2), 627–637.
(27) Bogati, S.; Georg, A.; Graf, W. Photoelectrochromic Devices Based on Sputtered WO_3 and TiO_2 Films. *Solar Energy Materials and Solar Cells* **2017**, *163*, 170–177.

CHAPTER IV: How does structure influence photo(electro)catalytic processes?

TABLE of CONTENTS

CHAPTER IV: How does structure influence photo(electro)catalytic processes?

Introduction

Anatase TiO_2 is one of the most studied light absorber in photocatalysis and photoelectrochemistry. When it comes to light-matter interaction, its strongest point is its favorable band-gap positions to drive various relevant redox reactions (OER, HER, ORR). Its weakest point lies in its large band-gap energy (3.2 eV), which restricts its photoactivity to UV light. Different approaches have been studied to widen its activity to the visible range; using different dopants to narrow the bandgap.[33] Very recently, community's massive interest has turned to black TiO_2.[1,3] The synthesis includes a hydrogen treatment that induces defect states (including Ti^{3+}) within the band gap giving rise to an increased light absorption in the visible and the near-infrared. However, numerous studies have shown that narrowing the bandgap does not automatically induce higher incident photon to charge carrier conversion in the visible region.

In this work, we would like to consider electrochemical lithiation to produce hydrogen. How electrochemical cation insertion impacting its photoelectrochemical activity have been quite disregarded. We believe that given their complexity, they hold a lot of promises. For example, Meekins et al[4] showed that the intercalation of H^+ and Li^+ into TiO_2 has a profound effect toward the photo-current generation under UV light irradiation. An enhancement of the photo-conversion efficiency (IPCE) has been observed upon intercalation of Li^+ ions into TiO_2 nanotube arrays. Sánchez-Tovar et al[5] highlighted that Li^+-doped TiO_2 nanostructures can be used as durable and stable photo-anodes for photoelectrochemical water splitting applications. Furthermore, doping TiO_2 with hydrogen generates black TiO_2, allowing better absorption of visible light[6]. However, this material performs poorly in Photo-Electrochemical Cell (PEC) oxidation processes due to the presence of defect sites at the surface. Furthermore, an enhancement of the performances is achieved through the passivation of the trap state by Li^+. But in all these studies, little attention was paid on how lithium distribution in the material could affect the photo-activity. Here, we will consider the visible activation of HER and how it depends on the lithium phases (poor and rich) structuration. Since here the UV region is filtered by the cell which is in glass. No significant improvement was observed using UV and visible region.

Our previous *in situ* UV-VIS-NIR experiments for our inserted materials (Li^+ doped TiO_2) have shown that light absorption increases along from 400 to 1000 nm, with the formation of the Li-rich phase. In the context of smart windows, nanosized lithiated TiO_2 phases have been reported to be active in NIR, thanks to their metallic type behavior, creating excitons through collective phonon vibration (surface plasmon resonance, SPR).[7,8] Our battery set-up is built to only allow visible light to access the working electrode, which excludes the activation of potential SPR, it also excludes any UV contribution from pure TiO_2 or Li-poor TiO_2. We will therefore solely rely on the visible range to activate the photoactivity. In this case, we will tend to highlight the non-trivial relationship between VIS absorption and photoactivity.

This chapter will also highlight the multipotentialities of these TiO_2 inserting electrodes. We will show that, because the solar production of H_2 using lithiated TiO_2 actually induces lithium extraction from TiO_2, in a battery configuration where TiO_2 plays the positive electrode. We can actually regenerate the electrode while producing H_2. The mechanism is illustrated in **schema 2**. Illuminating the system involves (i) the absorption of light and the creation of the exciton, (iia) the oxidation of Ti^{3+} by the hole and (iib) the reduction of water present in WIS by the photo-electron. To be more specific, after the formation of the exciton, to prevent recombination, the hole needs to react within the material itself (with the Li-rich phase) and Li^+ has to travel out of the particle. At the same time, the photo-electron needs to react with the water present at the surface of the particle (**schema 2a**) or at the counter electrode (**schema 2b**). In the WIS case, we can indeed attribute the fate of the photo-electron to its participation into producing H_2, since we purposely chose water to act as a photo-electron acceptor and the presence of dihydrogen was confirmed by Gas Chromatography (GC).

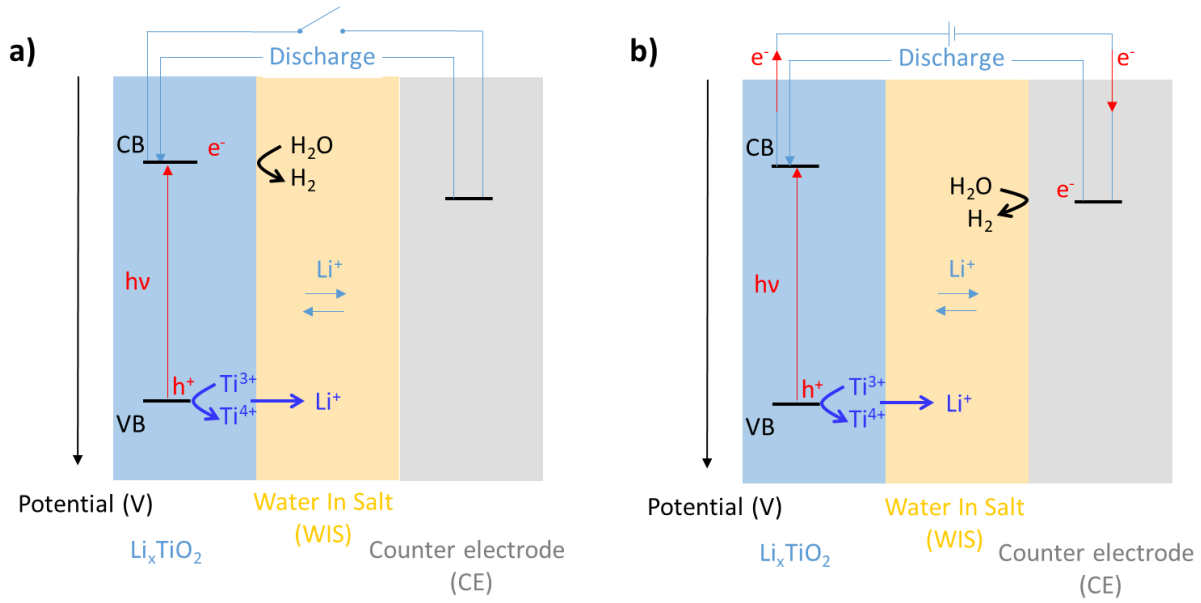

***Schema 2**: Representation of the photo-mechanism of the of TiO_2// LiTFSI water in salt (WIS) 20 m//AgAgCl KCl saturated/ Pt half-cell for (a) a photo-charge (OCV under illumination) experiment, (b) a photo-assisted charge (galvanostatic experiment under illumination) experiment.*

In this Chapter, we will discuss the mechanisms depending on the type of experiments used to induce lithiation/delithiation of the electrode. The first type of experiments (**Scheme 2a**) is performed when the electrode is illuminated at open circuit voltage (OCV). No current can flow through the external circuit during the illumination and solely photocatalytic reactions can be triggered. The term "Photo-charge" will be used to designate the experiment where the lithiated TiO_2 electrode is illuminated at OCV. This illumination will indeed induce lithium ions to come out and thereby regenerates TiO_2 (here considered as a positive electrode). Also, "photo-charge" is strictly speaking inappropriate, and we should better talk about electrode **regeneration**. Indeed, with this process only one electrode (here the positive one) is regenerated, in addition the photo-electron acceptor consumed (to produce H_2) is not regenerated. However, if the counter electrode could also be photo-regenerated, the system would present interesting features. In the second type of experiments (**Scheme 2b**), the electrode is illuminated while a potential or a current is applied to the cell. In this case, we can expect photoelectrocatalytic reactions to occur since the electron can go through the external circuit. These experiments will be later referred as "Photo-assisted" charge or discharge.

In Nguyen's thesis,[9] the mechanisms of light-induced processes were discussed regardless of the conditions (OCV or not). In this thesis, the mechanisms will be addressed separately. For each type of experiments, we will investigate how the structure of the electrode in terms of composition and phases distribution, depending on the SOC, will affect the photo-activity of the material.

IV.1. Study of the Photo-charge

This part is dedicated to the photo-charge of the electrode, i.e. regenerating the electrode at OCV using solar energy. We will start this section by highlighting how changing electrolyte, from LP30 to WIS, impacts the photo-charge. **Figure 37** presents the OCV evolutions of pre-lithiated electrodes in WIS and in LP30.

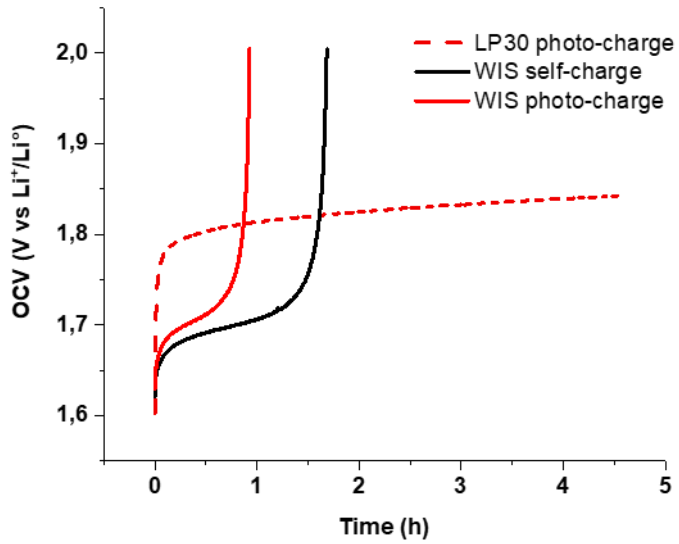

***Figure 37**: Comparison of OCV evolutions of pre-lithiated electrodes. The pre-lithiated electrodes were obtained after a discharge at 2C-rate in dark. Photo-charge in LP30 is presented in red dash, photo-charge in WIS is presented in red line. The Self-charge in WIS (OCV in dark) is presented in black as a reference.*

We observe that the photo-charge happens faster in WIS (1h) than in LP30 (more than 4h). For LP30, the experiment had to be stopped prematurely, however it is already clear that the photo-charge time is significantly higher. Besides, we observe that the plateau attributed to Li-deinsertion is shifted to much higher potential in LP30. The suggested mechanism is illustrated in **Schema 2a**.

Also, as mentioned in the introduction of this section, at OCV, the mechanism doesn't allow the charge carrier to travel throughout the electrode to the current collector, the reaction happens at the surface of each particle in contact with the electrolyte. It is purely photocatalytic. In this type of mesoporous electrodes, we expect a large part of the particle surface to interface the electrolyte.

The higher charge potential plateau in LP30 compared to WIS suggests a slower process in LP30. Slow lithium ions kinetics was already suggested for the LP30 system in the dark, given the large polarization between the charge and the discharge curves (**figure 30a**). We can also suggest that in the case of WIS, TiO_2 is known to have a better affinity with "aqueous" electrolyte than with organic ones, moreover water is a better electron-acceptor and it helps limiting the recombination of photo-generated holes and electrons.

This result seems to validate our choice to switch to WIS electrolyte regarding photo-charging. Nevertheless, in dark conditions at OCV (self-charge), it appears that lithium ions can be extracted very fast too (within less than 2h). This important self-charge is a feature that cannot be disregarded if we intend to take this system to an actual application level. In 2003, it was already reported that using a nanostructured TiO_2 improved the electrochromic properties[10] allowing a "self-extraction" of lithium ions. More recently, Makivic et al.[11] also mentioned not negligible self-discharge in aqueous solution for nanostructured anatase TiO_2 for battery applications (where TiO_2 is used as a negative electrode). The self-discharge process, has been described as follows: $2\ Ti^{III}OOH \xrightarrow{self\ k} 2\ Ti^{IV}O_2 + H_2$, with self k, the rate constant characterizing this spontaneous self-discharge reaction. They have shown that the charge storage could be modulated by the control of the competitive reactions that irreversibly produce H_2 (i.e. the faradaic hydrogen evolution reaction during the charge and the non-faradaic self-discharge of the reduced TiO_2 phase during discharge). The mechanism proposed in our work when light is applied is therefore a photo-acceleration of the self-extraction of the lithium thanks to the holes that oxidize Ti^{3+} to Ti^{4+}.

In **figure 37**, the photo-charge is performed starting from an initial lithiated electrode at the end of the discharge. While photo-charging, lithium ions are extracted and the state of charge evolves towards the non lithiated state.

We can expect that the photo-charge performance depends on the composition and the phase distribution within the illuminated particle. **Figure 38** illustrates the distribution of the Li-poor and the Li-rich phases within a particle for different initial state of charge.

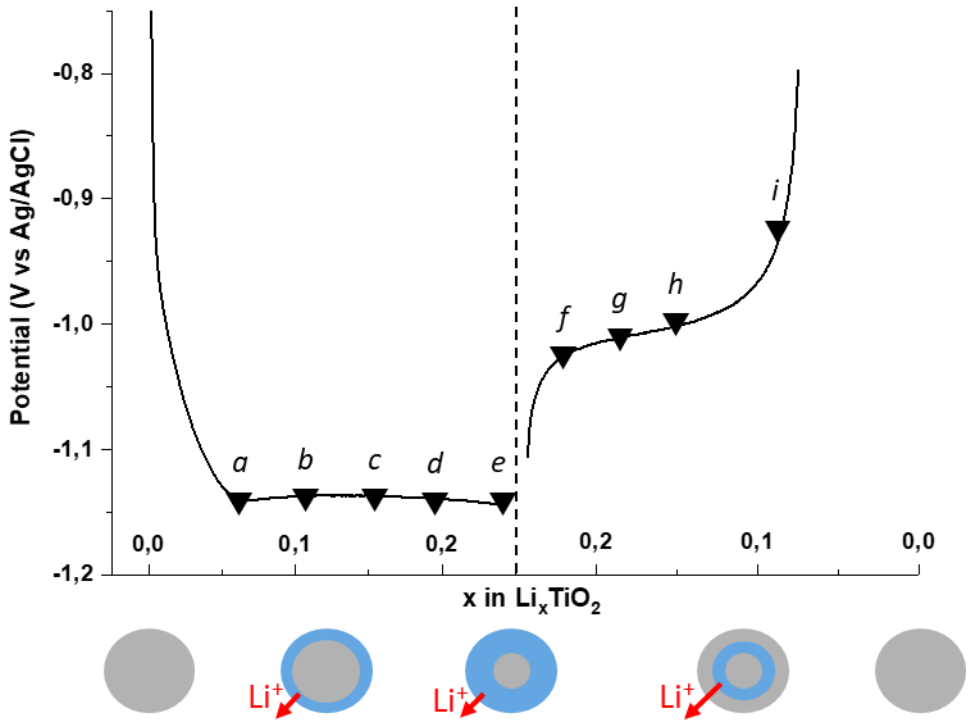

***Figure 38**: Galvanostatic discharge and charge curve at 2C in TiO_2// WIS (20 m)//AgAgCl KCl saturated/ Pt, the arrangement between the different phases at different SOC (from a to i) are illustrated under the galvanostatic experiment. Red arrows representing the photo-extraction of Li^+.*

According to this figure, upon discharge, the shell is mainly composed of the Li-rich phase and the core is composed of the Li-poor phase. Upon charge, the Li-rich phase lies in the more inner part of the particle. If we stop the discharge at different composition, we can easily imagine that this distribution (composition and organization) of the Li-rich and Li-poor phases, with respect to each other, but also with respect to the surface of the particle will affect the photo-charge. For example, a lithium rich phase, source of exciton, situated at the surface of the particle, in other words close to the particle/electrolyte interface, should favor the access of the photo-generated electron to the surface (**figure 38**, 2nd and 3rd particles). This is even more true that the Li-rich phase has shown to be a better electronic conductor. EIS experiments have been performed to confirm our hypotheses and results are summarized in **figure 39**.

A comparison of TiO_2 and $Li_{0.3}TiO_2$ impedance diagrams for the first charge indicates a change of the slope at low frequency, suggesting a modification of electrolyte/electrode interface due to Li insertion and a decrease of the semi-circle at high frequency. This change does reflect the formation of a Li-rich phase, unless it is only localized at the TiO_2 surface.

When the $Li_{0.3}TiO_2$ electrode is discharged i.e. going back to TiO_2, we observe a change of the slope at low frequency, confirming mechanical stresses occurring during charge/discharge in the electrode. The high frequency semi-circle did not go back to the same initial value; this could be linked to a modification of the electrode during cycling.

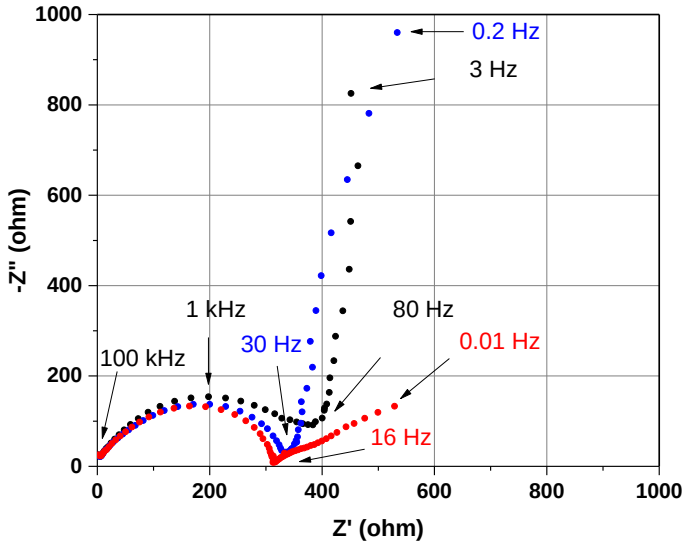

Figure 39: *Impedance of initial TiO_2 (•) , $Li_{0.3}TiO_2$ (•) and TiO_2 (after the charge, •).*

However, a Li-rich phase at the surface should also favor the extraction of the lithium ions, limiting their transport across the particle. If this is true, the configuration upon discharge should be ideal for the photocatalytic reaction to occur. On the contrary, the charge configuration would require the photo-electron to migrate to the surface of the particle through the Li-poor phase, together with the Li-ion. This extra transport means that the photo-electron would have a higher probability to recombine with the hole.

Another factor to take into account is the co-existence of an heterostructure created by interfacing the poor and the rich Li-phase that should generate a built-in electric field which should help, depending on the configuration, the charge carrier separation.[12]

In order to highlight how the Li-poor/Li-rich phases distribution affects the photocatalytic properties of the material, we designed an experiment where we vary the initial state of charge of the electrode before its photo-charge. We will consider various state of charge, obtained during a discharge ($SOC_{a\ to\ e}$), but also during a charge ($SOC_{e\ to\ i}$), in order to access the distributions schematized in **figure 38**.

First, the electrode is discharged at various SOC and then the electrode is illuminated at OCV the full sequence is described in **figure 40**.

One difficulty is to evaluate the actual lithium content for each selected SOC (state of discharge/charge). Indeed, we saw in **Chapter III**, that during discharge, for a lithium content as low as 40 mAh/g, lithium insertion and EC-HER both contributes to the electrochemical signal. In order to circumvent this difficulty, we designed the sequence reported in **figure 40**. First, the electrode is discharged in dark at 2C-rate to a specific state of charge, called SOC_i (PART I). After it is charged at 2C-rate in dark (PART II), and it is discharged again up to same SOC_i at 2C-rate (PART III). Finally, the electrode will be illuminated at OCV (PART IV). This whole sequence (PART I to IV) will be repeated for each SOC_i along the discharge curve.

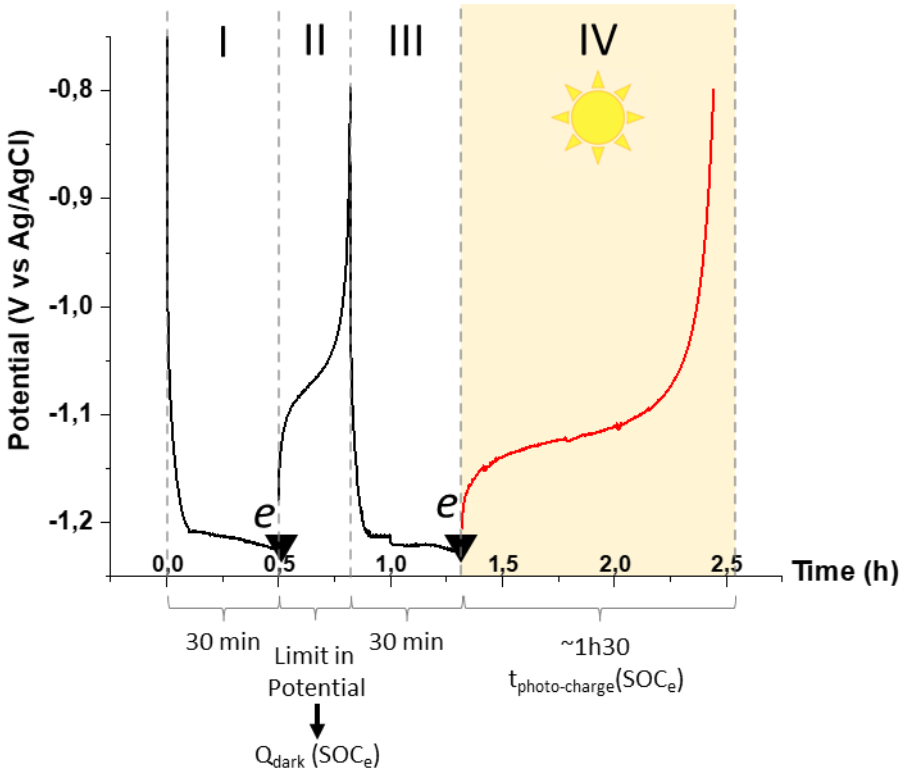

***Figure 40**: Sequence of the different steps from I to IV for one lithium composition (SOC_e), the sequence is repeated for each SOCs. Step I: galvanostatic discharge during 30 min (SOC_e) at 2C, step II: galvanostatic charge with a potential limit of -0.8 V vs Ag/AgCl KCl sat, step III: galvanostatic discharge during 30 min (SOC_e) at 2C, Step IV: Photo-charge (at OCV under illumination).*

The charge at OCV under light (PART IV) provides a time of photo-extraction or photo-regeneration at SOC_i.

Plotting the lithium photo-extracted versus the time of photo-charge at each (SOC_i) allow us to determine the rate of the photo-extraction. The sequence PART I to IV, for SOC_a to SOC_e was repeated on four different samples. From $SOC_{e'}$ to $SOC_{i'}$, the results are based on only one set of data on one sample, we shall therefore be careful about the interpretation. The results are summarized in **figure 41**.

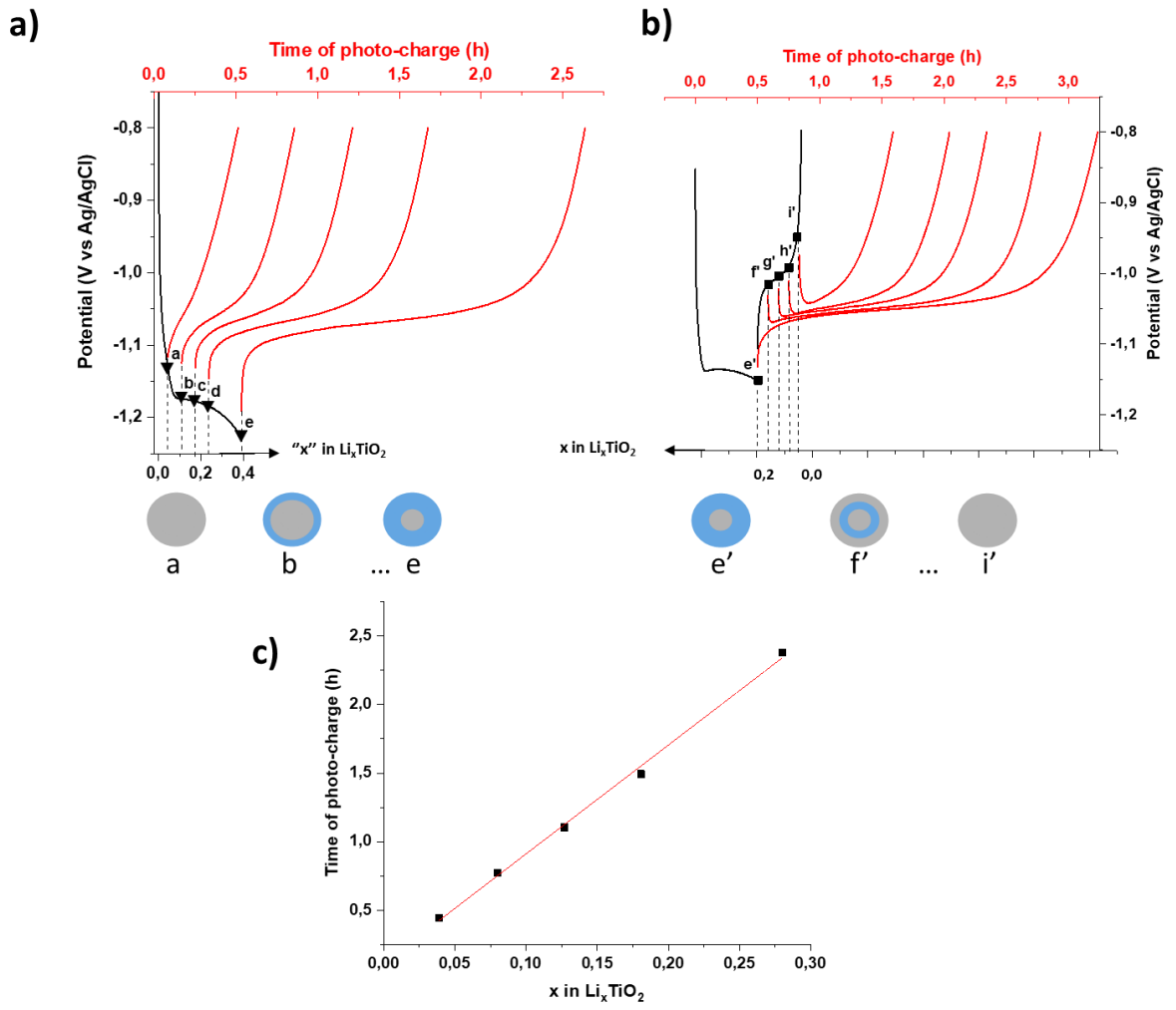

***Figure 41**: (a) Galvanostatic discharge stopped at different composition of lithium (a to e) followed by photo-charge (OCV under illumination), (b) galvanostatic charge stopped at different composition of lithium (e to i) followed by photo-charge (OCV under illumination), c) Time of photo-charge versus the lithium composition in the TiO_2.*

First of all, the results for the discharge configuration show that error bars on the photo-extraction rate are quite high and get even bigger for high initial lithium content.

This could be due to the fact that the H_2 produced during discharge could disturb the lithium insertion and therefore the lithium composition reached. An option to check this hypothesis would have been to change sample for each SOC_i or to help H_2 to diffuse using agitation.

Also, the photo-charge curves of the charge configuration exhibit a peculiar shape in the beginning of the photo-charge (**figure 41b**). Right after switching off the galvanostatic positive current, at OCV, the potential decreases to reach the plateau of the coexistence of the two-phases material usually observed in WIS at -1.1 V at 2C-rate. This is probably linked to accumulation of charges at the interface between the electrode and the electrolyte. Since

a current is applied during the charge, charges will be accumulated at the interface and will be dissipated after switching off the current (OCV). This phenomenon is independent of the light since the same experiment has been done in the dark and the same behavior is observed (**annex III**).

In **figure 41c**, where the time of photo-charge versus the lithium composition is plotted, we can see that the more lithium ions are inserted in the material the slowest the photo-extraction is. We can see a linear function which mean that the rate is constant during the experiment. The rate could be estimated by analyzing the slope of the linear function. We expected an increase of the rate with the increasing composition of lithium since the Li-rich is supposed to be the photo-active phase but this is not the case. The photo-charging rates of the 'discharge part' seems significantly higher than the 'charge part'. It tends to show that a Li-rich phase close to the particle surface shortens the lithium ion transport and ensure higher photocatalytic properties, as predicted. Indeed, literature data[13] show a shift of both the conduction and the valence band toward more positive value for lithiated phase, encouraging the photo-electron to react with water at the interface. In contrary, the positioning of the band is not favorable when the Li-poor phase is at the interface with the electrolyte. This is coherent with the speed evaluated in this experiment.

In order to illustrate the contribution of light, we also compared the photo-charge and self-charge at the same composition. **Figure 42a** presents 3 cycles of discharge (dark) – self-charge at OCV (dark). These result are compared to 3 cycles of discharge (dark)–photo-charge at OCV (**figure 42b**).

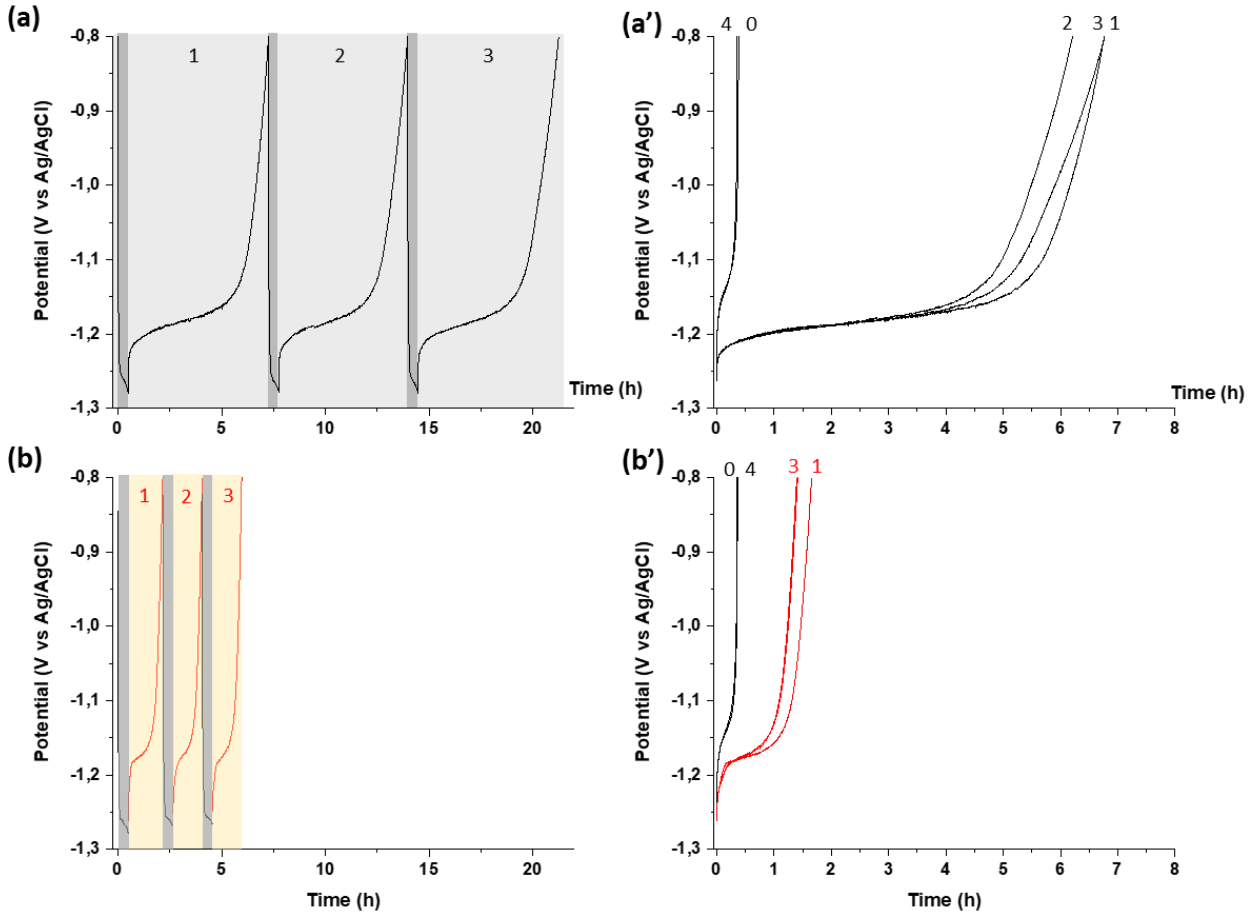

***Figure 42**: Galvanostatic experiments: 3 cycles of discharge at 2C-rate for 30 min and charge at OCV under dark and light conditions. The discharge capacity is constant (111 mAh/g).*
(a,a') Dark cycling: the OCV charge is performed in dark condition.
(b,b') Photo-charge cycling: the OCV charge is performed under illumination. In each case, two extra cycles, (not shown in a,b, but the charge curves are shown in a', b') are performed in the dark before (cycle 0) and after (cycle 4) the 3 cycles, as a control to check the evolution of the actual charge capacity before and after the 'photo-charge cycling'. In a' and b' charge curves of specific cycles from figures a and b, respectively, in order to allow an easy comparison.

The time of self-charge is about 3 times higher than the time of photo-charge. In both cases, the initial dark charge capacity (cycle 0) is equivalent to the final dark charge capacity (cycle 4) in both cases: 80 mAh/g. Both types of cycling present then an excellent capacity retention after 3 cycles.

Taking into account the dark charge capacity extracted from cycle 0 and 4, and the charging time of cycle 1 and 3, we evaluated the rate of lithium extraction. In the case of self-charge, the rate is constant at 0.035 Li^+/h. In the case of the photo-charge, the rate slightly increases from 0.15 up to 0.17 Li^+/h upon cycling. Both the difference in charge time (compared to

self-charge) and the good capacity retention lead us to conclude that light improves the efficiency of the charging at least for a few cycles. Long term cycling was not performed.

In this section, we demonstrated that water from WIS acts as an **efficient photo-electron acceptor**, producing H_2 upon photo-charging. The lithiated TiO_2 electrode can be photo-charged, in other words its lithium ions can be extracted, using visible light. We also showed that (1) there is no influence of the composition over the rate of photo-extraction of the lithium ions and (2) **when the lithium rich phase is situated at the surface of the particle**. This confirms the **key role of the lithium rich phase** in the photo-charge. It can be attributed to its better ability to absorb light and/or to a better electronic conductivity of the phase. The role of the co-existence of a Li-poor and Li-rich phase, which would create a built-in electric field is difficult to highlight. One way would be to show that, when there is no more Li-poor phase, the rate photo-charge rate decreases. However, in the here-studied electrodes no pure lithium-rich phase can be achieved.

IV.2. Study of the Photo-assisted Charge/Discharge

The photo-assisted charge is the charge of the electrode helped by solar energy. The electric charge and discharge could be realized by different experiments: galvanostatic, potentiostatic or even cyclic voltametry (CV). Each experiment could give us information on the mechanism of this photo-assisted charge.

We first studied the impact of light on galvanostatic experiments performed at 2C-rate and on 0.5 mV/s cyclic voltammetry experiments starting from the non lithiated TiO_2 (**figure 43**).

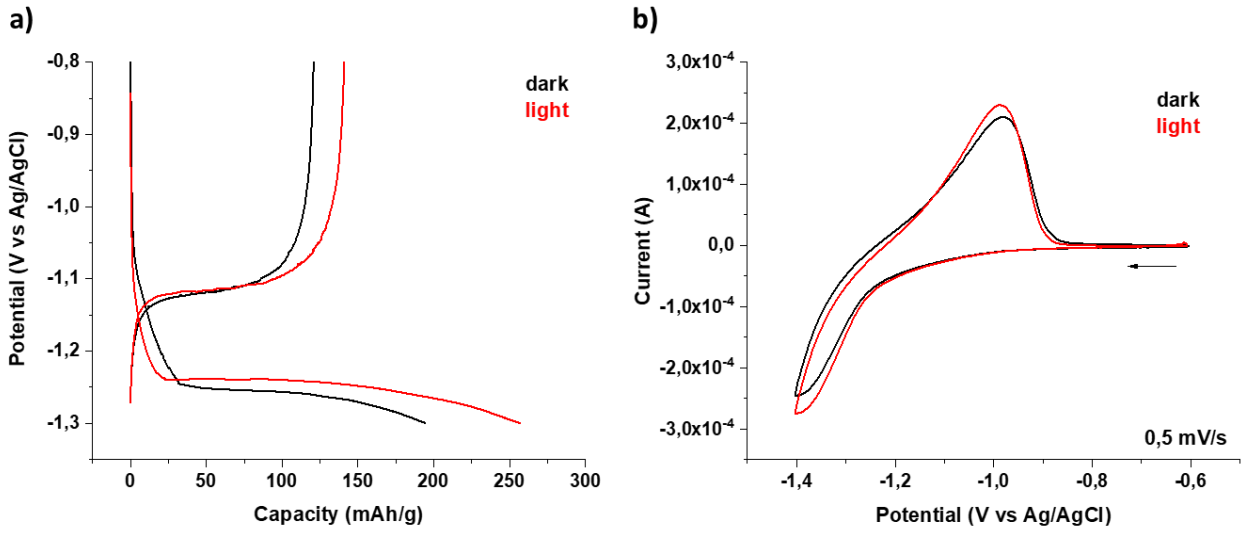

***Figure 43**: (a) Galvanostatic discharge and charge in dark conditions (black curves) and under illumination (red curves) at a 2C rate, (b) CV in dark conditions (black curves) and under illumination (red curves) at 0.5 mV/s from -0.6 V to 1.4 V vs Ag/AgCl of FTO/TiO_2// WIS (20 m)// Ag/AgCl (KCl sat)/ Pt.*

For both CV and galvanostatic cycles, a cycle in the dark is followed by a cycle under illumination. In both experiments, we can see that the signals change.

In CV (**figure 43b**), the intensity of both peaks slightly increases. In terms of capacities, for the reduction part (Li^+ insertion + HER), the capacity increases from 154 to 175 mAh/g with illumination. For the oxidation part (Li^+ extraction) however, the capacity exhibits a small increase under illumination. Concerning the galvanostatic experiment, both discharge and charge capacities significantly increase. Under illumination, the discharge capacities exhibit a 32 % increase (from 194 to 257 mAh/g), while the charge capacity increases from 121 to 141 mAh/g (17 % increase). Some differences appear for the discharge plateau whose potential is slightly higher under light; this is also seen on the CV curves where a slight decrease of the potential of the reduction peak is observed.

The same type of behavior under light was observed when LP30 was used as an electrolyte (**Cf. figure 20, Chapter I**) although the discharge capacity is more important in WIS. This difference may be related to the formation of H_2 since the positioning of the acceptor of electron (the water) limits the electron-hole recombination.

In the light of these results, and based on Nguyen's last work[9], here are our hypothesis for the reactions that take place at each step of the galvanostatic cycles for the WIS electrolyte.

In dark conditions (Cf. Chapter III):

Discharge:

(1) $TiO_2 + 0.5\ Li^+ = Li_{0.5}TiO_2$

(2) $H_2O + e^- = HO^- + ½\ H_2$ (HER)

Charge:

(1) $Li_{0.5}TiO_2 = TiO_2 + 0.5\ Li^+$

Under illumination (in red photo-induced reactions):

Discharge(Galvano)/Reduction(CV):

(1) $TiO_2 + 0.5\ Li^+ = Li_{0.5}TiO_2$

(2) $Li_{0.5}TiO_2 + 0.5\ h^+ = TiO_2 + 0.5\ Li^+$

(3) $H_2O + e^- = HO^- + ½\ H_2$

(4) $H_2O + e^- = HO^- + ½\ H_2$ (PHOTOCATALYTIC)

Charge (Galvano)/Oxidation(CV):

(1) $Li_{0.5}TiO_2 = TiO_2 + 0.5\ Li^+$

(2) $Li_{0.5}TiO_2 + 0.5\ h^+ = TiO_2 + 0.5\ Li^+$

(3') $H_2O + e^- = HO^- + ½\ H_2$ (at CE) (PHOTOELECTROCATALYTIC)

We will discuss only on the "under illumination" part since the "in dark condition" has already been discussed in chapter III. TiO_2 and $Li_{0.5}TiO_2$ designate respectively the Li-poor and Li-rich phase. The red reactions represent the photo-induced reactions. Reaction (2) represents the photo-extraction of the lithium ions thanks to the hole. We can distinguish two HER reactions: the (3) and (4). In equation (3), the electron comes from the current applied at the electrode, we will call it *EC-HER*; and in equation (4) the electron is photo-generated, we will call it *photo-HER*. The reaction (4) happens at the same electrode in the case of discharge, it happens at the other counter electrode in the case of charge (3).

In the latter case, and this is how it differs from the pure photocatalytic reaction, the photo-electron travels through the working electrode to the current collector to create *in fine* hydrogen at the counter electrode. We call it a photoelectrocatalytic reaction.

In the case of Charge/Oxidation, the extra electrochemical capacity comes from extra Li^+ extracted thanks to light. In the case of Discharge/Reduction, the 'apparent' extra capacity comes from the 'parking effect' already suggested in Nguyen et al.[9] This effect can be described as follow: during illuminating the electrode upon discharge, lithium is photo-extracted, it will then free some space, and extra lithium ions can be electrochemically inserted. This extra lithium gives rise to more electron going through the system and giving the appearance of a lithium capacity that increases, when it is actually only compensation the lithium ions that photocatalytically come out.

This assistance from light induces the ΔEp to slightly decrease in CV, and shifts the discharge plateau of the galvanostatic experiment towards higher potential. The potential of the charge plateau does not seem to be affected.

In the following experiments, we tried to **discriminate the impact of light on discharge and on charge**. Therefore, we performed the sequences presented in **figure 44**.

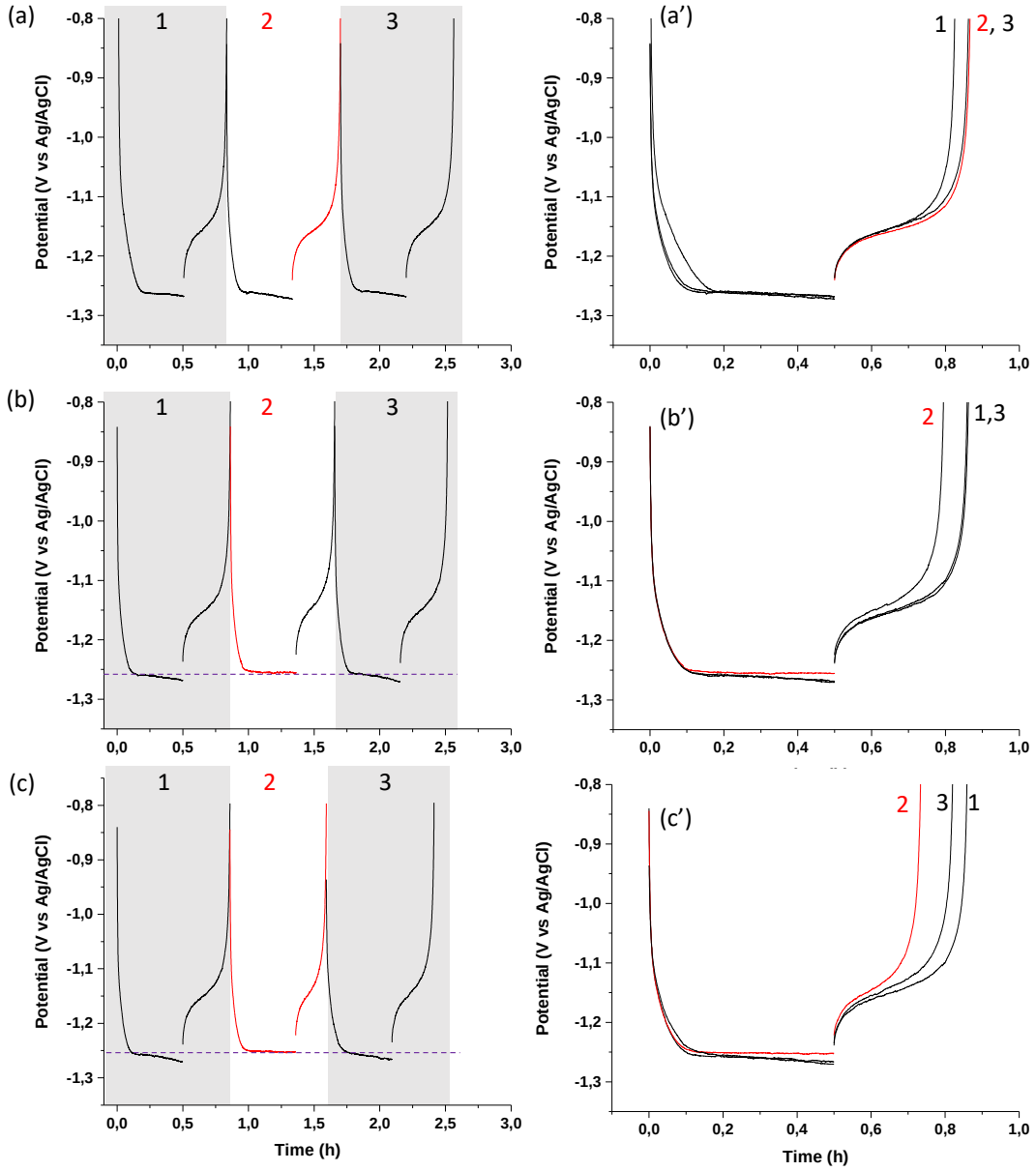

Figure 44: *Galvanostatic experiments performed at 2C-rate highlighting the impact on illumination on charge only (a), discharge only (b) and on both charge and discharge (c). Steps 1 and 3 consist in a cycle of discharge-charge performed in the dark, before and after the step of interest (i.e. step 2) respectively. The discharge time has been set to 30 min, which corresponds to 111 mAh/g. (a', b' and c') represent the same discharge and charge curves as in (a, b and c) starting all 3 discharge-charge curves at time 0 for an easier comparison. Black line are under dark and red line are under illumination.*

In this figure, we present the impact of light on charge only (a, a'), on discharge only (b, b') and on both charge and discharge (c, c'). The latter differs from the experiment illustrated in **figure 43a**, since in this set of experiments, the time of discharge is set to 30 min maximum (instead of a low potential limit).

Steps 1 and 3 are discharge-charge in dark before and after the step of interest (i.e. step 2, where the illumination takes place). Steps 1 and 3 are performed in order to follow the evolution of the system before and after. The results for the sequence a, b and c will be discussed successively.

(a, a') When the illumination is performed during charge only. The charge capacity "2" (under illumination) is 80 mAh/g, it is 11 % higher than charge capacity "1" (in dark, 72 mAh/g). Illumination seems to help extract more lithium ions, the charge is photo-assisted. The plateau potential is slightly lower, it could highlight the contribution of light on the potential (photovoltage), however it is very tiny. Interestingly, the charge capacity "3" stays at 80 mAh/g for the dark step after illumination. In this case, it looks like the extra space freed by the light-charge could be reused in the next discharge.

(b, b') When the illumination is performed during discharge only (discharge limited to 30 min = discharge capacity fixed). The charge capacity "2" (66 mAh/g) is 18 % lower than the capacities 1 and 3 (both at 80 mAh/g). Less lithium ions are extracted after a discharge under illumination. The shape of the plateau under illumination definitely changed: the potential stays perfectly constant even after 30 min. Whereas in the dark, the potential tends to decrease slowly but continuously. The initial and final charge discharge cycles (1 and 3) seem to be not affected at all by the existence of step "2".

(c, c') When the illumination is performed during charge and discharge (discharge limited to 30 min = discharge capacity fixed). As expected from experiment (b), we observe the change in the discharge plateau shape under illumination (2) versus in the dark (1/3). The charge capacity "2" (52 mAh/g) is here 35 % smaller than the charge capacity "1" (80 mAh/g). This value is even lower than the capacity "2" in b (66 mAh/g). The final charge capacity "3" does partially recover the loss (72 mAh/g instead of the initial 80 mAh/g). In addition, in this case, the charge plateau "2" is slightly higher than the charge plateau "1" and "3". It is interesting to compare this result (at least the results for 1 and 2) to the result presented in **Figure 43a**: a cycle of discharge-charge in dark is followed by an illuminated discharge charge, but the limit of the discharge curve is not time but a potential limit. In this case, as previously described, this system exhibits an increase of both charge and discharge capacities when the electrode is illuminated.

The same sequence of experiments has been done at 4C-rate, the results show the same trends but the differences are less pronounced. These results are gathered in **Annex IV**.

At this point, it is interesting to examine how this set of results challenges and/or comforts the hypotheses we made about the mechanisms of a photo-assisted discharge and charge; in brief a photocatalytic HER inducing Li^+ extraction, and its subsequent 'parking mechanism' during discharge and a photoelectrocatalytic HER inducing Li^+ extraction during charge (Equations 3').

In (a), an extra light charge capacity is expected given the existence of lithium ions photoelectrocatalytically extracted. In (b), the modification of the shape of the discharge plateau under illumination (b2) is also expected since the 'parking mechanism' previously described induces an elongation of the discharge plateau. In the (b) experiment however, the discharge has been stopped at 30 min, before the end of the discharge plateau. Plus, the dark charge capacity "2" is very small. These two features could highlight the consequence of lithium ions being photocatalytically extracted during discharge (b2) with no opportunity (discharge stopped) for more lithium ions to electrochemically insert the material. In the case of (c), the extremely small charge capacity c2 (54 mAh/g) can be puzzling regarding the suggested mechanism. How could it be smaller than the charge capacity (b2, 66 mAh/g)? We were expecting smaller capacities (around 7 %) from the 11 % increase observed in a2 (illuminated charge) tempered by the 18 % decrease of the amount of the lithium ion observed in b2 (illuminated discharge stopped). A feature that we didn't take into account in this discussion so far is the structure of the electrode. According to the suggested mechanism, the structure of an electrode particle at the end of an interrupted illuminated discharge (c2) is different from the structure of an electrode particle at the end of an interrupted dark discharge (a2). At the end of an interrupted dark discharge, the particle surface is composed of the Li-rich phase. At the end of an interrupted illuminated discharge, given the photocatalytic reaction happening at its surface (which would not be balanced by the parking phenomena in the 30 min discharge, as previously discussed), we expect the surface of the particle to form a surface layer composed of the Li-poor structure. This outer layer might initially contribute to explain why Li^+ extraction is impeded, as supported by the high charge voltage plateau of c2.

This experiment leads us to think that the particle composition and structuration might play a role in the photo-activity of the film. In order to highlight if/how the lithium content and its organization triggers/hinder a photo activity, a chopped CV and chopped potentiostatic experiments were performed. The results are illustrated in **figure 45**.

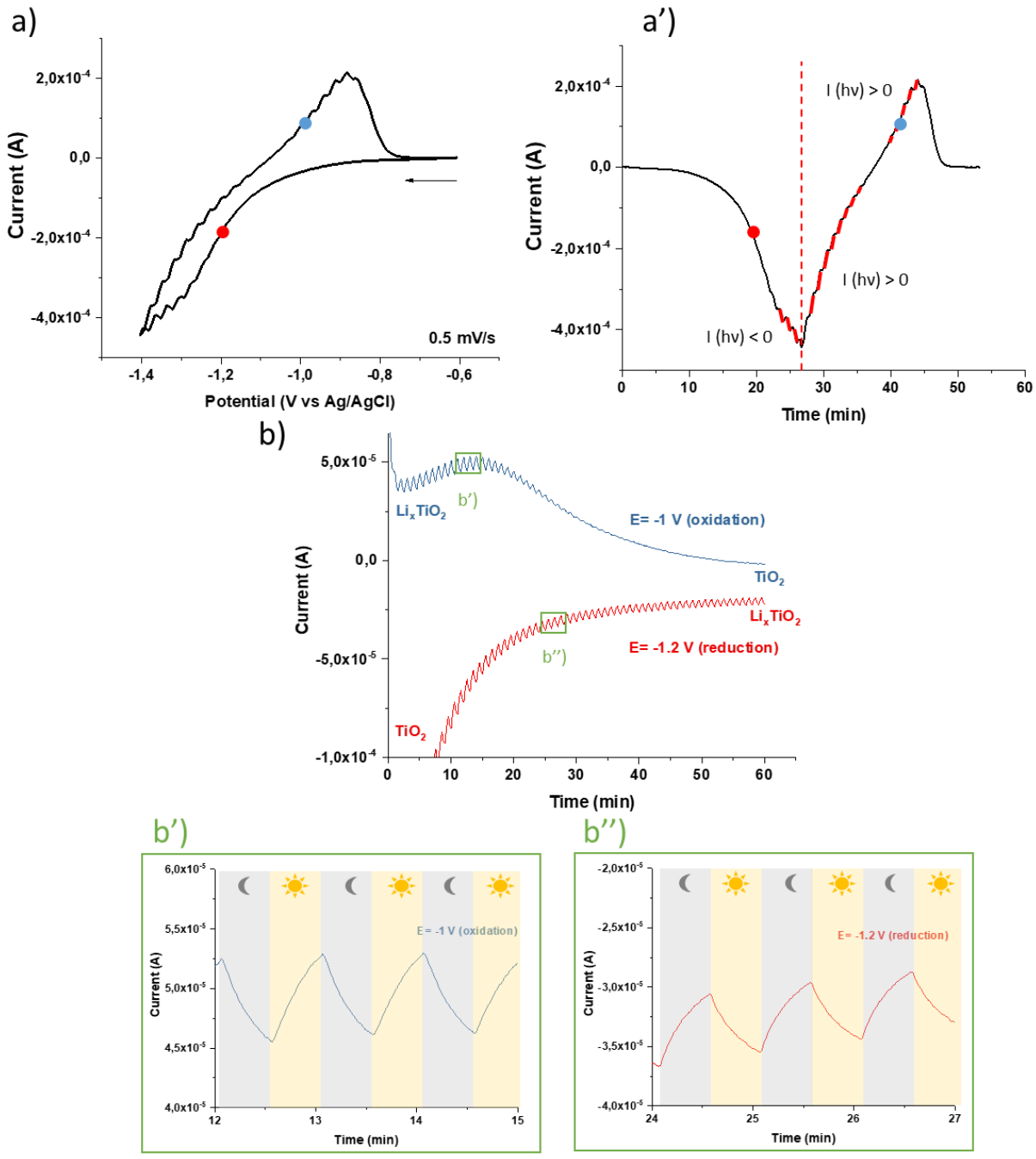

***Figure 45**: (a,a') CV at 0.5 mV/s starting from -0.6 to -1.4 V vs Ag/AgCl with chopped illumination every 30 seconds. (a') presents the same CV as (a) but a little differently for the sake of clarity. The portions of the curves highlighted in red correspond to times where the illumination takes place (b) Potentiostatic experiments under chopped illumination (light is switched on and off every 30 seconds) at -1 V (blue) and -1.2 V (red), a zoom of the photo-currents has been made for the zones b'), b'') for the oxidation and the reduction respectively.*

Compared to the activity of usual photoelectrocatalysts like TiO_2 for example, it is important to note that the observed photo-currents in this figure are relatively small. They appear as timid "fins" over the dark electrochemical signal. Another sign of their low intensity lies in the fact that photo-current do never reach a plateau. However, no spikes are observed when the light is turned on, this behavior demonstrates that few surface recombination occurs in the electrode, which is probably linked to the structure of the lithiated TiO_2 NPs, their composition gradient and their dynamics. This relatively low photo-current intensity might also explain the moderated impact of the photo-assistance on charge and discharge discussed in this chapter.

Figure 45 a and a' present a chopped CV experiment performed at 0.5 mV/s for 30 s-long illumination periods. Looking at the reduction wave**,** a photo-activity is observed starting at -1.2 V to the end of the reduction wave. It means that the electrode material becomes photo active almost as soon as lithium ions are inserted (starting at 0.21 Li^+ inserted with the hypothesis that at this potential a small amount of hydrogen is produced). On the oxidation wave, a photo-activity is present only from -1 V to -0.85 V, which corresponds to the first part of the oxidation wave. The photoactivity declines when the lithium content is too low (lower than 0.06 Li^+). **Figure 45a'** highlights in red, on the same CV, the portions of the curve that were illuminated during the chopped experiment, allowing us to track the sign of the photo-current along the chopped CV. It appears that, starting at around -1.2 V and as long as the potential is decreasing, a negative photo-current is observed: the material behaves as a "p-type" semiconductor. As soon as the potential changes direction heading towards higher potentials, the photo-current becomes positive and the material behaves as a "n-type" semi-conductor.[14,15] The positive photo-current also vanishes between -1.1 and -1.0 V. Depending both on the lithium content, and on the applied potential (including its direction), which impacts the occupation of the material electronic bands, the initially n-type TiO_2 material could turn p and back to n.[12] In this context, there is also a potential range, from -1.2 V to -1.4 V, where the material could be ambivalent ('n-like' and 'p-like' at the same time).

Potentiostatic experiments were also conducted under chopped illumination and are presented in **figure 45b**. Two values of potential (-1.2 V, and -1.0 V) are chosen, they constitute the starting point of the film photo-activities, they are illustrated by the blue and red dots in **figure 45a**.

The first experiment is performed at -1.0 V **(in blue, zoom in b')** and starts with the lithiated phase that is obtained after discharge at 2C-rate in dark. During the experiment, the film progressively turns from blue (color of the lithiated phase) to colorless (like TiO_2). We observe that the photo-activity (positive photo-current, n-type activity) dies progressively as the lithium ions get out of the structure.

The second potentiostatic experiment is conducted at -1.2 V **(in red, zoom in b'')** and starts with the non lithiated phase. In the experiment at -1.2 V, the initially transparent film turns progressively blue. In this case, the electrode exhibits a current different from zero over the entire experiment. Plus, the photo-current is always negative, which corresponds to a 'p-type' activity. According to the suggested mechanism and the 'parking phenomena', we attributed the extra negative current under illumination to more lithium ions electrochemically entering the structure, after that some Li^+ get photocatalytically extracted. There might be another way to consider to explain the photo-current upon reduction. If we apply the classical description of a 'p-type' semiconductor at our material, it could mean that the photogenerated holes travel through the external circuit, while the photogenerated electrons contributes to HER.

The reactions on discharge upon illumination would be reduced to:

Under illumination (in red photo-induced reactions):

<u>Discharge(Galvano)/Reduction(CV):</u>

(1) $TiO_2 + 0.5\ Li^+ = Li_{0.5}TiO_2$

(2) $H_2O + e^- = HO^- + ½\ H_2$ (photoelectrocatalytic reaction, the hole goes to the counter electrode)

In this case, the Li-rich phase acts a classical p-type photoelectrocatalyst active in the visible range of the light spectrum.

According to previous results (**figure 43 and 44**), this mechanism is plausible. However, for a pure photoelectrocatalytic reaction, we would expect very fast kinetics.

However here, the impact of light is more pronounced at slow rates (2C vs 4C), 30 seconds is also the shortest time period to actually visualize a “fin” in the CV curve for example. Even though at this point this hypothesis cannot be strictly excluded, we consider that for the reduction part (or discharge), a photocatalytic reaction, which would force lithium ions to diffuse out of the material, the most likely mechanism, the lithium diffusion being the rate determining step.

In the section dedicated to photo-charge, we clearly highlighted the advantage of a photo-charge compared to a self-charge upon limited cycling (three cycles). The mechanism of photo-charge at OCV (in brief: a photocatalytic HER with Li^+ extraction) is different from a photo-assisted charging (in brief: a photoelectrolocatalytic HER with Li^+ extraction). **In this case, is a photo-assisted cycling beneficial?** To answer this question, we compare the evolution of 10 cycles of discharge-charge performed at 2C-rate where the charge will be performed in the dark (dark cycling) or under illumination (photo-assisted cycling). The results are presented in **Figure 46**.

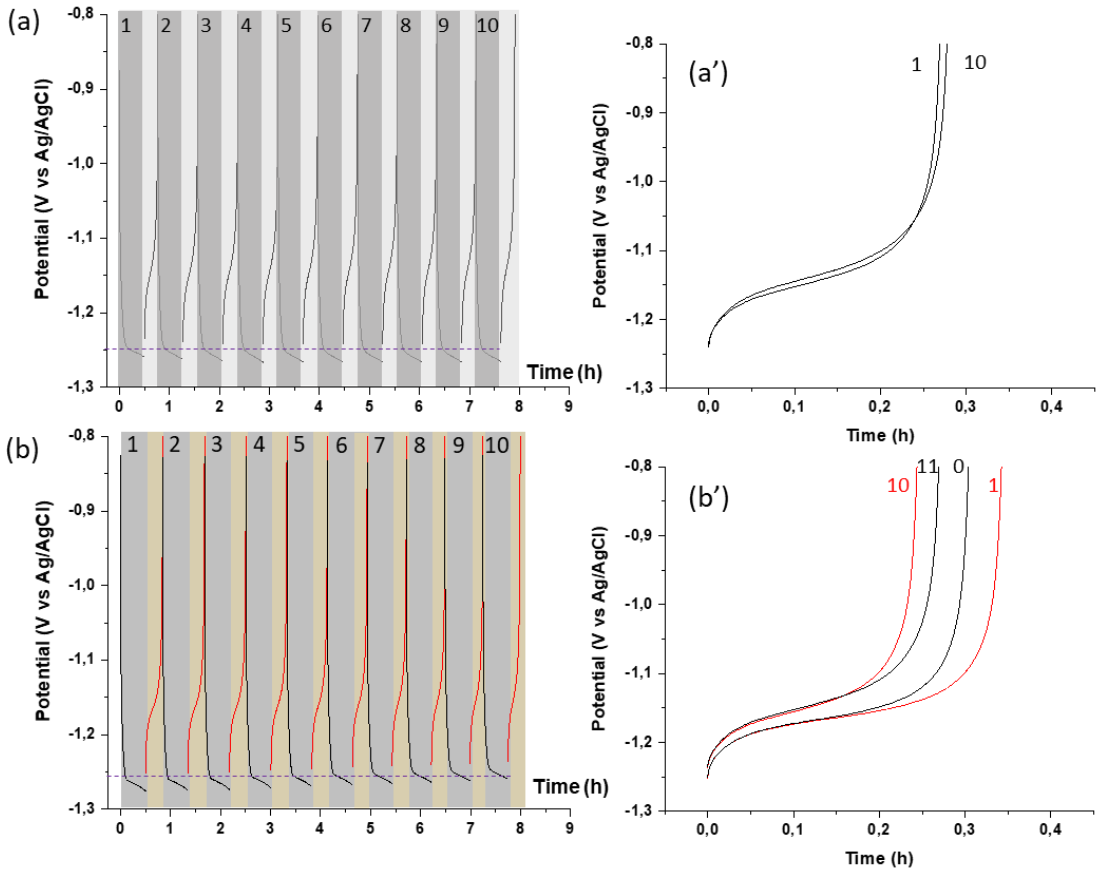

***Figure 46**: Galvanostatic experiments: 10 cycles of discharge-charge at 2C-rate. The discharge time was set to 30 min for all experiments, which corresponds to a constant discharge capacity of 100 mAh/g. (a,a') Dark cycling: the charge is performed in dark condition. (b,b')Photo-assisted cycling: the charge is performed under illumination. In this case, two extra cycles (not shown here) are performed in the dark before (cycle 0) and after (cycle 11) the 10 cycles, as a control to check the evolution of the actual charge capacity before and after the 'photo-assisted cycling'. In a' and b' charge curves of specific cycles from figures a and b, respectively, in order to allow an easy comparison. Horizontal dashed purple lines on figures a and b are a guide for the eye.*

The dark cycling exhibits no charge capacity change after 10 cycles (54 mAh/g and 55 mAh/g for cycle 1 and 10 respectively). The photo-assisted cycling suffers a small capacity loss: from an initial charge capacity of 60 mAh/g (obtained from the control initial dark charge on cycle 0), the final charge capacity reaches 55 mAh/g (obtained from the control final charge on cycle 11). In the case of dark cycling, the time required to charge the electrode is constant for each cycle (around 16 min). Given the charge capacity, it corresponds to a rate of 0.6 Li^+/h. In the case of 'photo-assisted cycling', the time required to charge the electrode varies upon cycling from 21 min, which corresponds to 0.5 Li^+/h (for a 60 mAh/g charge capacity) for the 1st cycle; to 15 min, which corresponds to 0.7 Li^+/h (for a 55 mAh/g charge capacity) for the cycle 10.

In the photo-assisted configuration, the rate of Li^+ extraction seems disfavored at first compared to the dark charge and it ends up increasing upon cycling up to 0.7 Li^+/h, which is faster than for the dark charge. The **figure 46b'** extracts from **figure 46** the charge curves of cycle "1" and "10", together with the control charges in the dark performed before (cycle "0") and after (cycle "11") the ten cycles. If we compare the charge curves of cycle "1" (light) and "0" (dark), the plateau voltages are similar. The same observation can be done when comparing the charge curves of cycle "10" (light) and cycle "11" (dark). There is no evidence of a photo-voltage, which would result in a decrease of the voltage plateau. However, there is a voltage shift between the charge plateau of cycle "0" vs. "1" and of cycle "10" vs. "11". The same shift is present for the discharge plateau (a horizontal purple dashed line on **figure 46b** allows to better apprehend the shift towards higher potential). This voltage evolution, present in both charge and discharge curves, can therefore be attributed to a progressive decrease in the cell ohmic resistance for the photo-assisted cycling, due to better electronic conductivity. This evolution is not observed during dark cycling.

Looking only at the overall time of the two experiments, which are very similar for a dark and a photo-assisted cycling, we might say that there is no significant advantage of a photo-assisted charge vs a dark charge. However, looking more closely at the evolution of the lithium ions extraction rate, the charge capacity and the ohmic drop during the photo-assisted charge, it is obvious that illuminating the system is not innocent. There are differences between the two cycling experiments. There is a positive impact of the photo-assistance on the lithium rate extraction, however it appears to be slightly detrimental to the charge capacity retention.

The results of this section show that the WIS system exhibits similar behavior compared to the LP30 system with respect to illuminating the (photo)electrode, during CV, galvanostatic, chopped CV/potentiostatic experiments. Although the **mechanism that we propose is different upon discharge/reduction and charge/oxidation**. It involves **photocatalysis during discharge** and **photoelectrocatalysis during charge**. We observe a limited benefit for the photo-assisted cycling. The **lithium rich phase** plays an important role in the activation of the photoactivity.

Conclusion

In this Chapter, we managed to induce visible production of HER using lithiated anatase TiO_2 mesoporous films in WIS electrolyte. We used a battery configuration where TiO_2 is at a positive electrode to electrochemically insert lithium ions. Discharging the battery involves lithium insertion in TiO_2, and using solar illumination, we could charge the electrode producing H_2. We studied the impact of the material structuration, in terms of lithium content and of phases (Li-poor/Li-rich) distribution within the particle. We showed that photocatalytic or photoelectrocatalytic both required Li-rich content starting around $Li_{0.2}TiO_2$ to become active in the visible. A configuration where the Li-rich phase was located at the surface seems to be key to reach higher rate of photoactivity.

In the next Chapter, we will change the current collector to be able to work with Li-rich TiO_2 with a concentration in Li of 0.5. In addition, we will be using structured substrate for better light absorption and stability in potential. To do so, we used black silicon substrate. Finally, we will study the proposed mechanism when solid electrolyte is in contact with the TiO_2 nanostructured electrode. In this situation, we will voluntary push the photo-electron to pass through external circuit to favor Li deposition at the counter electrode.

Bibliography

(1) Naldoni, A.; Allieta, M.; Santangelo, S.; Marelli, M.; Fabbri, F.; Cappelli, S.; Bianchi, C. L.; Psaro, R.; Dal Santo, V. Effect of Nature and Location of Defects on Bandgap Narrowing in Black TiO_2 Nanoparticles. *J. Am. Chem. Soc.* **2012**, *134* (18), 7600–7603.

(2) Serpone, N. Is the Band Gap of Pristine TiO_2 Narrowed by Anion- and Cation-Doping of Titanium Dioxide in Second-Generation Photocatalysts? *J. Phys. Chem. B* **2006**, *110* (48), 24287–24293.

(3) Chen, X.; Liu, L.; Huang, F. Black Titanium Dioxide (TiO_2) Nanomaterials. *Chem. Soc. Rev.* **2015**, *44* (7), 1861–1885.

(4) Meekins, B. H.; Kamat, P. V. Got TiO_2 Nanotubes? Lithium Ion Intercalation Can Boost Their Photoelectrochemical Performance. *ACS Nano* **2009**, *3* (11), 3437–3446.

(5) Sánchez-Tovar, R.; Blasco-Tamarit, E.; Fernández-Domene, R. M.; Lucas-Granados, B.; García-Antón, J. Should TiO_2 Nanostructures Doped with Li^+ Be Used as Photoanodes for Photoelectrochemical Water Splitting Applications? *Journal of Catalysis* **2017**, *349*, 41–52.

(6) The Mystery of Black TiO_2: Insights from Combined Surface Science and In Situ Electrochemical Methods | ACS Materials Au https://pubs.acs.org/doi/full/10.1021/acsmaterialsau.1c00020 (accessed **2021** -12 -06).

(7) Agrawal, A.; Cho, S. H.; Zandi, O.; Ghosh, S.; Johns, R. W.; Milliron, D. J. Localized Surface Plasmon Resonance in Semiconductor Nanocrystals. *Chem. Rev.* **2018**, *118* (6), 3121–3207.

(8) Dahlman, C. J.; Agrawal, A.; Staller, C. M.; Adair, J.; Milliron, D. J. Anisotropic Origins of Localized Surface Plasmon Resonance in N-Type Anatase TiO_2 Nanocrystals. *Chemistry of Materials* **2019**, *31* (2), 502–511.

(9) Nguyen, O. Towards a Li-Ion Photo-Rechargeable Battery. thesis, Sorbonne Université, 7 place Jussieu, **2018**.

(10) Bogati, S.; Georg, A.; Graf, W. Photoelectrochromic Devices Based on Sputtered WO_3 and TiO_2 Films. *Solar Energy Materials and Solar Cells* **2017**, *163*, 170–177.

(11) MAKIVIĆ, N.; Balland, V. Reversible Proton-Coupled Charge Storage in Nanostructured Amorphous and Anatase TiO_2. thesis, Université de Paris, Laboratoire l'Electrochimie Moléculaire, Université de Paris.

(12) Xia, T.; Zhang, W.; Murowchick, J.; Liu, G.; Chen, X. Built-in Electric Field-Assisted Surface-Amorphized Nanocrystals for High-Rate Lithium-Ion Battery. *Nano Lett.* **2013**, *13* (11), 5289–5296.

(13) Andriamiadamanana, C.; Sagaidak, I.; Bouteau, G.; Davoisne, C.; Laberty-Robert, C.; Sauvage, F. Light-Induced Charge Separation in Mixed Electronic/Ionic Semiconductor Driving Lithium-Ion Transfer for Photo-Rechargeable Electrode. *Advanced Sustainable Systems* **2018**, *2* (5), 1700166.

(14) McCann, J. F.; Pezy, J. The Measurement of the Flat band Potentials of N-Type and P-Type Semiconductors by Rectified Alternating Photocurrent Voltammetry. *J. Electrochem. Soc.* **1981**, *128* (8), 1735.

(15) Hankin, A.; E. Bedoya-Lora, F.; C. Alexander, J.; Regoutz, A.; H. Kelsall, G. Flat Band Potential Determination: Avoiding the Pitfalls. *Journal of Materials Chemistry A* **2019**, *7* (45), 26162–26176.

CHAPTER V: Challenges and perspectives

TABLE of CONTENTS

Introduction

In this thesis few challenges could be highlighted. We studied in this manuscript an innovative way to collect and store the solar energy by the use of a photo-battery with different architecture throughout the literature and especially the use of TiO_2 bi-functional photo-electrode. The objective was to study the photo-mechanism. Indeed, the light absorption and the change of composition of the TiO_2 upon lithiation is a very challenging approach since the properties evolve with the composition. That's why we decided to choose a model electrode without dye or carbon in order to have a composition as simple as possible to study this complex but rich topic of bi-functional electrode. A pending question in the literature upon these system is the fate of the photo-charges. Indeed, since the band diagram of the semiconductor could be modified by the insertion of cations and the energy of the photo-charges are dependent on the position of the conductive and valence band; it is a challenging task to well identify the energies of these photo-charges and so their fate. Moreover, during lithiation a coexistence between two phases occur resulting in different organization in space but also in energy of the band diagram.

Previous studies[1–3] on this bi-functional electrode TiO_2 showed the formation of a Solid Electrolyte Interface (SEI) exacerbate under illumination, specifically when organic electrolyte is used. The hypothesis was the reduction of the electrolyte by the photo-electron. This SEI is detrimental to this system since (1) it wastes one photo-charge and (2) reduces the battery efficiency. To overcome this issue, we used a Water In Salt (WIS) electrolyte to use both photo-generated charges for the storage. Indeed, the electron is used to transform the water into dihydrogen which is a chemical storage since the energy is stored in the chemical band between the hydrogen and the hole is used to extract the lithium ion from a battery material, so an electrochemical storage. We managed in this thesis, to control the fate of these photo-charges and this change of electrolyte does not modify the battery properties of the material. However, since the Hydrogen Evolution Reaction (HER) consume the water of the electrolyte a compensation system need to be found.

This HER occur also during the insertion of the lithium in our mesoporous TiO_2 anatase thin film in the dark and is in competition with it. The electrochemical dissociation between these two phenomena is not an easy task. In this thesis, we used an operando UV-VIS-NIR spectroscopy to follow the evolution of the absorbance of the material during the charge and discharge of the system, this allow us to follow the composition of lithium in the TiO_2 and separate the contribution of the HER from the lithium insertion during a discharge. A complementary experiment to future investigate the lithium composition is the use of Raman spectroscopy in order to follow the oxidation state of the titanium center since it is closely linked with the composition of lithium and the state of charge.

We also studied this same evolution of composition on (1) the photo-charge of the material and (2) the electrochemical production of hydrogen. We showed an increase of the rate of charge under illumination and also an increase production of hydrogen in the dark. The use of solar energy allows fast charging but also energy saving since for the same speed the charging time is reduced under illumination.

As a perspective, we used a solid electrolyte (LiPON) more stable than liquid in order to avoid the photo-electron to react with the electrolyte allowing the lithium ion to be reduced at the counter lithium electrode. An optimization of the deposition of the LiPON and the lithium metal still need to be done. The study of the influence of the cation insertion pave the way of the use of multifunctional material[4]. A study of the influence of the type of cation, the type of electrolyte, the concentration of the cations, the influence of the pH or the crystallinity could be done toward the efficiency of HER or (oxygen Evolution Reaction) OER. The investigation could be extend to other semiconductor and insertion material like $LiFePO_4$[5], $LiWO_3$[6], $LiMn_2O_4$[7] or perovskite[8,9].

Here we saw the conclusion of this work with the battery point of view but a different approach could be done. We show a way to boost the production of hydrogen by inserting cation in a semiconductor in the dark. This kind of dynamic material could be used in photo-catalyst for HER or OER.

This thesis open prospects in different field like photo-catalyst for hydrogen production and the concept could be extended to other semiconductors[10] reported In the literature if they are able to insert ions in there structure. This work also paves the way of the battery field with innovative ways to charge a battery with renewable energy. For the battery part we can couple this photo-electrode with another one in order to have a full device rechargeable by the solar energy using even less electrical energy.

The first one is the limitation in reductive potential due to the substrate of FTO. We saw that under a certain potential and depending on the pH if an aqueous electrolyte is used the FTO is not stable.

A second challenge is the cost of the WIS electrolyte. Indeed, since it is a highly concentrated electrolyte the cost of the prepare electrolyte should be taken into account for further application.

And last but not least we can see in the literature that the trend tends to move to solid electrolyte instead of liquid ones in order to avoid safety issue and to have a more compact device. We are going to investigate few perspectives in order to overcome challenges.

V.1. Reaching high lithium content

The currently used substrate FTO tends to be reduced at potential lower than 1V vs $Li^+/Li°$, it thereby limits the potential range accessible. Going to lower potential should help increase the lithium content in TiO_2, since it would give access to the fully lithiated $LiTO_2$. An approach would be to change substrate.

Therefore, we considered a plasma-etched black-silicium nano-needles (b-Si)[11] material as substrate. It has been used instead of the FTO in an organic electrolyte (LP30) to avoid predominant EC-HER. We chose to work in LP30, rather than in WIS, to prevent a large contribution of EC-HER expected at lower potential. The b-Si is a better conductor (20 Ω compared with 80 Ω for the FTO). We studied the electrochemical behavior of the usual mesoporous anatase TiO_2 films deposited on b-Si substrate in LP30. A CV at 0.35 mV/s down to 0.5V vs $Li^+/Li°$ is performed in order to increase lithium insertion. The rate of the scan is reduced compared to previous study in order to allow the lithium to be inserted in the TiO_2.

The potential window of the scan is broadening in the reduction area in order to reach higher composition of lithium (from 3 V to 0.5 V vs Li^+/Li). The results are summarized in **figure 47**.

From the CV, the typical wave of the Ti^{4+} to Ti^{3+} reduction between 2 and 1 V and the reverse wave between 2 to 3 V are observed. A new signal under 1 V (**figure 47a**) appears and could be linked to the conversion reaction of the silicium substrate with the lithium ion. Indeed, since the TiO_2 is porous and thin, the electrolyte can pass through it and reach the b-Si substrate. The silicium is known as conversion material and form upon lithiation a $Li_{15}Si_4$ (3 578 mAh/g) phase with an increase of volume about 300 % limiting its usage along with an non stable SEI[12].

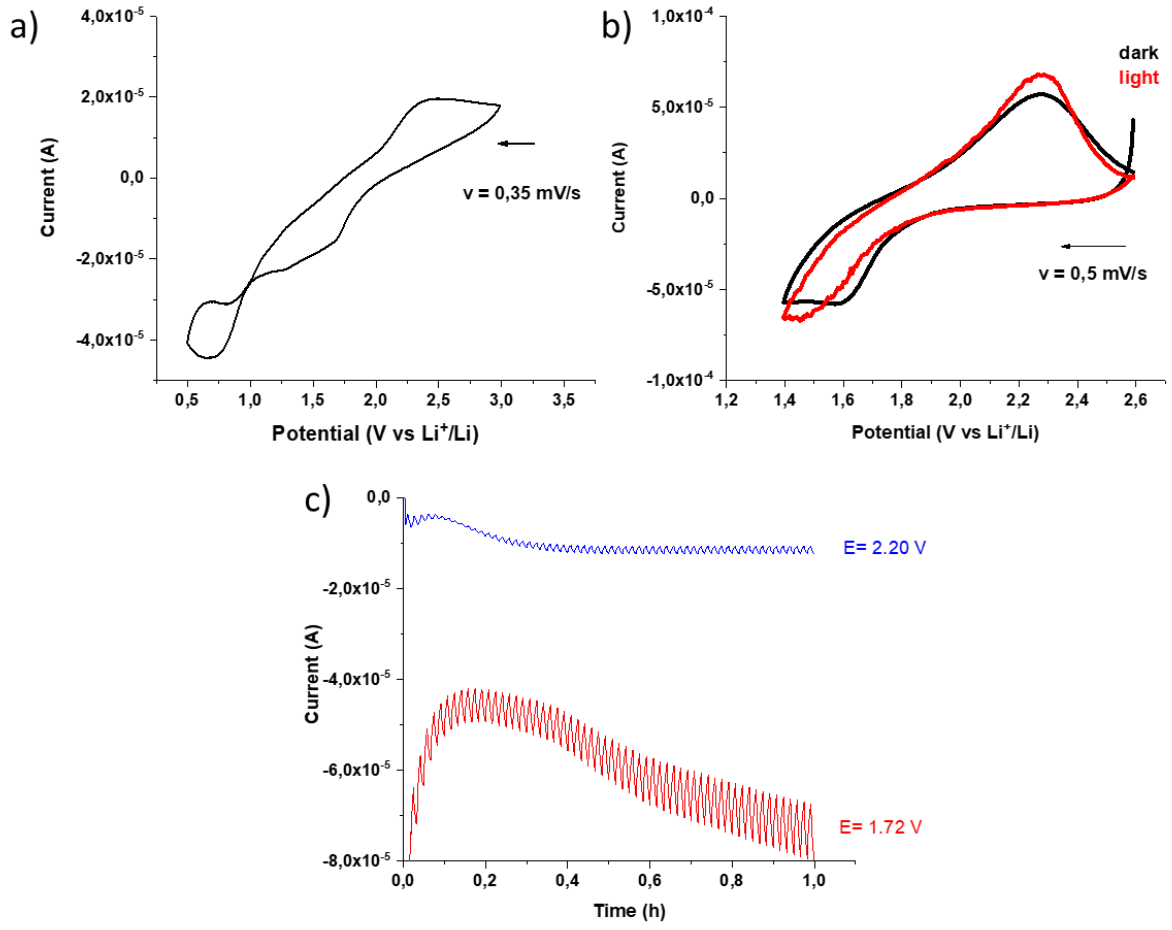

***Figure 47**: (a) CV at 0.35 mV/s starting from 3 to 0.5 V vs $Li^+/Li°$, (b) CVs at 0.5 mV/s from 2.6 to 1.4 V vs $Li^+/Li°$ under dark (black line) and under illumination (red), (c) potentiostatic chopped (30s under illumination, 30 s under dark conditions at 2.2 V (blue line) and 1.7 V (red line) the set up used is (+) b-Si/TiO_2//LP30 (1M)//Li°, Li° (-).*

To compare this substrate with the FTO used previously, the same CV experiments (with the same potential window and the same rate) were realized under dark and light conditions. We can also notice that the intensity of the wave is smaller than on FTO, this is quite surprising since the substrate is less resistive, so the intensity should be higher on b-Si than on FTO. The potential between the reduction and the oxidation wave of the redox couple of the titanium increases (0.4 V vs 0.3 V in WIS with the FTO substrate). It means that the reaction is less reversible with the b-Si substrate. Under illumination, the difference between the two substrates increases which is surprising, the reverse effect was expected as we saw in the LP30 and the WIS studies. The light should reduce the overpotential of reactions, here it seems that the light is detrimental to the insertion of lithium ions on this b-Si substrate and no explanation was found.

The same potentiostatic experiments under chopped illumination were realized (**figure 47c**). Here, the photo-current under oxidative potential does not disappear like shown in the LP30 and WIS experiment. We can also notice that a small photo-current was observed, 12 µA and 2 µA for the reduction and the oxidation potential, respectively. We need also to take into account that the photo-current on oxidative potential are under 0 A unlike the previous studies.

One hypothesis for these modest results was that the change of volume leading to a bad contact between the silicium and the TiO_2 mesoporous film. We try to change de density of the first layer of the TiO_2 by changing the Pb-*b*-PEO concentration in order to have more space for the b-Si to “breath”. SEM-FEG images are shown in **figure 48** to visualize the different contact made.

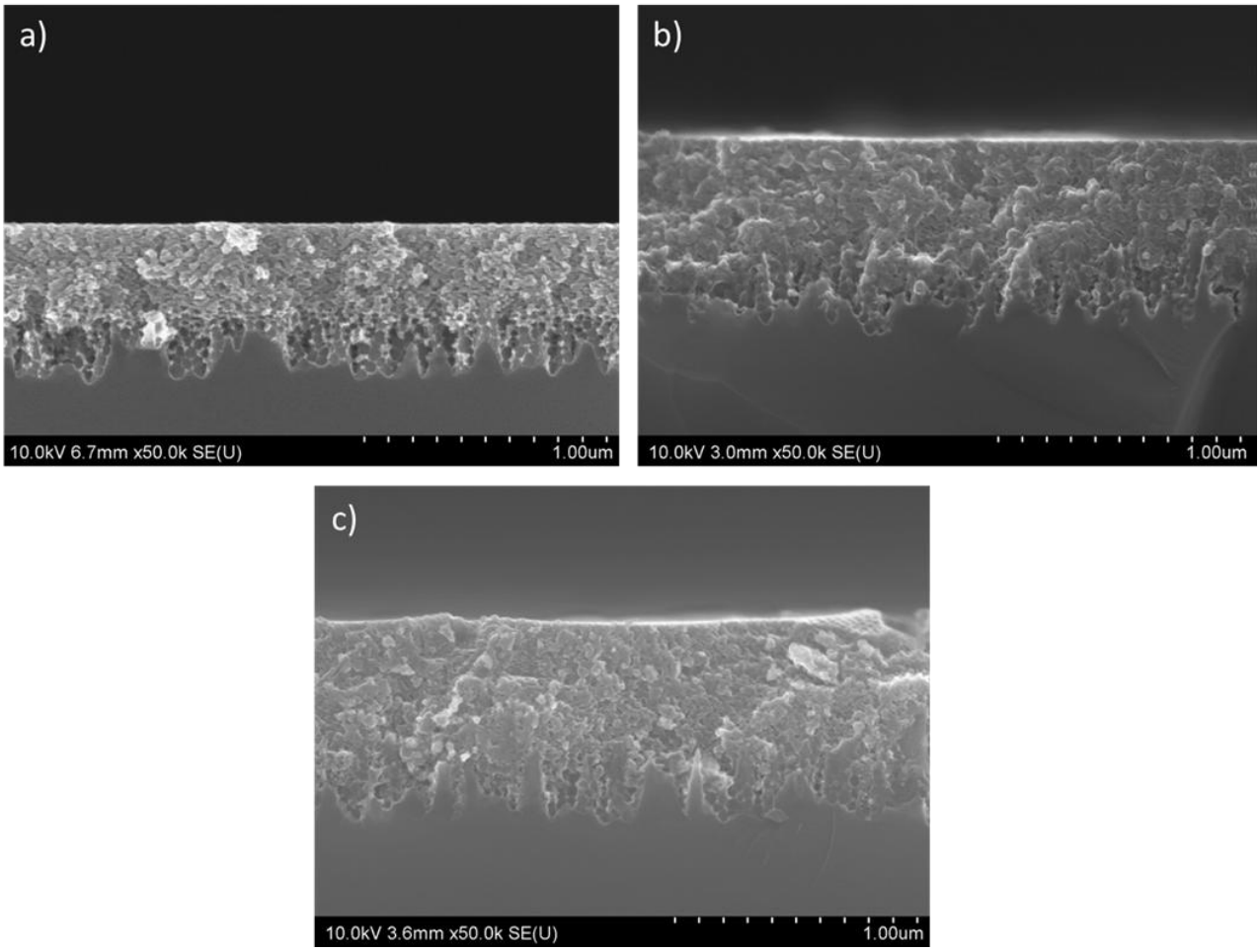

Figure 48: *Side view of the film by SEM-FEG images. Study on the density of the first layer of TiO_2 on the b-Si substrate. (a) 200 mg of Pb-b PEO, (b) 100 mg, (c) 50 mg.*

No significant results were reach at the moment. One perspective is to make the second layer of TiO_2 denser to avoid the electrolyte to reach the b-Si.

V.2. Problem of photo-electron and reactivity toward solid electrolyte

In this thesis, we used the photo-electron for the production of hydrogen. One perspective is to conserve the photo-electron in the process and avoid the reaction with species in the electrolyte or the electrolyte itself. We need to find a stable electrolyte in order to avoid these reactions. Solid state electrolyte are good candidates since they are less reactive; a Lithium Phosphorus Oxynitride (LiPON) was investigated because of its large electrochemical stability window (0 - 5.5 V vs Li^+/Li) and its stability against TiO_2 and lithium metal and make the LiPON the perfect candidate for our photo-all-solid state battery.

Since the photo-electron should not react with the solid electrolyte, it is supposed to pass through the external circuit and reduce the lithium ions at the lithium electrode. A figure summarizing the idea is presented below (**figure 49**).

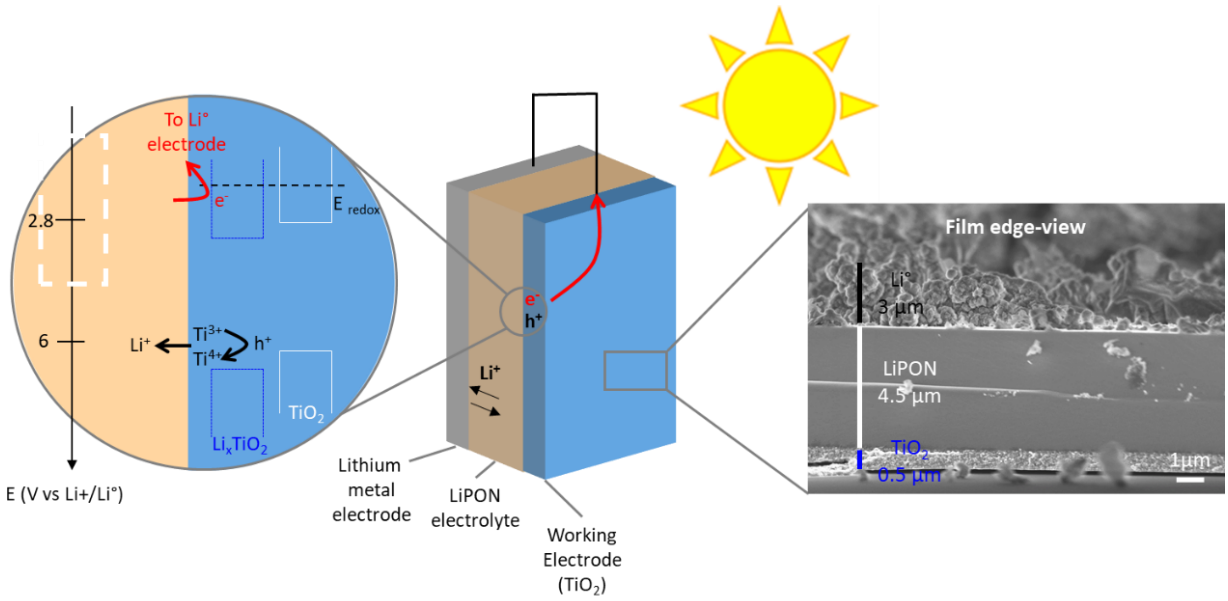

***Figure 49**: Schema of the system: glass/FTO/TiO_2// LiPON// Li°. With a schema of the band diagram of TiO_2 and Li_xTiO_2 and the LiPON electrochemical stability window in white dots scare on the left and on the right SEM-FEG images of the battery on an edge-view.*

V.2.1. Experimental section

In this section, we will detail the experimental part of the work, from the synthesis of the electrolyte, the deposition of the lithium metal, their structural characterizations to their (photo-)electrochemical characterizations, and post mortem characterizations. The same TiO_2 electrode was prepared on a bigger substrate of FTO (area: 75 x 25 mm) for practical reason.

V.2.1.1. LiPON (Lithium Phosphorus Oxynitride) deposition

LiPON thin films (1-3 µm) were deposited onto TiO_2 by rf magnetron sputtering from an Li_3PO_4 (Aldrich, 99.9%) target in a pure N_2 atmosphere with a MP 300 T apparatus. Plasma ignition was performed with argon before introduction of nitrogen. Prior to the deposition of thin films, a presputtering of 30 min was performed. This deposition was realized in the EDF lab at Les Renardières with the help of Philippe Stevens and Gwenaelle Toussaint.

V.2.1.2. Lithium deposition

The lithium metal were deposited on the LiPON by evaporation under 100 A and a pressure in the chamber of $5*10^{-6}$ Torr. Rate 19 A/s for a thickness of 23.13 kÅ. This deposition was realized in the EDF lab at Les Renardières with the help of Philippe Stevens and Gwenaelle Toussaint.

V.2.1.3. Scanning Electron Microscopy

The microstructure of the films and film thickness were observed by Field Emission Gun Scanning Electron Microscopy (FEG- SEM) on a SU-70 Hitachi FEG-SEM, instruments facilitated by the IMPC (Institut des Matériaux de Paris Centre FR2482) financially supported by the C'Nano projects of the Region Ile-de-France. FEG-SEM images were collected under 10 kV tension. Measurements were performed with MONTERO David from the IMPC (Institut des Matériaux de Paris Centre FR2482). The all solid state battery is set on the analytical plot in the glove box in order to avoid contact with the air. If needed it is cut also in the glove box applying a diamond blade on the glass. The sample is transported to the SEM-FEG in a hermetic box under argon.

V.2.2. Result and discussion

First the comparison with our previous system needs to be done. Cyclic voltammetry were realized under dark and light condition through the glass of the glove box to avoid any reactions with the air of the lithium electrode (**figure 50**). The photo-performances should not be disturbed since we already worked in a glass cell from the LP30 and WIS studies.

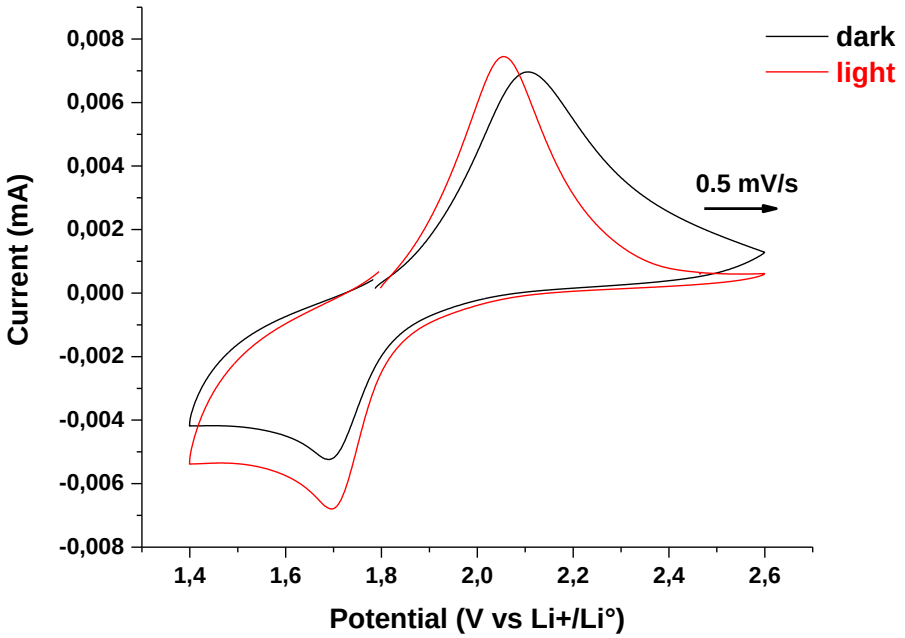

***Figure 50**: Cyclic voltammetry at 0.5 mV/s from 2.6 and 1.4 V of (+) FTO/TiO_2/LiPON/Li° (-) under dark (black line) and light (red line) conditions. (Here the area is not normalized by the surface)*

From the CV in the dark, it seems that the intensity of the waves is lower than in liquid electrolyte, this is probably due to the interface between LiPON and the metallic lithium, that it is not optimized. It might also explain the high the resistance measured (13 kΩ). The peak potential difference (ΔEp) insertion and extraction of the lithium ions are around 0.4 V (against 0.3 V for the WIS study and 0.4 V with the b-Si substrate). Under illumination, an increase intensity of both waves is observed and a small reduction of the overpotential attesting a better reversibility under illumination. SEM-FEG images from the side view were realized in order to investigate the interfaces between the different materials (**figure 51**).

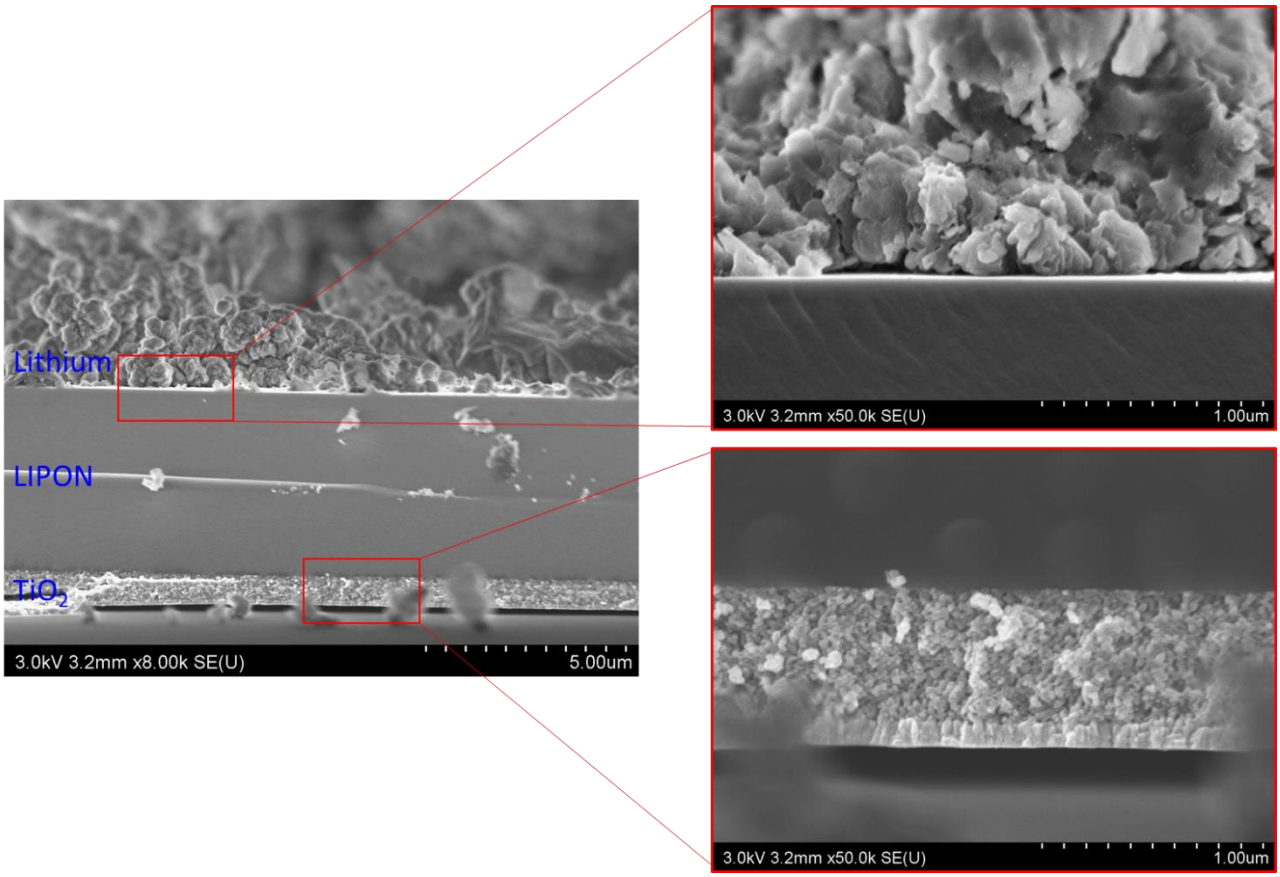

***Figure 51**: SEM-FEG images of the (+) FTO/TiO_2/LiPON/Li° (-) from side view with a zoom of the LiPON/Li° interface (top) and a zoom of the TiO_2/LiPON interface (bottom).*

From these images, we can see that the interface between the LiPON and the TiO_2 seems good (bottom right) but we cannot see if the LIPON impregnates the mesoporous structure of the TiO_2. Nevertheless, on the top right we can see that the interface between the lithium and the LiPON seems not good but could also be due to the oxidation during the transfer of the cell to the SEM-FEG chamber even though it last less than 10 second it could be enough. We try different method of lithium deposition but without any success. The technics used were melting of lithium, anodeless or even applying pressure on a metallic foil of lithium. During some deposition of the LiPON, we have noticed a reduction of the TiO_2 since the substrate turns blue. It could be due to the plasma in the chamber that is reductive or some pollution in the chamber. Both deposition of the LiPON and the lithium metal are not optimized yet and needs further optimization.

Bibliography

(1) Nguyen, O. Towards a Li-Ion Photo-Rechargeable Battery. thesis, Sorbonne Université, 7 place Jussieu, **2018**.

(2) Nguyen, O.; Courtin, E.; Sauvage, F.; Krins, N.; Sanchez, C.; Laberty-Robert, C. Shedding Light on the Light-Driven Lithium Ion de-Insertion Reaction: Towards the Design of a Photo-Rechargeable Battery. *Journal of Materials Chemistry A* **2017**, *5* (12), 5927–5933.

(3) Nguyen, O.; Krins, N.; Laberty-Robert, C. Harvesting Light with Semiconductor: Role of Interface in the Processes of Charge Transfer. *Materials Science in Semiconductor Processing* **2018**, *73*, 2–12.

(4) Sood, A.; Poletayev, A. D.; Cogswell, D. A.; Csernica, P. M.; Mefford, J. T.; Fraggedakis, D.; Toney, M. F.; Lindenberg, A. M.; Bazant, M. Z.; Chueh, W. C. Electrochemical Ion Insertion from the Atomic to the Device Scale. *Nat Rev Mater* **2021**, *6* (9), 847–867.

(5) Paolella, A.; Faure, C.; Bertoni, G.; Marras, S.; Guerfi, A.; Darwiche, A.; Hovington, P.; Commarieu, B.; Wang, Z.; Prato, M.; Colombo, M.; Monaco, S.; Zhu, W.; Feng, Z.; Vijh, A.; George, C.; Demopoulos, G. P.; Armand, M.; Zaghib, K. Light-Assisted Delithiation of Lithium Iron Phosphate Nanocrystals towards Photo-Rechargeable Lithium Ion Batteries. *Nature Communications* **2017**, *8*, 14643.

(6) Wang, Z.; Chiu, H.; Paolella, A.; Zaghib, K.; Demopoulos, G. P. Lithium Photo-intercalation of CdS-Sensitized WO_3 Anode for Energy Storage and Photoelectrochromic Applications. *ChemSusChem* **2019**, *12* (10), 2220–2230.

(7) Lee, A.; Vörös, M.; Dose, W. M.; Niklas, J.; Poluektov, O.; Schaller, R. D.; Iddir, H.; Maroni, V. A.; Lee, E.; Ingram, B.; Curtiss, L. A.; Johnson, C. S. Photo-Accelerated Fast Charging of Lithium-Ion Batteries. *Nat Commun* **2019**, *10* (1), 1–7.

(8) Gurung, A.; Chen, K.; Khan, R.; Abdulkarim, S. S.; Varnekar, G.; Pathak, R.; Naderi, R.; Qiao, Q. Highly Efficient Perovskite Solar Cell Photocharging of Lithium Ion Battery Using DC–DC Booster. *Advanced Energy Materials* **2017**, *7* (11), 1602105.

(9) Ahmad, S.; George, C.; Beesley, D. J.; Baumberg, J. J.; De Volder, M. Photo-Rechargeable Organo-Halide Perovskite Batteries. *Nano Lett.* **2018**, *18* (3), 1856–1862.

(10) Chen, S.; Wang, L.-W. Thermodynamic Oxidation and Reduction Potentials of Photocatalytic Semiconductors in Aqueous Solution. *Chemistry of Materials* **2012**, *24* (18), 3659–3666.

(11) Light-induced reflectivity transients in black-Si nanoneedles | Elsevier Enhanced Reader (accessed **2020** -03 -05).

(12) Monconduit, L.; Croguennec, L.; Dedryvère, R. *Electrodes de batteries Li-ion volume 2*, ISTE.; Collection Energie; **2015**; Vol. 2.

General Conclusion

General Conclusion

There is a growing interest in the literature for developing systems able to combine solar conversion and storage. Chapter I presented a few examples of the growing research on the topic. Numerous works study the three-electrode systems: a photo-electrode that harvests light while charging the two electrodes of the battery, or better most often while *assisting* their charge. Different battery technologies (Li/Na-ion, redox flow, Li-S, Li-O_2) are investigated and various strategies are suggested to ensure the transfer the harvested light energy from the photo-electrode to the battery, like redox shuttles in the electrolyte, soluble storage redox couples or physically contacting one electrode with the cathode. Fewer works investigate two-electrode set-up, where one of the battery electrode endorse the role of harvesting light and storing it. And within this category, we distinguish the electrodes that combine a storage material modified on the surface by a photosensitizer, from the bifunctional electrodes where the storage material is also doing the work of light conversion. This thesis studies the latter and presents a mesoporous anatase TiO_2 film as bifunctional electrode candidate. We chose to work with a model electrode: phase pure, carbon-free electrode, which offers a homogeneous exposition to the electrolyte throughout the electrode. It can host lithium ions and we will demonstrate that its Li-rich phase can harvest visible light.

This work follows up on the work of Nguyen et al. [1], which uses with these electrodes LP30 as an electrolyte and Li° as a counter electrode. Photo-extraction of lithium ions at OCV and during electrochemical cycling was demonstrated. The role played by the photogenerated holes seemed clear, however the fate of the electrons was not elucidated. In this thesis, we chose to control and orient the fate of the electrons by adding water as a photo-electron acceptor, thereby choosing a water-based electrolyte (i.e. water-in-salt, WIS) to also be able to access a large storage capacity of lithium ions.

In our system, in the dark, TiO_2 can reversibly host up to 0.3 lithium ions per TiO_2. However, capacities achieved during discharge are much higher because of the electrochemical contribution of the water reduction reaction (HER for Hydrogen Evolution Reaction). From the discharge-charge cycle, the global quantity of H_2 produced represents the irreversible part of the capacity, the reversible part corresponding to the reversible Li^+ storage.

In Chapter I, we were interested in evaluating how the HER could be influenced by the state of charge of TiO_2, in other words its lithium content.

We used *operando* UV-VIS to discriminate the lithium insertion from the HER, following the optical absorbance of the material since only Li^+ insertion is responsible for the change in opto-electronic properties of the material. We could plot the quantity of H_2 produced as a function of the Li^+ content. **The higher the lithium content, the higher the HER production. The Li-rich phase of TiO_2 appears to play the role of a HER electrocatalyst**. Using inserting materials as electrocatalysts have recently attracted attention mainly for OER and with this example, we showed that electrochemically lithiated TiO_2 HER could also be investigated as a cheap and eco-friendly candidate HER, and easy to regenerate electrocatalyst.

If inserting materials are envisioned as good candidate for electrocatalytic reaction, they should also be considered for their promising photocatalytic or photoelectrocatalytic reactions. This is where this field merges with the one of bifunctional electrode. In Chapter IV, we showed that it was possible and interesting, in terms of time, to **photo-charge in the visible the TiO_2 electrode**. A photocatalytic mechanism is proposed, where the photogenerated holes oxidizes TiO_2 while extracting lithium ions, and the photo-electrons contribute to HER at the surface of the electrode. We also demonstrated that the Li-rich phase is responsible for visible light harvesting, and that its distribution within the particle matters. The photoactivity increases when the lithium-rich phase is located at the surface, which is the case when the electrode is being discharged. Lithium rich phase TiO_2 acts as a photocatalyst for HER active in the visible range. A catalyst is supposed to be left unchanged after a reaction, here the material is changing. It could however be regenerated electrochemically.

We also examined the possibility of performing a **photo-assisted charge**. After 10 cycles at 2C-rate, the cumulated time of 10 photo-charges was the same compared to 10 charges in the dark. In a first approach there was **no obvious benefit** to photo-assisted charging. However, light had **an actual impact** on the experiment: a slight decrease in charge capacity, but also an improved lithium diffusion rate and a lower ohmic drop. We investigated in more details this impact on charge and discharge, separately and together and we showed that a better understanding of the system is necessary to conduct a beneficial photo-assisted cycling.

We also examined when, depending on the potential on a cyclic voltammogram, the electrode was photoactive. The material behaves as a p-type semiconductor or a n-type semi-conductor depending on different parameters, the Li-content, the potential, but also the direction of the potential ramping (towards electronic band filling or emptying).

For a same lithium content, or even a same potential, it could be ambivalent. The lithiated phase acts this time as a **photoelectrocatalyst for HER upon illuminated charge)**.

The different sections of this thesis convert to one important perspective that is to investigate the promises of these inserting material (TiO_2, but also $LiFePO_4$[2], $LiWO_3$[3], $LiMn_2O_4$[4] or perovskite[5,6].) In the fields of (photo)(electro)catalysis in general, and HER/OER in particular. We could this time use pure aqueous solutions and various cations (H^+, Li^+, Na^+). We could again play on the Li-rich/Li-poor organization electrochemically to build-in electrical field (BIEF). This study would also have its share of challenges, including the use of operando techniques to follow electronic structure evolution during the reaction of interest (the opto-electronic properties of the materials, the band diagram, BIEF). And we could of course use this combination to building photo-rechargeable systems.

In parallel to the WIS approach, we also tempted to build a photo-rechargeable all-solid-state battery. Preliminary results are shown in **Chapter V.2.** with LiPON. The idea behind is to remove all potential photo-electron acceptor from the electrolyte to encourage the photo-electron to reduce lithium anode. It seems unlikely given the electronic band structure of the composite Li-poor/Li-rich TiO_2, however it still holds a lot of unknown. At this stage the conception of the battery itself, and the management of electrode/electrolyte interface is challenging.

In addition to these perspectives, another point, which would deserve to be investigated is the lithium content. This system holds us back with a Li-rich phase $Li_{0.5}TiO_2$ (and a global composition at $Li_{0.3}TiO_2$). For nanosized systems, a Li-richer phase has been reported, $LiTiO_2$. All the properties studied in this thesis relate to Li content. Reaching higher Li^+ content would certainly be worth studying. In LP30, the main issue would be to access a lower range of potential. For now, FTO is not stable, we suggest to switch to a doped Si one. Preliminary tests are presented in **Chapter V.1**. This perspective holds new challenges if we want to switch to aqueous or even solid state electrolytes.

Here we saw the conclusion of this work with the battery point of view but a different approach could be done. We show a way to boost the production of hydrogen by inserting cation in a semiconductor in the dark. This kind of dynamic material could be used in photo-catalyst for HER or OER.

Bibliography

(1) Nguyen, O. Towards a Li-Ion Photo-Rechargeable Battery. thesis, Sorbonne Université, 7 place Jussieu, **2018**.

(2) Paolella, A.; Faure, C.; Bertoni, G.; Marras, S.; Guerfi, A.; Darwiche, A.; Hovington, P.; Commarieu, B.; Wang, Z.; Prato, M.; Colombo, M.; Monaco, S.; Zhu, W.; Feng, Z.; Vijh, A.; George, C.; Demopoulos, G. P.; Armand, M.; Zaghib, K. Light-Assisted Delithiation of Lithium Iron Phosphate Nanocrystals towards Photo-Rechargeable Lithium Ion Batteries. *Nature Communications* **2017**, *8*, 14643.

(3) Wang, Z.; Chiu, H.; Paolella, A.; Zaghib, K.; Demopoulos, G. P. Lithium Photo-intercalation of CdS-Sensitized WO_3 Anode for Energy Storage and Photoelectrochromic Applications. *ChemSusChem* **2019**, *12* (10), 2220–2230.

(4) Lee, A.; Vörös, M.; Dose, W. M.; Niklas, J.; Poluektov, O.; Schaller, R. D.; Iddir, H.; Maroni, V. A.; Lee, E.; Ingram, B.; Curtiss, L. A.; Johnson, C. S. Photo-Accelerated Fast Charging of Lithium-Ion Batteries. *Nat Commun* **2019**, *10* (1), 1–7.

(5) Gurung, A.; Chen, K.; Khan, R.; Abdulkarim, S. S.; Varnekar, G.; Pathak, R.; Naderi, R.; Qiao, Q. Highly Efficient Perovskite Solar Cell Photocharging of Lithium Ion Battery Using DC–DC Booster. *Advanced Energy Materials* **2017**, *7* (11), 1602105.

(6) Ahmad, S.; George, C.; Beesley, D. J.; Baumberg, J. J.; De Volder, M. Photo-Rechargeable Organo-Halide Perovskite Batteries. *Nano Lett.* **2018**, *18* (3), 1856–1862.

Annex

Annex I – Air Mass Global

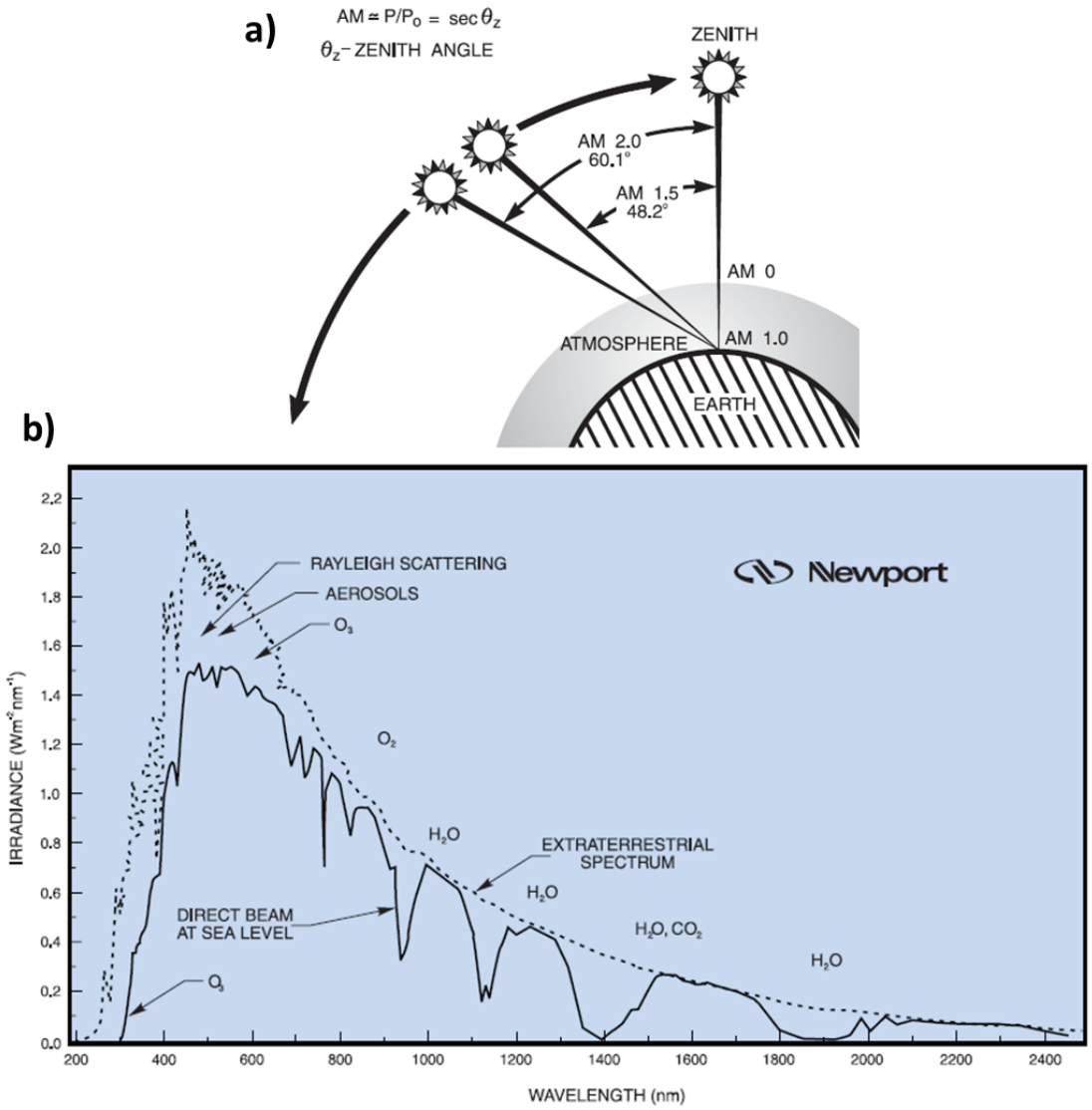

(a) the path length in units of Air Mass, changes with the zenith angle, (b) Normally incident solar spectrum at sea level on a clear day (AM 1). The dotted curve shows the extrarrestrial spectrum (AM 0).[1]

Annex II – Electrode stabilization in LP30 and WIS electrolyte

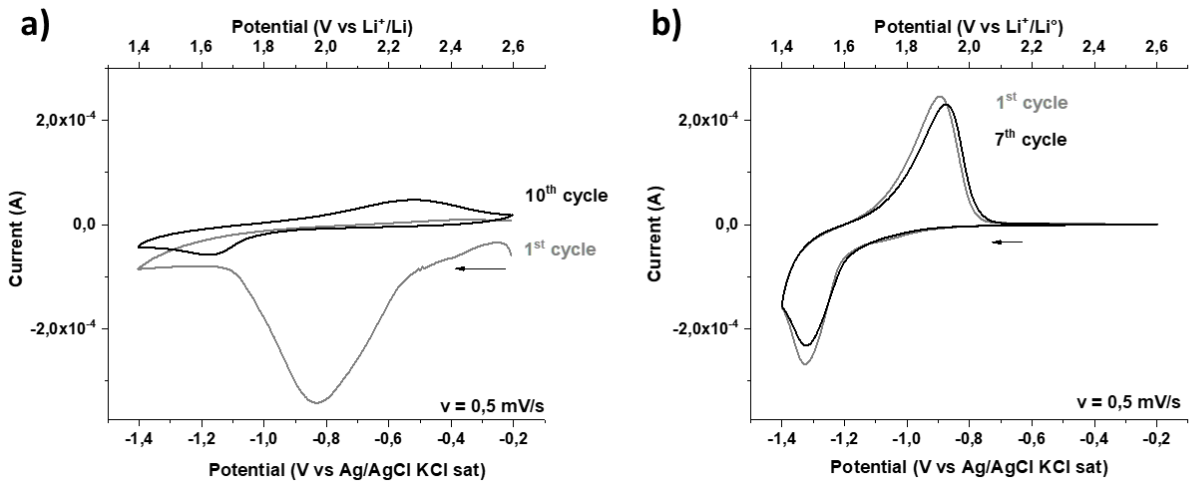

a) *1st and 10th cyclic voltammetry (CV) at 0.5 mV/s starting from 2.6 V to 1.4 V vs Li+/Li° in LP30 electrolyte (TiO_2/$LiPF_6$ 1 M in EC: DMC (1: 1 vol) (LP30) // Li°/Li°), b) 1st and 7th cyclic voltammetry (CV) at 0.5 mV/s starting from -0.2 V to -1.4 V vs Ag/AgCl (KCl saturated) in Water In Salt (WIS) electrolyte (TiO_2// WIS (20 m) // Li°/Li°).*

Annex III – Self extraction of Li^+ at different State of Charge

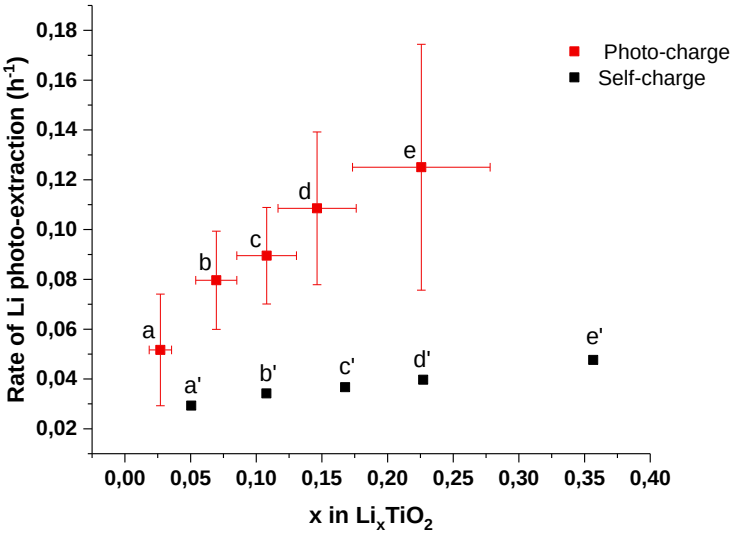

(red) Rate of the photo-extraction of the Li^+ over different composition of lithium (a to e) in the TiO_2, (black) Rate of the self-extraction of the Li^+ over different composition of lithium (a' to e') in the TiO_2.

Annex IV – TiO_2 electrode behavior under illumination at 4C-rate

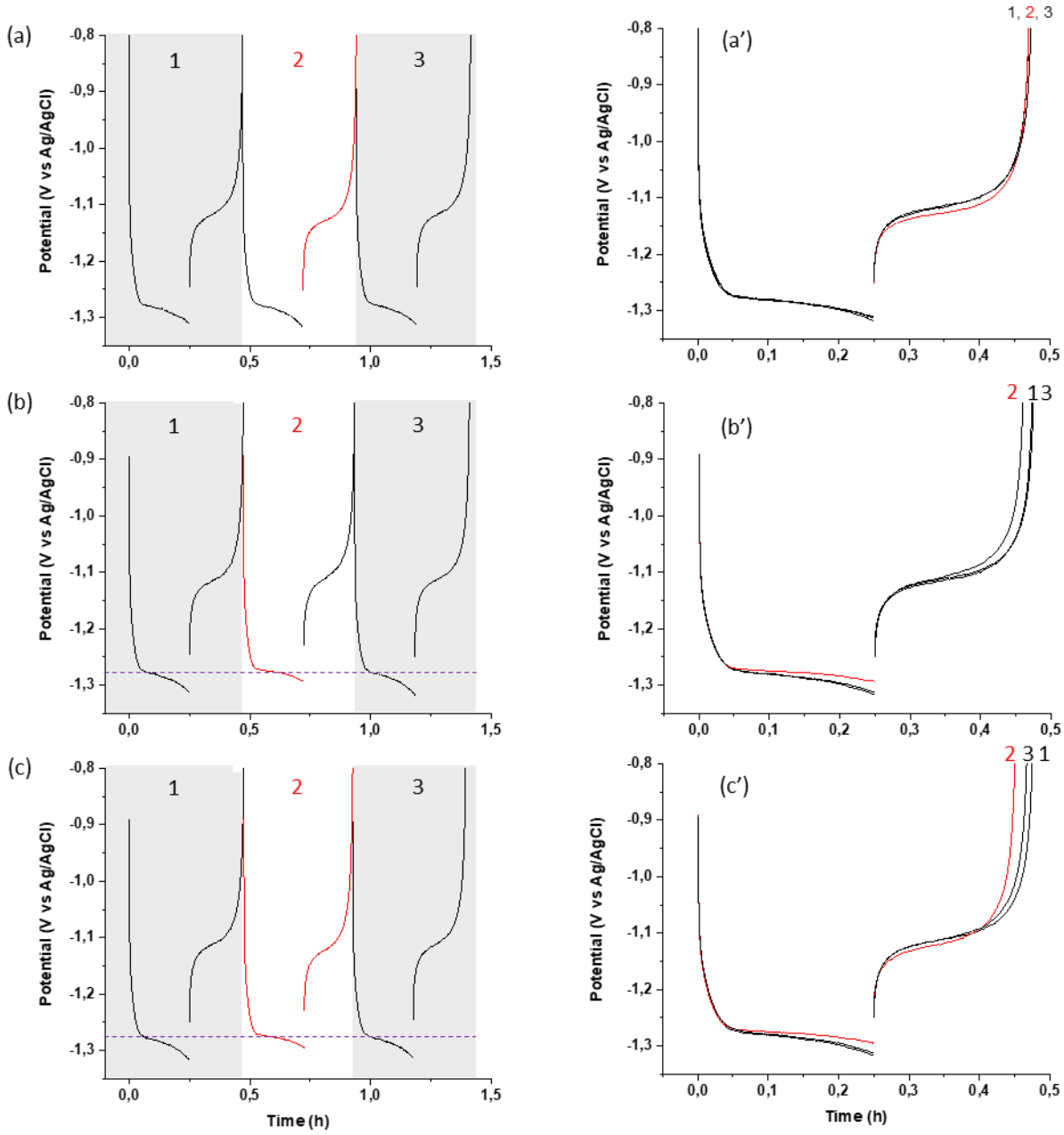

Galvanostatic experiments performed at 4C-rate highlighting the impact on illumination on charge only (a), discharge only (b) and on both charge and discharge (c). Steps 1 and 3 consist in a cycle of discharge-charge performed in the dark, before and after the step of interest (i.e. step 2) respectively. The discharge time has been set to 30 min, which corresponds to 111 mAh/g. (a', b' and c') represent the same discharge and charge curves as in (a, b and c) starting all 3 discharge-charge curves at time 0 for an easier comparison.

Annex IV – Absorption spectra evolution from 3500 to 250 nm upon lithiation

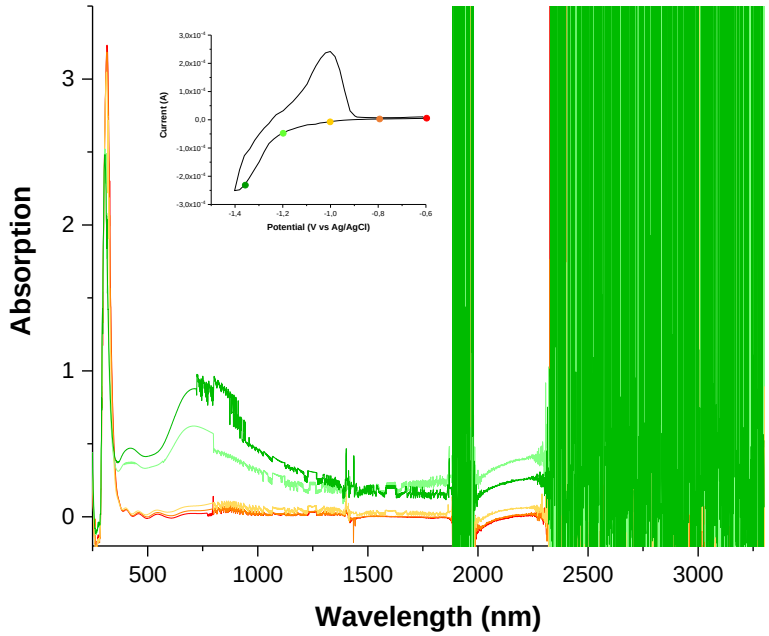

Absorption spectra from 3500 nm to 250 nm at different state of charge during the reduction of the TiO_2 electrode at 0.5 mV/s.

Annex V – Impedance spectra of TiO_2 and $Li_{0.3}TiO_2$ under dark and light conditions

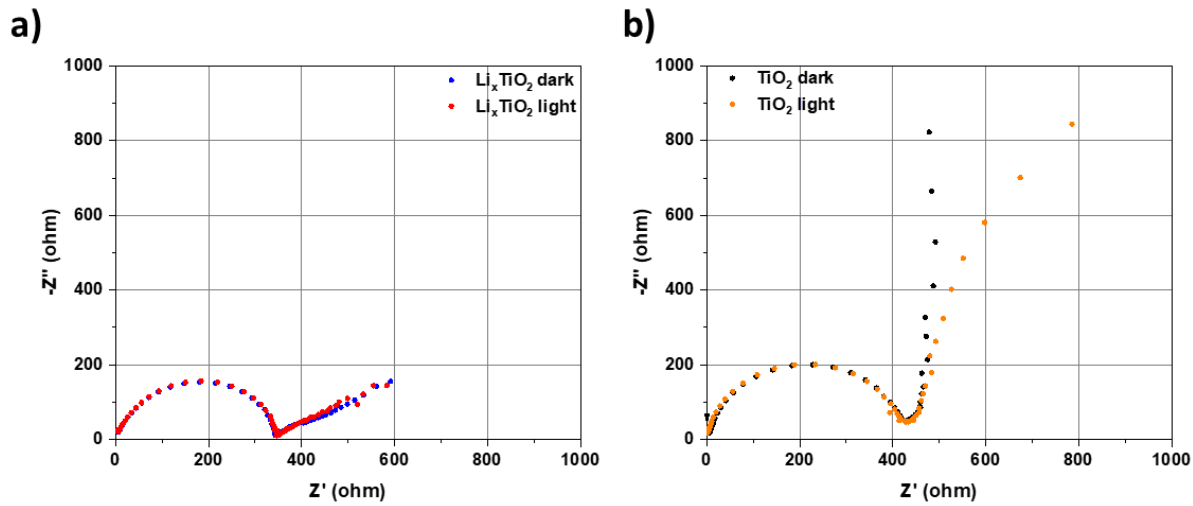

Impedance spectra of (a) $Li_{0.3}TiO_2$ under dark (blue dots) and light (red dots), and (b) TiO_2 under dark (black dots) and light (orange dots).

Annex VI – Pictures illustrating the change of color upon galvanostatic cycle at 2C-rate.

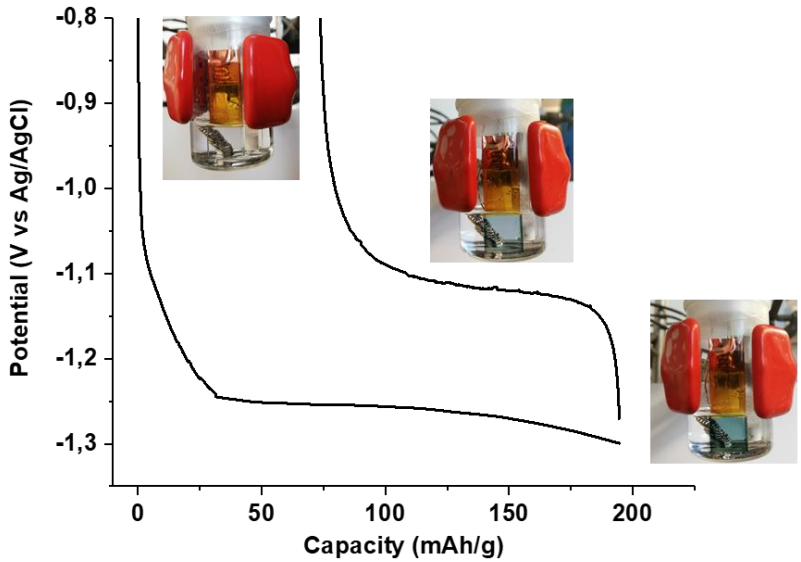

Pictures illustrating the change of color upon galvanostatic cycle at 2C-rate of FTO/TiO_2// WIS (20m) // AgAgCl KCl saturated /Pt.

Abstract

Our approach to alleviate the solar intermittency is to combine, in a single photo-electrochemical cell, solar energy conversion and storage. Starting from a Li-ion battery configuration, we propose to use Li-ion host photo-electrodes, which could both harvest solar energy and store it. We will be presenting the case of mesoporous TiO_2 anatase, as a positive electrode. The illumination of the lithiated electrode (after discharge) induces a lithium-ion extraction reaction (i.e. the recharge of the battery), opening the way to Li-ion photo-rechargeable batteries. Photo-extraction of lithium ions at open circuit voltage and during electrochemical cycling was demonstrated. The holes' photo-generated seems to oxidize the Ti^{3+} into Ti^{4+} resulting in the extraction of the lithium ion, however the fate of the photo-electrons was not elucidated. In this thesis, we chose to control and orient the fate of the electrons by adding water as a photo-electron acceptor, thereby choosing a water-based electrolyte (i.e. water-in-salt, WIS) to also be able to access a large storage capacity of lithium ions and produce a storage molecule, the dihydrogen. Depending of the state of charge of the battery, the electrode composition varies a lot: from a single crystalline phase to a two-phase material. The impact of this composition change in the dynamics of, the production of hydrogen and the light-induced processes, both will be discussed in this thesis. This work constitutes a proof of concept that low potential Li-ion batteries could solely be recharged by exposure to light.

Résumé

Ce projet de thèse vise la conception d'un seul dispositif électrochimique capable de collecter l'énergie solaire, la convertir et la stocker de façon réversible. Pour ce faire, nous avons choisi de travailler avec un matériau d'électrode bi-fonctionnel qui doit à la fois absorber une partie du spectre solaire et aussi accueillir réversiblement les ions lithiums dans sa structure. Dans ce contexte, nous avons travaillé avec un film de TiO_2 anatase mésoporeux comme électrode positive bi-fonctionnelle. L'illumination de l'électrode lithiée (après décharge) induit une réaction d'extraction des ions lithium (c'est-à-dire la recharge de la batterie), ouvrant la voie aux batteries Li-ion photo-rechargeables. La photo-extraction des ions lithium à tension de circuit ouvert et pendant le cyclage électrochimique a été démontrée. Le mécanisme proposé envisage l'oxydation du Ti^{3+} en Ti^{4+} par les trous photo-générés, entraînant ainsi l'extraction de l'ion lithium. Cependant, le sort des photo-électrons n'a pas été élucidé. Dans cette thèse, nous avons choisi de contrôler et d'orienter le devenir des photo-électrons en ajoutant de l'eau comme accepteur. Ainsi, nous avons travaillé avec un électrolyte à base d'eau (ie Water In Salt, WIS) pour accéder à une grande capacité de stockage des ions lithium et produire une molécule de stockage, le dihydrogène. Selon l'état de charge de la batterie, la composition de l'électrode varie : d'une phase monocristalline à un matériau bi-phasique. L'impact de ce changement de composition sur la dynamique de la production d'hydrogène et les processus induits par la lumière seront tous deux discutés dans cette thèse. Ce travail constitue une preuve de concept que les batteries Li-ion à faible potentiel pourraient être rechargées uniquement par exposition à la lumière.